PB85-242139

# Destruction of Hazardous Wastes Cofired in Industrial Boilers: Pilot-Scale Parametrics Testing

Acurex Corp., Mountain View, CA

Prepared for

Environmental Protection Agency, Cincinnati, OH

Aug 85

U.S. Department of Commerce
National Technical Information Service
NTIS

PB85-242139

EPA/600/2-85/097
August 1985

# DESTRUCTION OF HAZARDOUS WASTES COFIRED IN INDUSTRIAL BOILERS: PILOT-SCALE PARAMETRICS TESTING

by
C. D. Wolbach and A. R. Garman
Acurex Corporation
Energy & Environmental Division
555 Clyde Avenue
P.O. Box 7555
Mountain View, California 94039

EPA Contract No. 68-02-3176

EPA Project Officer: Robert A. Olexsey
Incineration Research Branch
Hazardous Waste Engineering Laboratory
Cincinnati, Ohio 45268

HAZARDOUS WASTE ENGINEERING RESEARCH LABORATORY
OFFICE OF RESEARCH AND DEVELOPMENT
U.S. ENVIRONMENTAL PROTECTION AGENCY
CINCINNATI, OH 45268

REPRODUCED BY
NATIONAL TECHNICAL
INFORMATION SERVICE
U.S. DEPARTMENT OF COMMERCE
SPRINGFIELD, VA. 22161

## TECHNICAL REPORT DATA

*(Please read Instructions on the reverse before completing)*

1. REPORT NO.
EPA/600/2-85/097

2.

3. RECIPIENT'S ACCESSION NO.
PB85 242139/AS

4. TITLE AND SUBTITLE
Destruction of Hazardous Wastes Cofired in Industrial Boilers: Pilot-Scale Parametrics Testing

5. REPORT DATE
August 1985

6. PERFORMING ORGANIZATION CODE

7. AUTHOR(S)
C. D. Wolbach and A. R. Garman

8. PERFORMING ORGANIZATION REPORT NO.
FR 84-146/EED

9. PERFORMING ORGANIZATION NAME AND ADDRESS
Acurex Corporation
Energy & Environmental Division
555 Clyde Avenue, P.O. Box 7555
Mountain View, CA 94039

10. PROGRAM ELEMENT NO.
D 109

11. CONTRACT/GRANT NO.
68-02-3176

12. SPONSORING AGENCY NAME AND ADDRESS
HAZARDOUS WASTE ENGINEERING RESEARCH LABORATORY
OFFICE OF RESEARCH AND DEVELOPMENT
U.S. ENVIRONMENTAL PROTECTION AGENCY
CINCINNATI, OH 45268

13. TYPE OF REPORT AND PERIOD COVERED
Final Report

14. SPONSORING AGENCY CODE
EPA/600/12

15. SUPPLEMENTARY NOTES

16. ABSTRACT

Thermal destruction of wastes by direct incineration or by cofiring with conventional fuels in boilers, furnaces, or kilns is one of the most effective methods currently available for disposal of hazardous organic material. However, more information is needed on the potential for emissions to the environment during thermal destruction.

The specific objectives of the current study were to identify which of several boiler operational parameters have a major impact on boiler destruction and removal efficiency; and to evaluate and if practical, establish a mathematical model for predicting an upper limit on the amount of cofired waste that could be emitted. The program was carried out in three phases: a detailed characterization of thermal history and environment of a pilot-scale furnace under various sets of operating conditions; a study of the DRE of one compound as conditions were varied; and finally, a study of DRE's of several compounds burned simultaneously (a composite "soup"). Parameters studied included excess air rate, fuel firing rate, amount of water wall surface area, burner swirl setting, and waste type. In addition, a model was constructed that predicts the thermal profile and destruction efficiency of the combustor. The model runs on a microcomputer.

17. KEY WORDS AND DOCUMENT ANALYSIS

| a. DESCRIPTORS | b. IDENTIFIERS/OPEN ENDED TERMS | c. COSATI Field/Group |
|---|---|---|
| | | |

18. DISTRIBUTION STATEMENT
Release unlimited

19. SECURITY CLASS *(This Report)*
Unclassified

20. SECURITY CLASS *(This page)*
Unclassified

21. NO. OF PAGES
174

22. PRICE

EPA Form 2220-1 (9-73)

# NOTICE

This document has been reviewed in accordance with U.S. Environmental Protection Agency Policy and approved for publication. Mention of trade names of commercial products does not constitute endorsement of recommendation for use.

# FOREWORD

Todays's rapidly developing and changing technologies and industrial products and practices frequently carry with them the increased generation of solid and hazardous wastes. These materials, if improperly dealt with, can threaten both public health and the environment. Abandoned waste sites and accidental releases of toxic and hazardous substances to the environment also have important environmental and public health implications. The Hazardous Waste Engineering Research Laboratory assists in providing an authoritative and defensible engineering basis for assessing and solving these problems. Its products support the policies, programs, and regulations of the Environmental Protection Agency, the permitting and other responsibilities of State and local governments and the need of both large and small businesses in handling their wastes responsibly and economically.

This report documents the results of pilot-scale parametric testing of hazardous waste material mixtures cofired with conventional fuels in a test combustor facility. The testing was intended to simulate industrial boilers cofiring hazardous wastes. The research effort is part of the multidisciplinary research program to develop the information necessary for boiler cofiring regulatory development. For further information, please contact the Alternative Technologies Division of the Hazardous Waste Engineering Research Laboratory.

David G. Stephan, Director
Hazardous Waste Engineering Research Laboratory

# ABSTRACT

Thermal destruction of wastes by direct incineration of by cofiring with conventional fuels in boilers, furnaces, or kilns is one of the most effective methods currently available for disposal of hazardous organic material. However, more information is needed on the potential for emissions to the environment during thermal destruction.

The specific objectives of the current study were to identify which of several boiler operational parameters have a major impact on boiler destruction and removal efficiency; and to evalute, and if practical, establish a mathematical model for predicting an upper limit on the amount of cofired waste that could be emitted. The program was carried out in three phases: a detailed characterization of thermal history and environment of a pilot-scale furnace under various sets of operating conditions; a study of DRE's of several compounds burned simultaneously (a composite "soup"). Parameters studied included excess air rate, fuel firing rate, amount of water wall surface area, burner swirl setting, and waste type. In addition, a model was constructed that predicts the thermal profile and destruction efficiency of the combustor. The model runs on a microcomputer.

This report was submitted in fulfillment of Contract No. 68-02-3176 by Acurex Corporation under the sponsorship of the U.S. Environmental Protection Agency. This report covers a period from July 1982 to July 1984, and work was completed as of July 1984.

# CONTENTS

Foreword . . . . . . . . . . . . . . . . . . . . . . . . . . . . . iii
Abstract . . . . . . . . . . . . . . . . . . . . . . . . . . . . . iv
Figures . . . . . . . . . . . . . . . . . . . . . . . . . . . . . vii
Tables . . . . . . . . . . . . . . . . . . . . . . . . . . . . . x

1. Introduction . . . . . . . . . . . . . . . . . . . . . . . . 1
    1.1 Background . . . . . . . . . . . . . . . . . . . . . . 2
    1.2 Purpose . . . . . . . . . . . . . . . . . . . . . . . . 3
    1.3 Generalized Approach . . . . . . . . . . . . . . . . . 3

2. Conclusions and Recommendations . . . . . . . . . . . . . . 5
    2.1 Conclusions . . . . . . . . . . . . . . . . . . . . . . 5
    2.2 Recommendations . . . . . . . . . . . . . . . . . . . . 6

3. Technical Approach and Program Description . . . . . . . . . 8
    3.1 Model Description . . . . . . . . . . . . . . . . . . . 8
    3.2 General Approach and Test Matrix . . . . . . . . . . . 10
    3.3 Facility Description . . . . . . . . . . . . . . . . . 14
    3.4 Test Description . . . . . . . . . . . . . . . . . . . 16
    3.5 Sampling and Analysis Protocols . . . . . . . . . . . . 17

4. Results and Discussion . . . . . . . . . . . . . . . . . . . 19
    4.1 Summary of Tests . . . . . . . . . . . . . . . . . . . 19
    4.2 Summary of DRE Results . . . . . . . . . . . . . . . . 19
    4.3 Parameter Effects . . . . . . . . . . . . . . . . . . . 19
    4.4 Other DRE Correlations . . . . . . . . . . . . . . . . 39
    4.5 Products of Incomplete Combustion . . . . . . . . . . . 39
    4.6 Compound Composition . . . . . . . . . . . . . . . . . 42

5. Model Development . . . . . . . . . . . . . . . . . . . . . 44
    5.1 Background . . . . . . . . . . . . . . . . . . . . . . 47
    5.2 Goals . . . . . . . . . . . . . . . . . . . . . . . . . 47
    5.3 Approach . . . . . . . . . . . . . . . . . . . . . . . 48
    5.4 Bulk Gas Temperature Model . . . . . . . . . . . . . . 48
    5.5 Boundary Layer Destruction Model . . . . . . . . . . . 63
    5.6 Bulk Gas Temperature Model Results . . . . . . . . . . 67
    5.7 Boundary Layer Model Results . . . . . . . . . . . . . 78
    5.8 Summary and Conclusions . . . . . . . . . . . . . . . . 94

## CONTENTS (CONCLUDED)

References . . . . . . . . . . . . . . . . . . . . . . . . . . . . 96

Appendices

A. Test Facility Detailed Description . . . . . . . . . . . . . . . . 99
B. Detailed Furnace Operation . . . . . . . . . . . . . . . . . . . . 121
C. Sampling and Analysis . . . . . . . . . . . . . . . . . . . . . . 126
D. Data Handling and Reduction Procedures . . . . . . . . . . . . . . 130

## FIGURES

| Number | | Page |
|---|---|---|
| 1 | Typical plot of a boiler time-above-temperature curve overlain by a compound time-at-temperature curve . . . . . . | 9 |
| 2 | Schematic of the Acurex pilot-scale furnace . . . . . . . . . . | 15 |
| 3 | Schematic of sampling train used for the B series of tests . . . . . . . . . . . . . . . . . . . . . . . . . | 18 |
| 4 | Samplified schematic of the pilot-scale furnace showing location of temperature profile cross sections . . . . . . . | 25 |
| 5 | A typical set of cross sectional temperature profiles . . . . | 27 |
| 6 | Axial temperature profiles are various radial distances from centerline including refractory wall temperatures . . . | 28 |
| 7 | Conterline axial temperature profiles for four firing conditions without waterwalls . . . . . . . . . . . . . . . . | 29 |
| 8 | Centerline axial temperature profiles for six firing conditions with waterwalls . . . . . . . . . . . . . . . . . . | 30 |
| 9 | Centerline temperature profiles with (Run B-8) and without waterwalls (Runs B-2 and B-3) . . . . . . . . . . . . | 31 |
| 10 | Plot of fractional breakthrough of chlorobenzene versus firing conditions . . . . . . . . . . . . . . . . . . | 32 |
| 11 | Effects of excess air on temperature for three firing conditions without waterwalls . . . . . . . . . . . . . . . . | 34 |
| 12 | Effect of excess air on fractional breakthrough for carbon tetrachloride and chlorobenzene . . . . . . . . . . . | 35 |
| 13 | Effect of burner swirl setting on temperature profiles . . . | 37 |
| 14 | Correlation of NO emissions to fractional breakthrough of chlorobenzene . . . . . . . . . . . . . . . . . . . . . . | 41 |
| 15 | Turbulent spray flame processes affecting waste destruction efficiency . . . . . . . . . . . . . . . . . . . . | 45 |

FIGURES (CONTINUED)

| Number | | Page |
|---|---|---|
| 16 | Processes undergone by materials during thermal destruction | 46 |
| 17 | Furnace model flow diagram | 49 |
| 18 | Bulk temperature module zone energy balance | 50 |
| 19 | Sample boundary layer module predictions of axisymmetric mass breakthrough fractions | 51 |
| 20 | Plan view schematic of package watertube boiler with 44 MW capacity; furnace height 2.7m | 53 |
| 21a | Case I zone energy balance without interaction between zones | 54 |
| 21b | Case II zone energy balance including recirculation and radiative transfer between zones | 54 |
| 22 | Surface radiation fluxes | 56 |
| 23 | Circuit analog and radiative equilibrium between a nonadiabatic refractory, waterwall sink, and an absorbing gas | 59 |
| 24 | Typical radial temperature and velocity profiles for a zone showing slices | 64 |
| 25 | Program flow chart for Case I bulk gas temperature model | 69 |
| 26a | Baseline bulk temperature model major inputs printout | 73 |
| 26b | Baseline bulk temperature model major outputs printout | 74 |
| 27 | Comparison of model to experimental bulk gas temperature data | 79 |
| 28 | Comparison of model and experimental waterwall heat losses | 80 |
| 29 | Baseline axial carbon tetrachloride concentration profiles | 87 |
| 30 | Effect of 20 percent increase in Arrhenius constants on baseline bulk concentration profiles | 88 |

## FIGURES (CONCLUDED)

| Number | | Page |
|---|---|---|
| 31 | Effect of firing rate on three-annuli baseline $CCL_4$ destruction . . . . . . . . . . . . . . . . . . . . . . . . | 89 |
| 32 | Effect of excess air level on baseline weighted average $CCL_4$ destruction at various axial furnace positions . . . . . | 91 |
| 33 | Comparison of weighted average model prediction and pilot-scale carbon tetrachloride destruction data at variable excess air . . . . . . . . . . . . . . . . . . . . . . | 93 |

## TABLES

| Number | | Page |
|---|---|---|
| 1 | Matrix of independent and depentent variables measured by task | 11 |
| 2 | Test matrix of variables and nominal values | 13 |
| 3 | Nominal independent variable settings for the firing conditions tested | 14 |
| 4 | Summary of runs | 20 |
| 5 | Summary of destruction and removal efficiencies | 22 |
| 6 | Average fractional breakthrough $C/C_0$ for each waste and firing condition | 23 |
| 7 | Semiquantitative estimation of the effects of the independent variables on temperature profile and DRE | 24 |
| 8 | Reproducibility of temperature measurements at four selected points within the pilot-scale furnace | 24 |
| 9 | Flame geometry estimation for baseline condition IIa | 38 |
| 10 | Effect of 10 percent chlorobenzene on temperature profile for firing condition IV | 38 |
| 11 | Effect of waste on average bulk gas temperatures for firing condition II | 40 |
| 12 | Summary of run C-7 | 43 |
| 13 | Baseline bulk temperature model inputs | 72 |
| 14 | Bulk gas temperature profile sensitivity | 76 |
| 15 | Sensitivity ranking of bulk temperature model inputs | 77 |
| 16 | Baseline boundary layer model inputs | 83 |
| 17 | Baseline boundary layer model output for three annuli and bulk conditions | 85 |

# SECTION 1

# INTRODUCTION

Thermal destruction of wastes by direct incineration or by cofiring with conventional fuels in boilers, furnaces, or kilns is one of the most effective methods currently available for disposal of hazardous organic material. While direct incineration of hazardous wastes is regulated by Part 264 of the Resource Conservation and Recovery Act (RCRA) as adopted in January 1981, boiler cofiring is currently exempt from RCRA provisions. However, the potential for boiler cofiring regulations has been evaluated by the Environmental Protection Agency (EPA) and they are now in the process of preparing regulatory positions and drafting regulations for promulgation. To support this effort, EPA's Incineration Research Branch (IRB) in conjunction with the Office of Solid Waste is conducting research and development programs on various thermal destruction devices, incineration effectiveness and associated regulatory impacts.

There are two basic regulatory strategies that are readily applicable to regulating the combustive destruction of hazardous wastes: design certification and performance certification. Design certification is usually thought of as specifying the type or size of equipment that must be used, or banning certain classes of equipment from use. In the particular case of hazardous waste combustion, it may also be used to limit the type or class of wastes that may be combusted. Conversely, performance certification does not limit the type of equipment that can be used, but rather sets performance goals that must be met by the equipment. Most workers in the environmental area are familiar with this strategy in the form of emission limits. However, for the combustion of hazardous wastes, two other performance criteria have evolved with potential for regulatory application. These are the performance of the combustor in generating a specific environment (time, temperature, and turbulence) and its ability to achieve a given destruction and removal efficiency (DRE) with respect to a given material.

The global purpose of this study was to gather data to aid the EPA in selecting a strategy or set of strategies for regulating the combustion of hazardous wastes in boilers. The following subsections present the technical background leading to this study, the specific goals for this study, and the general approach used to achieve these goals.

## 1.1 BACKGROUND

During the mid-1970's the disposal of hazardous materials began to come to the fore as an area of major concern in the field of environmental protection. This concern is exemplified by the passage of the RCRA. One identified method of disposal for high organic content wastes was incineration. Studies were initiated by EPA to determine the conditions necessary for the destruction of some particularly hazardous materials in order to promulgate regulations for their incineration (1,2). Other workers began to look at specific applications of incineration technology to pollution control (3,4). By 1980, papers on incineration were being included in research symposia on hazardous waste treatment and by 1982 sufficient work was being supported to require parallel symposia with one dedicated solely to destruction by combustion (5,6).

With the advent of the energy crisis of 1978-79, industry began to look for ways to lower fuel costs. It was quickly recognized that much organic waste had high heat content, since some industries had been using some waste streams from a few processes as supplemental fuel sources for many years. In 1979 EPA commissioned a study to determine if there was a hazard potential from combusting hazardous wastes in devices other than incinerators (7). The conclusions drawn from the study were that the potential for hazard was high but that there was insufficient data available on:

- How much material could be expected to be burnt
- What classes of compounds would be burnt
- What types of combustors would be used
- How much destruction would be achieved
- What other (hazardous) materials might be emitted

The major conclusion was that the (then) current regulatory status concerning waste combustion in boilers was in a state of limbo.

A follow-on report was then prepared by Castaldini, et al. (1-8) which attempted to answer many of the questions raised by the previous study. Specifically, this report documented the following efforts:

- A survey of hazardous waste generated and disposal practice
- Assembly of an inventory of industrial boiler capacity capable of hazardous waste combustion
- Compilation of the combustion characteristics of typical boilers
- Characterization of hazardous wastes suitable for use as a fuel supplement and

- Attempts to identify the matrix of wastes/boiler types suitable for hazardous waste combustion.

Within reference 8, a simplistic and conservative mathematical model was developed to predict destruction efficiencies as functions of compound and boiler (9). The model was offered for use as a tool to reduce the number of boilers that might have been required to (1) undergo full-scale testing on the advent of a regulatory strategy based on performance, or (2) meet design criteria under a design certification stragegy.

A further report was prepared to investigate various engineering aspects of boiler destruction of wastes (10). Within that report five major topics were covered:

- Identification of candidate test sites
- Preparation of generic sampling and analysis protocol
- Evaluation and prediction of potential air emissions
- Risk assessment considerations
- Estimation of impacts on boiler operation

Within the topic of air emissions the potential for thermal destruction modeling was suggested. However, in order to model, the magnitude of the effects of as many of the known parameters as possible must be known.

## 1.2 PURPOSE

The specific objectives of the current study were twofold: to identify which of several boiler operational parameters have a major impact, positive or negative, on boiler destruction and removal efficiency; and, to evaluate and if practical, establish a mathematical model for predicting a maximum amount of cofired waste that a particular boiler configuration might emit. In particular, those parameters that could be easily changed by an operator or might represent major differences between boiler types were studied. A secondary objective of the study was to gain sufficient information to allow judgements of what particular parameters to monitor closely during full-scale testing. Within that objective was the intent to establish some common basis for comparing full-scale boilers. A final objective was to obtain information that would give insight on how regulations might be cast so that trial burns would not be needed.

## 1.3 GENERALIZED APPROACH

The facility used to achieve the purpose and objectives of the study was a pilot-scale furnace whose thermal characteristics approximated closely a 12-megawatt (40 million Btu/hr) packaged D-type watertube boiler. The program was carried out in the three phases: a detailed characterization of the thermal history and environment of the furnace under various sets of operating conditions; a study of the DRE of one compound as conditions were varied, and finally, a study of DRE's of several compounds burned simultaneously (a composite "soup"). Parameters studied included excess air rate, fuel firing rate, amount of water wall surface area, burner swirl setting, and waste type. The selection of waste types for the composite "soup" encompassed a large range of predicted destructibility.

This report details the results of this study. Section 2 presents the conclusions and recommendations arising from the study. Section 3 presents an in-depth description of the program. Section 4 presents and discusses the results of the tests. Section 5 presents a detailed description of the thermal and kinetic modeling effort.

# SECTION 2

# CONCLUSIONS AND RECOMMENDATIONS

The primary purpose of this study was to determine which boiler operational variables play the most significant part in boiler Destruction and Removal Efficiencies (DRE's). The study determined that within the pilot-scale unit the use of water walls and the variation of excess air were significant, and that there appeared to be an optimal excess air rate. The study also demonstrated that operational variables could change DRE's by two to three orders of magnitude. Further experimental work should be carried out to verify some of the findings. The modeling results should be applied to full-scale units to estimate their applicability to permitting.

## 2.1 CONCLUSIONS

- Of the variables studied, the order of influence on DRE is: water walls > compound ≥ excess air > firing rate > flame shape. The order of influence on temperature profiles is: water wall > excess air > firing rate > compound = flame shape.

- Except for waste composition, the influence of operational variables on DRE corresponds to the influence on temperature

- From comparison of DRE with high-heat extraction and low-heat extraction in the combustor, it is concluded that in-flame destruction accounts for only about 90 to 99 percent of the DRE. The remaining destruction must be achieved from postflame thermal oxidation and decomposition.

- Residence time within the flame is insufficient to destroy both Principal Organic Hazardous Constituents (POHC's) and Products of Incomplete Combustion (PIC's). Without sufficient postflame time and temperature, the quantity of PIC's passing out of the boiler will be significant.

- This program clearly demonstrated the effect of compound selection on DRE. Of the four POHC's used in this test program, carbon tetrachloride was the most refractory compound. Chloroform and 1,2-dichloroethane were equal in destructability. Chlorobenzene was the easiest compound to destroy.

- For this test program, maximum DRE was achieved in the excess air region of 20 to 50 percent

- Reduced DRE was primarily caused by material following aerodynamic paths outside of the bulk gas flow

- Carbon monoxide levels showed minimal variations over the range of DRE observed. No relationships between CO and DRE could be established from this data.

- Thermal $NO_x$ appears to show a strong bounding correlation. For a given $NO_x$ level, at each test condition, the DRE will be at least a certain amount.

- Significant PIC's emitted during combustion of chlorinated organics include methylene chloride, ethylene trichloride, perchloroethylene, and the ethylene dichlorides. Suspected but not positively identified PIC's include chloromethane, chloroethane, chloroethylene, and propylene chloride.

- A model capable of predicting within a few degrees the temperature profile within a furnace has been validated. The model can be used to predict within an order of magnitude the destruction efficiency of the modeled furnace.

- The weakest point in the model appears to be the availability of reliable psuedo-first-order empirical global kinetic data for the thermal destruction of a wide range of compounds.

## 2.2 RECOMMENDATIONS

This study showed that certain variables play a major role in determining DRE, and gave insight on underlying physical and chemical mechanisms. Results of the program suggest the following areas of research which need to be addressed:

- The study strongly reinforced the concept that only a fraction of the destruction of a compound is achieved in the flame zone. Verification and quantification of the breakthrough phenomenon is necessary with flames closely approximating full-scale boiler flames.

- In close conjunction with the study of breakthrough of compounds from the flame zone, there should be studies on the formation and destruction of PIC's in both the flame and postflame zones

- The fact that certain compounds appear to be more refractory than others (e.g. carbon tetrachloride) should be applied to testing of potential surrogates (such as sulfur hexafluoride) for establishing boiler and incinerator capabilities

- A key operating criterion that should be considered when using boilers for waste destruction is the placing of upper and lower limits on excess air rates

- The current thermal destruction model should be applied to full-scale boiler data to calibrate empirical approximations and evaluate the level of conservatism

- Further work on obtaining psuedo-first-order empirical global kinetic data would broaden the range of compounds to which the boiler model could be applied

- The optimum excess air region conclusion should be verified on a full-scale unit

- Studies of DRE breakthrough mechanisms and their relative significance should be conducted

# SECTION 3

# TECHNICAL APPROACH AND PROGRAM DESCRIPTION

The technical goal for this program was to gather information to assist in defining operational limits for boilers cofiring hazardous wastes. This was achieved by:

- Defining the magnitude of the effects of controllable operational variables on the thermal environment within a boiler firebox
- Determining destruction efficiencies for known thermal environments (approximating environments in full-scale boilers) for selected compounds
- Refining the simple thermal destruction model as a tool to help quantitate the variables which impact the cofiring of wastes in boilers

The following subsections detail the problem addressed by this program and the technical approach used. The first section explains the basic model and the specific comments which were studied. The second section describes the general approach and the program test matrix. The third section describes the main features of the test facility, while the last two sections outline a typical test and briefly describe the sampling and analysis protocols. Further detail on the facility, sampling train, and organic analysis methodology are provided in the appendices.

## 3.1 MODEL DESCRIPTION

The original model for the destruction of wastes in boilers consisted of two parts, a boiler "time-above-temperature" profile and a compound "time-at-temperature" profile. An example of such a plot is shown in Figure 1. The boiler time-above-temperature profile is a plot of the residence time of gases within the boiler above a given temperature. The period of time the gases exceed a given temperature is plotted on the abscissa and the corresponding temperature is plotted on the ordinate. Time-temperature points to the right and above the plotted line are inaccessible within the boiler under the firing conditions plotted. The compound time-at-temperature plot is the plot of time and temperature requirements to achieve a given destruction efficiency. This plot (the DRE curve) is overlayed on the boiler curve. If any point on the DRE curve lies below and to the left of the boiler curve, then there is a path within the boiler with sufficient time and temperature to achieve the amount of

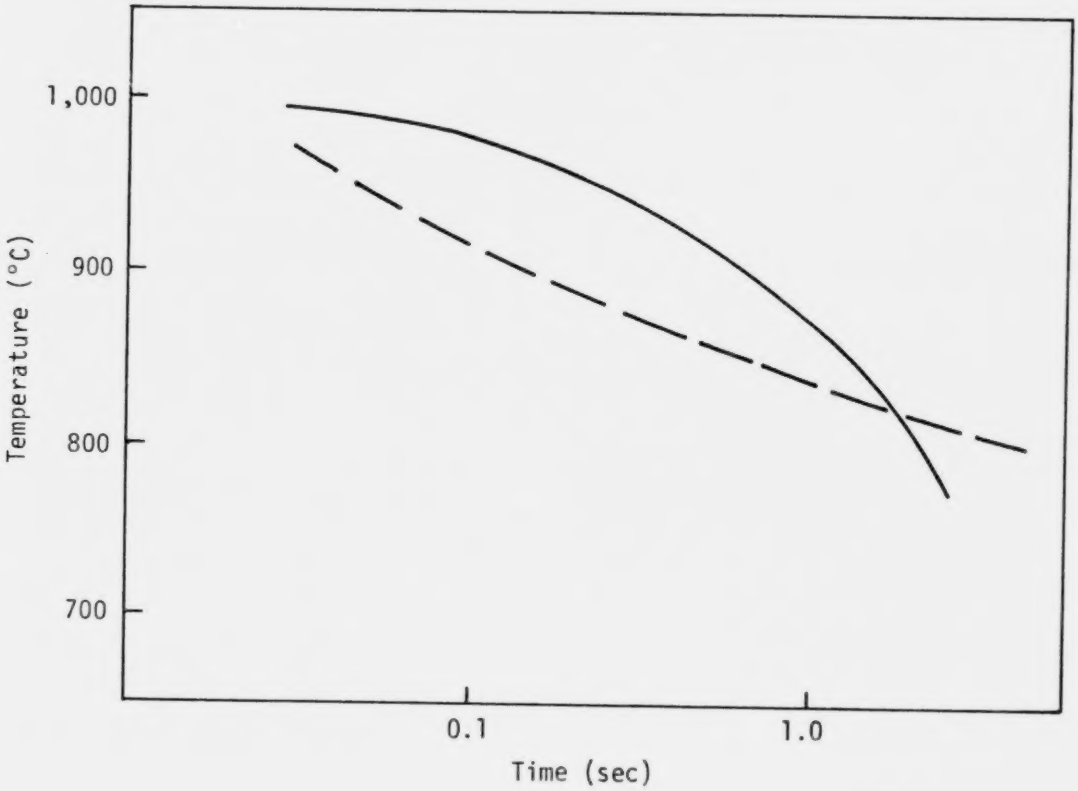

Figure 1. Typical plot of a boiler time-above-temperature curve (solid line) overlain by a compound time-at-temperature curve (dashed line).

destruction for which the compound curve was plotted. However, this only establishes minimum achievable destruction limits; it does not predict destruction rates. To predict DRE one must model the time-temperature history of the compound through the boiler.

The problem with respect to boiler operational variables is to define a sequence of time-temperature paths that are functions of the variables. Such a solution will allow determination of a boiler time-above-temperature curve that will give a reasonable approximation to the worst case path with respect to destruction. The solution used is to divide the boiler into a series of zones and estimate the volume flowrate and temperature in each zone. From this a conservative estimate of destruction can be made. A detailed description of the approach is given in Section 5.6.

## 3.2 GENERAL APPROACH AND TEST MATRIX

The experimental goals of the program, in sequence, were to:

- Determine the furnace operating parameters which affect the furnace three-dimensional time-temperature environment
- Quantify these effects
- Identify the relationships between operating parameters, time-temperature history, and destruction of hazardous waste components in the fuel

The test plan divided the tests into three subsets: a baseline study burning only distillate oil, a single compound study of one hazardous waste compound cofired with distillate oil, and a multiple compound study burning more than one compound simultaneously. The baseline study was designed to define the thermal environment within the facility under the various operating conditions of choice, to define the magnitude of the effects of changes in variables on the thermal environment, and to demonstrate the ability of a simulation to predict the thermal environment resulting from a specific set of variable settings. The single compound studies had two goals: to define the magnitude of variable effects on destruction efficiency; and to define the effects of cofiring wastes on the expected thermal environment. The final, multiple compound studies were to determine the destruction efficiencies of several compounds with known thermal environments.

Within each of these tasks a set of independent variables were identified that are relevant to the operation of incinerators and boilers. The variables studied (both independent and dependent) are shown by task in Table 1. The variables, or parameters, are defined and discussed in the following paragraphs.

TABLE 1. MATRIX OF INDEPENDENT AND DEPENDENT VARIABLES MEASURED BY TASK

| Task | Independent variables | Dependent variables |
|---|---|---|
| Baseline study | Firing rate (load)<br>Flame basket shape (swirl)<br>Excess air rate<br>Waterwall surface area | Temperature profile (measure)<br>Horizontal<br>Vertical<br>Axial<br>Residence time (calculated)<br>Exit gas composition (measured)<br>CO<br>$CO_2$<br>$O_2$<br>THC<br>$NO_x$ |
| Single compound studies | Baseline study variables and waste to fuel ratio | Baseline study variables and destruction efficiencies |
| Multiple compound studies | Baseline study variables and compound composition | Single compound study variables |

### Firing Rate or Load

The firing rate, or furnace load is defined as the mass flow rates of fuel and waste multipled by their heating values. Firing rates ranged from 0.2 to 0.38 megawatts (0.7 to 1.3 million Btu/hr).

### Excess Air Rate or Stoichiometry

This is the air-to-fuel ratio expressed as "excess air", or the percentage of air in excess of that required for stoichiometric combustion of the fuel and waste based on their ultimate analysis. Excess air values in this program ranged from 10 to 50 percent.

### Flame Shape or Burner Swirl Setting

This is the ratio of circumferential to axial momentum applied to combustion air injected around the fuel delivery tube. The swirl setting is arbitrarily defined on a scale of 0 to 8, where 0 corresponds to the smallest axial velocity and 8 corresponds to the largest axial velocity. High swirl flames tend to be short and bushy with large cross sections, while low swirl flames are long and thin. Significant recirculation occurs at high swirl settings (above 6).

### Waterwall Area

Up to six radiant cooling panels can be inserted along the wall of the furnace firebox. These panels can represent up to 7.6 percent of the inside surface area. The walls allow simulation of a range of bulk gas temperatures and thermal boundary layers. During this test program all panels were either in or out.

### Waste Compounds

These are a set of liquid chlorinated wastes representing a range of predicted incinerability. Chlorinated wastes were selected for sensitivity and ease of analysis. There are chloride specific detectors that eliminate interference from other nonchlorinated species. Chlorobenzene was selected for the single compound tests because of its high heat content, compatibility with distillate oil, and simple structure. For the multiple compound tests chlorobenzene was fired with carbon tetrachloride, chloroform, methylene chloride, and dichloroethane.

Table 2 shows the test matrix of nominal operating conditions used in the program. Firing rate and stoichiometry parameter values are listed at nominal conditions based on analysis of the pure distillate oil fuel. As shown, two nominal firing rates (0.2 and 0.38 megawatts) and three nominal stoichiometries (10, 25, and 50 percent excess air) were used. In the data analysis these values (the mass firing rate of the fuel plus waste mixture and the fuel plus waste stoichiometry) were adjusted for the presence of waste compounds in the fuel. The maximum amount of the waste in the fuel was dictated by the necessity of maintaining HCl emission levels below 1,200 ppm

TABLE 2. TEST MATRIX OF VARIABLES AND NOMINAL VALUES

| Variable | Values |
|---|---|
| Firing rate (load) | 0.23, 0.35 ± 0.03 megawatts<br>(0.8, 1.2 ± 0.10 million Btu/hr) |
| Flame shape (swirl) | 7.5, 5.0, 2.0 |
| Excess air rate (stoichiometry) | 10, 25, 50 percent, ±2 percent |
| Waste to fuel ratio | 10, 3, 1.5 percent |
| Waterwall area | 0, 7.6 percent |
| Compounds | 4 |

to prevent undue corrosion of the downstream equipment. The highest concentration of waste to fuel was achieved with chlorobenzene (10 percent v/v). Other materials were injected at levels of approximately 1.5 to 3.5 percent (v/v). Since the waste compound heating value is lower than that of distillate oil, at a given total volume feedrate the firing rate is lower when the waste contribution is considered. Therefore the absolute flowrate was increased to maintain the desired firing rate. Similarly the combustion air flow requirements were changed because of the adjustment in the carbon-to-hydrogen ratio and the hydrogen scavenging by chlorine.

The various nominal firing conditions actually used in the program are identified in Table 3. For run identification, those runs in the baseline studies are prefixed with an "A". The single compound and multiple compound tests are prefixed with a "B" and a "C", respectively. Test series A, the baseline studies, consists of seven runs, all with no waterwalls present. Three swirl settings, two nominal firing rates, and three nominal stoichiometries were considered. Baseline firing conditions (no waste in the fuel) were not repeated with waterwalls in place because it was found that chlorobenzene had no significant effect on the thermal environment. It was believed that firing with chlorobenzene would give the same time temperature history as firing without. Thus work could immediately start on DRE studies. Test series B, the single compound tests, consists of ten runs, seven without waterwalls and three with waterwalls. Two nominal firing rates, three stoichiometries, and two swirl settings were studied. Test series C, the multiple compound tests, included 32 runs, all with waterwalls present in the firebox. It was decided to forego further testing without waterwalls because DRE's were higher than the range of interest and emission levels were near the detection level of the sampling and analytical procedures. A detailed description of each run is given in Table 13 of Section 5.

TABLE 3. NOMINAL INDEPENDENT VARIABLE SETTINGS FOR THE FIRING CONDITIONS TESTED (WASTES FIRED ARE LISTED IN TABLE 22)

| Condition* | Firing rate (million Btu/hr) | Excess air rate (percent) | Swirl setting |
|---|---|---|---|
| I | 0.8 | 10 | 7.5 |
| Ia | 0.8 | 10 | 7.5 |
| II | 0.8 | 25 | 7.5 |
| IIa | 0.8 | 25 | 7.5 |
| III | 0.8 | 50 | 7.5 |
| IIIa | 0.8 | 50 | 7.5 |
| IV | 1.2 | 10 | 7.5 |
| IVa | 1.2 | 10 | 7.5 |
| V | 1.2 | 25 | 7.5 |
| Va | 1.2 | 25 | 7.5 |
| VI | 1.2 | 50 | 7.5 |
| VIa | 1.2 | 50 | 5.5 |
| VII | 0.8 | 25 | 5.0 |
| VIIa | 0.8 | 25 | 5.0 |
| VIII | 0.8 | 25 | 2.0 |
| IX | 1.2 | 25 | 5.0 |

* Conditions followed by an "a" do not have waterwalls; all other conditions have waterwalls.

## 3.3 FACILITY DESCRIPTION

All tests were performed in the Acurex Pilot-Scale Furnace. The furnace has a single burner, front wall fired, into a horizontally oriented firebox. The arrangement and gas flow pattern are shown schematically in Figure 2. The premixed fuel oil/waste mixture is pumped out of drums through a pressure-atomizing nozzle and stabilized at the front wall. The fuel flow is monitored by rotometer. Combustion air is preheated and injected in the annular region around the fuel delivery tube. The IFRF/Acurex burner design allows swirl adjustment by rotating swirl blocks. Air flow is monitored by hot wire anemometer.

The postflame gases travel down the 4.55m (15-ft) by 83.5 cm (33-in.) diameter radiant section tunnel. The walls are refractory lined with optionally mounted waterwalls. Ports along the top and sides of the furnace accommodate ceramic type R thermocouple probes for gas temperature profiles. Type K probes are embedded in the refractory for wall temperature determinations. Thermocouples are also placed at the manifold inlet to and

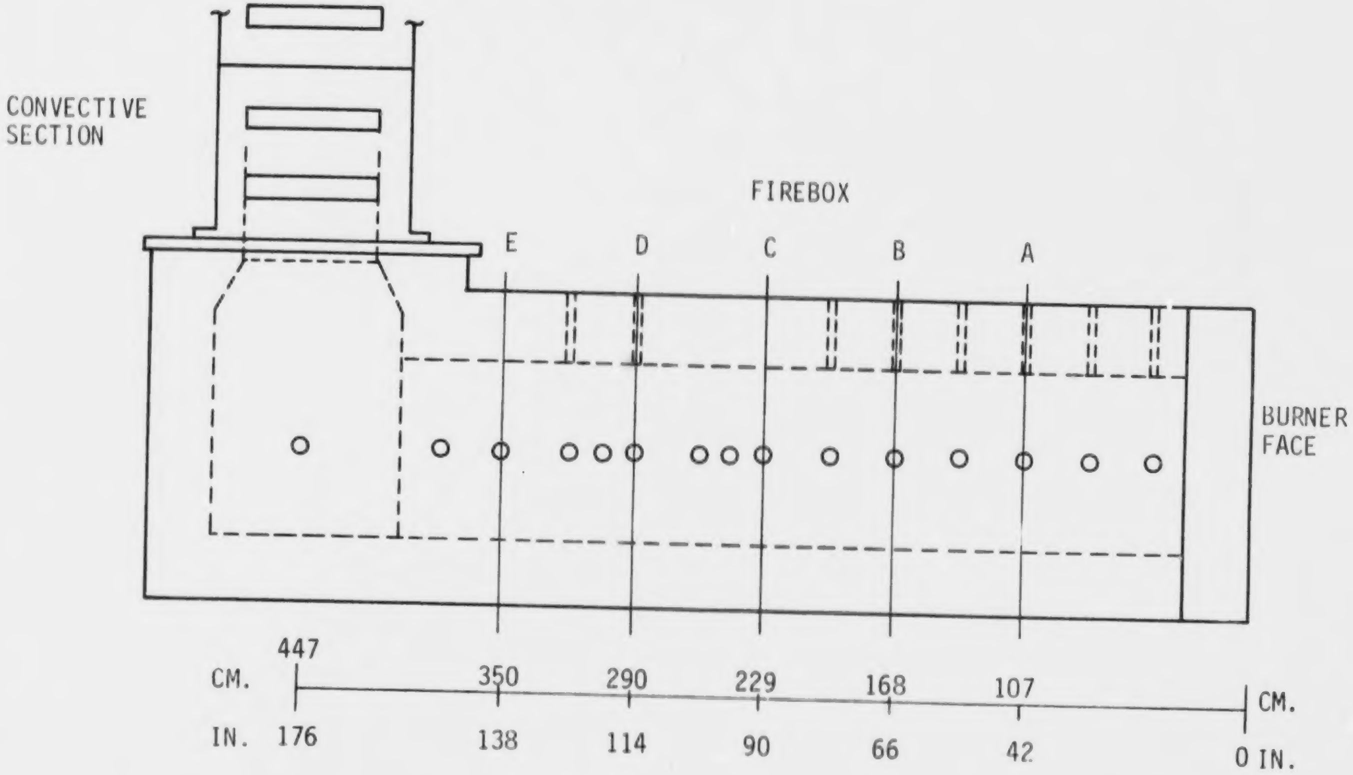
CONVECTIVE SECTION
FIREBOX
E
D
C
B
A
BURNER FACE
CM.
447
350
290
229
168
107
CM.
IN.
176
138
114
90
66
42
0 IN.

Figure 2. Schematic of the Acurex pilot-scale furnace. (Cross sections a through E represent temperature profile locations)

the outlet of each cooling panel, and to and from the burner quarl. Cooling fluid flow measurements are by rotameter.

After traversing the radiant section, the hot gases make a 90° turn and pass upward through the convective section. The U-tube cooling drawer assemblies extract heat from the gas stream as necessary to bring the temperature down to levels that can be handled by the bag house. Downstream of the last tube bank a stainless steel probe extracts gas samples for continuous emissions analysis. Electro-optical analyses are used to define levels of CO, $CO_2$, $O_2$, $NO_x$, and total unburnt hydrocarbon (THC) (Appendix A.5). Samples for the Volatile Organics Sampling Train (VOST) are extracted with a stainless steel probe from the end of an 8-in. diameter 15-ft long duct. The gases are then exhausted to a 45-ft high stack. A detailed description of the facility is given in Appendix A.

## 3.4 TEST DESCRIPTION

A test can be divided into four stages: fuel preparation, furnace heatup, sampling, and analysis. Fuel was prepared by mixing known volumes of waste and distillate oil in clean 55-gal drums. Furnace heatup could occur either from a cold start or a hot start, and involved bringing the furnace walls to a preset temperature (below the expected run temperature) with natural gas firing and then switching to the test fuel until the temperature reached the final run temperature. This heating phase could take from 4 to 16 hr. Sampling was done for the temperature and flow readings and gas samples specified for the program. Analysis encompassed both the prerun preparation and QC of sampling trains and collection media as well as postrun analysis of the collected samples.

Fuel oil-waste mixtures were usually prepared at least 24 hours in advance. A metered volume of oil was placed in a 55-gal drum, followed by the requisite volume of pure technical grade (>99 percent) waste. The oil was subjected to analysis (see Appendix B), while the "waste" of interest was pure technical ultimate and proximate analyses (see Appendix B). The precise waste content was later back-calculated from fuel chloride analysis.

As discussed in Appendix B, consistency of heatup procedures was very important. Because radiative heat loss through the refractory walls plays such a large role in the heat balance of the furnace, it was imperative that the start of each run be from a fixed temperature point. Thus, wall temperature was used as the start point in each case. When the wall temperature reached the specified starting temperature, the fuel was switched from gas to the fuel/waste mixture to be used for the sample. Otherwise, the firing rate on gas was increased until the desired temperature was reached. The furnace was allowed to operate at the desired firing conditions for 4 hr before sampling was started.

Three VOST samples, one HCl sample, and all temperature, pressure, and flow measurements were made for each run. Each VOST sample was usually extracted for 20 min at a flowrate of 200 mL/min. However, some samples were taken for shorter or longer periods when expected concentration levels of

PHOC's in the emissions were not known. In this manner, the amount of PHOC on a trap could be adjusted to maximize the confidence in the analysis. The HCl sampling train was usually run for 30 min at a rate of 1 $ft^3$/min to collect a total volume of 30 $ft^3$. This train was also used for the moisture determination. Fuel samples for total chloride analyisis were drawn during this period.

Analysis was conducted on the Tenax traps from the VOST for volatile chlorinated organics. In each case, procedures were optimized to identify and quantify PHOC's; information about PIC's was secondary. That is to say, in the effort to maximize the precision and quantity of data on the fired PHOC's, only cursory efforts were made to identify and quantify other chlorinated organics that might have been emitted. Section 6.5 describes these findings.

## 3.5 SAMPLING AND ANALYSIS PROTOCOLS

### 3.5.1 Sampling

The VOST protocol was in a major state of change during the beginnings of this program. This is reflected in the use of two different train configurations during the program. The sampling train used during the B series of tests is schematically presented in Figure 3. A later VOST configuration (using a second Tenax® trap downstream from the condensate trap) was used for the C series. Basically, samples were pumped from the furnace exhaust gas stream (at temperatures of 200°C ±50°C) through a heat traced teflon sampling line designed to keep the gases above their dew point temperature. The gases were then passed downward through a condenser into an impinger train, and then through the monitoring and pumping equipment. Each sample was taken nominally at 200 ml/min for 20 min. Total volume sampled was measured with a dry gas meter. A separate train was used to collect HCl using an impinger partially filled with 0.1 M NaOH solution. Three Tenax trap samples for organics and one HCl train sample were taken for each run. In the single compound tests, runs B-4 and B-5 were replicate conditions. Runs C-2 and C-3 were replicates as were runs C-4 and C-5 in the multiple compound series of tests.

### 3.5.2 Analytical Procedures

To analyze for volatile organic species, the Tenax trap was thermally desorbed directly onto the head of a gas chromatographic column with nitrogen at 200°C. The column, a 6-ft SP-1000 Carbopak, was held at 60°C. After desorption for 2 min, the analysis was begun by temperature programming the column for 5 min at 60°C then increasing temperature at 20°/min to 220°C and held for 20 min. Chlorinated species were detected and quantitated with a Hall conductivity detector. Species were identified by relative retention time against an internal standard of bromobenzene injected upstream of the Tenax trap prior to desorption. Quantitation was by relative response factors. Each day of analysis, a column blank, a directly injected standard, a trap blank, and a trap injected standard were run. Each trap was subjected to QC procedures to verify that it was clean to less than 10 ng total chromatographable hydrocarbons by FID prior to use.

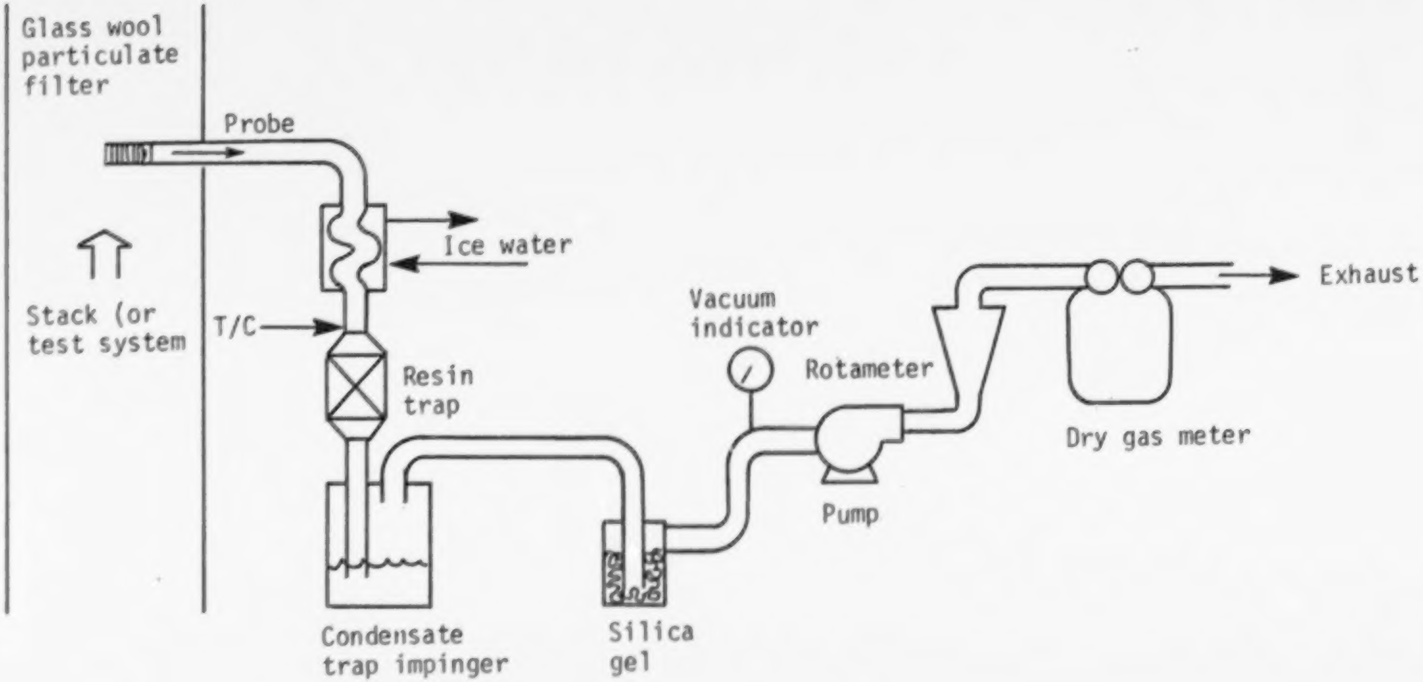
Glass wool
particulate
filter
Probe
Ice water
Stack (or
test system
T/C
Resin
trap
Condensate
trap impinger
Silica
gel
Vacuum
indicator
Rotameter
Pump
Dry gas meter
Exhaust

Figure 3. Schematic of sampling train used for the B series of tests.

# SECTION 4

# RESULTS AND DISCUSSION

## 4.1 SUMMARY OF TESTS

A summary of test runs is given in Table 4. The conditions, given in Roman numerals, are summarized in Table 3. Baseline runs were conducted to establish background conditions without waste firing, and were not sampled for specific organic emissions. Runs with approximately 10 percent (v/v) chlorobenzene in the fuel are called single compound runs. Multiple compounds runs usually contained approximately 3.8 percent chlorobenzene and about 1.5 percent of carbon tetrachloride, chloroform, or 1,2-dichloroethane.

## 4.2 SUMMARY OF DRE RESULTS

A summary of destruction and removal efficiencies (DRE's) for all runs is given in Table 5. The values are percent DRE and are averages for several data points. DRE's were calculated from the data in Table 6, which gives the average penetration value, $C/C_o$, (mass of waste out per unit time/mass rate of waste in), the value of one standard deviation, and (in parentheses) the number of data points. The relationship is: $DRE = 1-C/C_o$. The effects of the various firing conditions on DRE's are discussed in the following sections. A semiquantitative summary on the variable effects is given in Table 7. These values are rough estimates of the difference between either temperature or DRE for two runs where only the specified parameter was varied. For example, a change in firing rate between 0.8 million Btu/hr and 1.2 million Btu/hr changed the temperature profile by about 110°C (200°F). The corresponding change in DRE was about a factor of three.

## 4.3 PARAMETER EFFECTS

For each firing condition, radial temperature profiles were measured at five cross sections (locations A through E shown in Figure 4). During the first several runs about 120 individual temperature points were measured. After establishing the reproducibility of the individual location temperatures, the number of points measured per run was reduced to 40. The reproducibility of the temperature measurements is presented in Table 8. The following sections detail the effects of each of the variables on temperature profiles and DRE's.

TABLE 4. SUMMARY OF RUNS

| Run No. | Condition* | Waste (vol %) |
|---|---|---|
| Baseline | | |
| A-1 | IIa (0.8, 25, 7.5, 0) | None |
| A-2 | VIIa (0.8, 25, 5.0, 0) | |
| A-3 | VIIIa (0.8, 25, 2.0, 0) | |
| A-4 | Ia (0.8, 10, 7.5, 0) | |
| A-5 | Va (1.2, 25, 7.5, 0) | |
| A-6 | Va (1.2, 25, 7.5, 0) | |
| A-7 | IVa (1.2, 10, 7.5, 0) | |
| Single Compound | | |
| B-1 | IIIa (0.8, 50, 7.5, 0) | Chlorobenzene, 10% |
| B-2 | IIa (0.8, 25, 7.5, 0) | |
| B-3 | IIa (0.8, 25, 7.5, 0) | |
| B-4 | Ia (0.8, 10, 7.5, 0) | |
| B-5 | Ia (0.8, 10, 7.5, 0) | |
| B-6 | Va (1.2, 25, 7.5, 0) | |
| B-7 | VIa (1.2, 50, 5.5, 0) | |
| B-8 | II (0.8, 25, 7.5, 0) | |
| B-9 | I (0.8, 10, 7.5, 8) | |
| B-10 | V (1.2, 25, 7.5, 8) | |
| Multiple Compound | | |
| C-1 | III (0.8, 50, 7.5, 8) | Chlorobenzene, 3.6%; Carbon tetrachloride, 1.4% |
| C-2 | II (0.8, 25, 7.5, 8) | |
| C-3 | II (0.8, 25, 7.5, 8) | |
| C-4 | I (0.8, 10, 7.5, 8) | |
| C-5 | I (0.8, 10, 7.5, 8) | |
| C-6 | VII (0.8, 25, 5.0, 8) | |
| C-7 | VI (1.2, 50, 7.5, 8) | |
| C-8 | V (1.2, 25, 7.5, 8) | |
| | IV (1.2, 10, 7.5, 8) | |
| C-10 | IX (1.2, 25, 5.0, 8) | |

(continued)

*Firing rate in million Btu/hr, percent excess air, swirl setting, percent waterwall surface area.

TABLE 4. Concluded

| Run No. | Condition* | Waste (vol %) |
|---|---|---|
| Multiple Compound (Concluded) | | |
| C-11 | III (0.8, 50, 7.5, 8) | Chlorobenzene, 3.8%; |
| C-12 | II (0.8, 25, 7.5, 8) | Chloroform, 1.5% |
| C-13 | I (0.8, 10, 7.5, 8) | |
| C-14 | VI (1.2, 50, 7.5, 8) | |
| C-15 | V (1.2, 25, 7.5, 8) | |
| C-16 | IV (1.2, 10, 7.5, 8) | |
| C-21 | III (0.8, 50, 7.5, 8) | Chlorobenzene, 3.8%; |
| C-22 | II (0.8, 25, 7.5, 8) | 1,2-Dichloroethane, 3.8% |
| C-23 | I (0.8, 10, 7.5, 8) | |
| C-24 | VI (1.2, 50, 7.5, 8) | |
| C-25 | V (1.2, 25, 7.5, 8) | |
| C-26 | II (0.8,250, 7.5, 8) | Carbon Tetrachloride, 1.7%; |
| C-27 | I (0.8, 10, 7.5, 8) | Chloroform, 1.7%;<br>and Methylene Chloride, 1.7% |

*Firing rate in million Btu/hr, percent excess air, swirl setting, percent waterwall surface area.

TABLE 5. SUMMARY OF DESTRUCTION AND REMOVAL EFFICIENCIES

| Condition* | | Chlorobenzene | Carbon tetrachloride | Chloroform | 1,2 Dichloro-ethane |
|---|---|---|---|---|---|
| Ia[†] | (0.8, 50, 7.5, 0) | 99.9996 | --[‡] | -- | -- |
| IIa | (0.8, 25, 7.5, 0) | 99.9999† | -- | -- | -- |
| IIIa | (0.8, 50, 7.5, 0) | 99.9999† | -- | -- | -- |
| IVa | (1.2, 10, 7.5, 0) | 99.9999† | -- | -- | -- |
| Va | (1.2, 25, 7.5, 0) | 99.9999† | -- | -- | -- |
| VIa | (1.2, 50, 7.5, 0) | 99.9999† | -- | -- | -- |
| I | (0.8, 10, 7.5, 8) | 99.986 | 99.9984 | 99.9984 | 99.9995 |
| II | (0.8, 25, 7.5, 8) | 99.9986 | 99.9950 | 99.9974 | 99.9999 |
| III | (0.8, 50, 7.5, 8) | 99.9911 | 99.979 | 99.9980 | 99.9999 |
| IV | (1.2, 10, 7.5, 8) | 99.9940 | 99.988 | 99.9968 | -- |
| V | (1.2, 25, 7.5, 8) | 99.9996 | 99.9975 | 99.9912 | -- |
| VI | (1.2, 50, 7.5, 8) | 99.9947 | 99.9921 | 99.989 | 99.9992 |
| VII | (0.8, 25, 5.0, 8) | -- | 99.9937 | -- | -- |
| IX | (1.2, 25, 5.0, 8) | 99.9998 | 99.985 | -- | -- |

*Firing rate in million Btu/hr, percent excess air, swirl setting, percent waterwall surface area.

[†] Conditions followed by an "a" do not have waterwalls; all other conditions have waterwalls.

[‡] -- Not tested.

## TABLE 6. AVERAGE FRACTIONAL BREAKTHROUGH $C/C_0$ FOR EACH WASTE AND FIRING CONDITION

| Condition | | Chlorobenzene*,† | Carbon tetrachloride | Chloroform | 1,2 Dichloroethane |
|---|---|---|---|---|---|
| I‡ | (0.8, 10, 7.5, 8) | $1.4 \pm 0.1 \times 10^{-4}$ (4) | $1.6 \pm 0.2 \times 10^{-4}$ (2) | $1.6 \pm 0.2 \times 10^{-5}$ (3) | $5 \pm 2 \times 10^{-6}$ (3) |
| Ia§ | (0.8, 10, 7.5, 0) | $4.2 \times 10^{-6}$ (1) | --‖ | -- | -- |
| II | (0.8, 25, 7.5, 8) | $1.4 \pm 0.3 \times 10^{-5}$ (4) | $5 \pm 3 \times 10^{-5}$ (5) | $2.6 \pm 2 \times 10^{-5}$ (5) | $1 \pm 0.5 \times 10^{-6}$ (2) |
| IIa | (0.8, 25, 7.5, 0) | $4 \pm 3 \times 10^{-7}$ (6) | -- | -- | -- |
| III | (0.8, 50, 7.5, 8) | $8.9 \pm 6 \times 10^{-5}$ (5) | $2.1 \times 10^{-4}$ (1) | $2.0 \pm 0.8 \times 10^{-5}$ (3) | $1 \pm 0.2 \times 10^{-6}$ (3) |
| IIIa | (0.8, 50, 7.5, 0) | $2.5 \pm 2 \times 10^{-7}$ (3) | -- | -- | -- |
| IV | (1.2, 10, 7.5, 8) | $6 \pm 8 \times 10^{-5}$ (5) | $1.2 \pm 0.3 \times 10^{-4}$ (2) | $3.2 \pm 0.5 \times 10^{-5}$ (3) | -- |
| IVa | (1.2, 10, 7.5, 0) | $2.2 \pm 0.5 \times 10^{-7}$ (3) | -- | -- | -- |
| V | (1.2, 25, 7.5, 8) | $4.5 \pm 2 \times 10^{-6}$ (5) | $2.5 \pm 1 \times 10^{-5}$ (2) | $8.8 \pm 2 \times 10^{-5}$ (3) | -- |
| Va | (1.2, 25, 7.5, 0) | $0.5 \pm 0.3 \times 10^{-7}$ (3) | -- | -- | -- |
| VI | (1.2, 50, 7.5, 8) | $5.5 \pm 2 \times 10^{-5}$ (4) | $7.9 \pm 6 \times 10^{-5}$ (3) | $1.1 \pm 0.02 \times 10^{-4}$ (2) | $8 \pm 4 \times 10^{-6}$ (2) |
| VIa | (1.2, 50, 7.5, 0) | $3.4 \pm 0.7 \times 10^{-7}$ (3) | -- | -- | -- |
| VII | (0.8, 25, 5.0, 8) | -- | $6.3 \pm 3 \times 10^{-5}$ (3) | -- | -- |
| IX | (1.2, 25, 5.0, 8) | $2.0 \pm 0.5 \times 10^{-6}$ (3) | $1.5 \pm 0.3 \times 10^{-4}$ (3) | -- | -- |

* ± represents 1 standard deviation from average.
† ( ) indicates number of valid data points.
‡ See Table 3 for run conditions.
§ Run conditions suffixed with an "a" are without waterwalls. All other conditions are with waterwalls in place.
‖ Not tested under that condition.

TABLE 7. SEMIQUANTITATIVE ESTIMATION OF THE EFFECTS OF THE INDEPENDENT VARIABLES ON TEMPERATURE PROFILE AND DRE

| Variable | Range of temperature changes °C (±°F) | Range of DRE changes (Factor)* |
|---|---|---|
| Waterwalls | 275 (500) | 100 |
| Excess air rate | 165 (300) | 10 |
| Firing rate | 110 (200) | 3 |
| Burner swirl | 30 (50) | 1 |
| Compound | 30 (50) | 20 |

*$C/C_0$ is mass rate of waste out divided by mass rate of waste in.

TABLE 8. REPRODUCIBILITY OF TEMPERATURE MEASUREMENTS AT FOUR SELECTED POINTS WITHIN THE PILOT-SCALE FURNACE*

|  | Number of points | Average difference °C (°F) | Standard deviation °C (°F) |
|---|---|---|---|
| Within run (with waterwalls) | 40 | 10 (18) | 6 (10) |
| Within run (without waterwalls) | 48 | 7 (13) | 4 (7) |
| Between all runs | 40 | 29 (53) | 17 (30) |

*The points are at 8 and 12 in. from the wall and at cross sections C-3 and E-2.

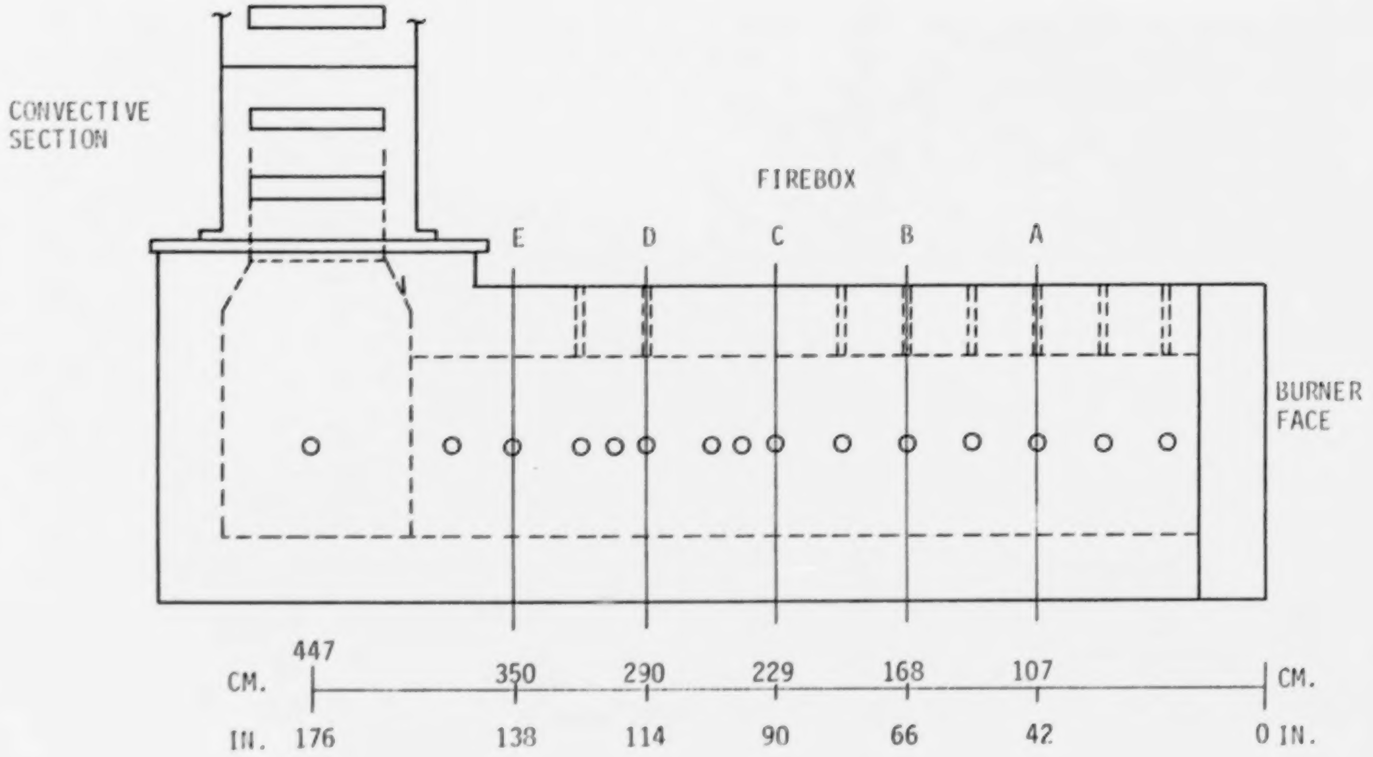
CONVECTIVE SECTION
FIREBOX
E
D
C
B
A
BURNER FACE
447
CM.
350
290
229
168
107
CM.
IN.
176
138
114
90
66
42
0 IN.

Figure 4. Simplified schematic of the pilot-scale furnace showing location of temperature profile cross sections.

### 4.3.1 Time-Temperature Profiles

A typical set of cross sectional profiles is shown in Figure 5 for firing condition Ia. These profiles clearly show a thermal boundary layer within four inches of the furnace wall. (A description of the various firing conditions is given in Section 3, Table 3.) This boundary layer is significant, since it represents greater than 40 percent of the volume or thermal environment of the furnace. Because temperature and velocity are the dominant factors in volume flowrate and destruction, this zone will be significant when considering destruction efficiencies in this furnace.

Axial temperature profiles were measured at several radial distances from the centerline of the furnace are shown in Figure 6. Centerline axial temperature profiles for four firing conditions without waterwalls are shown in Figure 7. The profiles for the same conditions but without waterwalls are shown in Figure 8. These figures demonstrate the range of thermal environments achieved during this study. Centerline temperatures at the first measured cross section (B-4) ranged over 400°C (700°F), while temperatures at the exit from the furnace box (cross section F-1) ranged over 825°C (1,500°F). Mean residence times ranged from 3 to 6 sec and heat release rates in the flame zone ranged from approximately 140,000 to 220,000 Btu/ft$^3$. The heat release rates are comparable to those for industrial boilers, but the pilot scale residence times are longer. Residence times in industrial boilers usually range from 0.7 to 2 sec. Residence time in the pilot unit with waterwalls was in the 1 to 2 sec range.

### 4.3.2 Effect of Waterwalls on Thermal Environments and DRE's

Addition of waterwall panels replaced about 8 percent of the refractory surface area but extracted 50 to 60 percent of the heat input (as measured by the rise in temperature of the cooling fluid). An example of the effect of the waterwall on longitudinal temperature profiles is shown in Figure 9. Runs B-2 and B-3, with similar firing conditions, were conducted one month apart. This demonstrates the reproducibility of the thermal history. The waterwall effects can also be seen by comparing the temperature scales on Figures 7 and 8. Not only does the waterwall lower the overall temperature profile, but it also steepens the slope. From heat flow calculations the average waterwall surface temperature is estimated to be 77°C (170°F). This is compatible with the observed condensation on the rear panels, implying that the surface temperature of the panels must range from above to below the flue gas dew point at 55°C (130°F). With the waterwalls in place the thermal environment of the first six feet of the firebox was comparable to a D-type packaged watertube boiler. However, the pilot-scale waterwall surface temperature is much lower than for industrial boilers (600° to 800°F). The effect will be to lower DRE in the pilot unit with respect to an industial boiler through wall quenching. This is offset by the larger industrial boiler waterwall surface area (>50 percent) compared to the pilot unit.

Waterwalls have a dominant effect on DRE. This is shown in Table 6 and in Figure 10. For chlorobenzene DRE varied over two orders of magnitude with the introduction of wall cooling. Qualitatively, this was to be expected

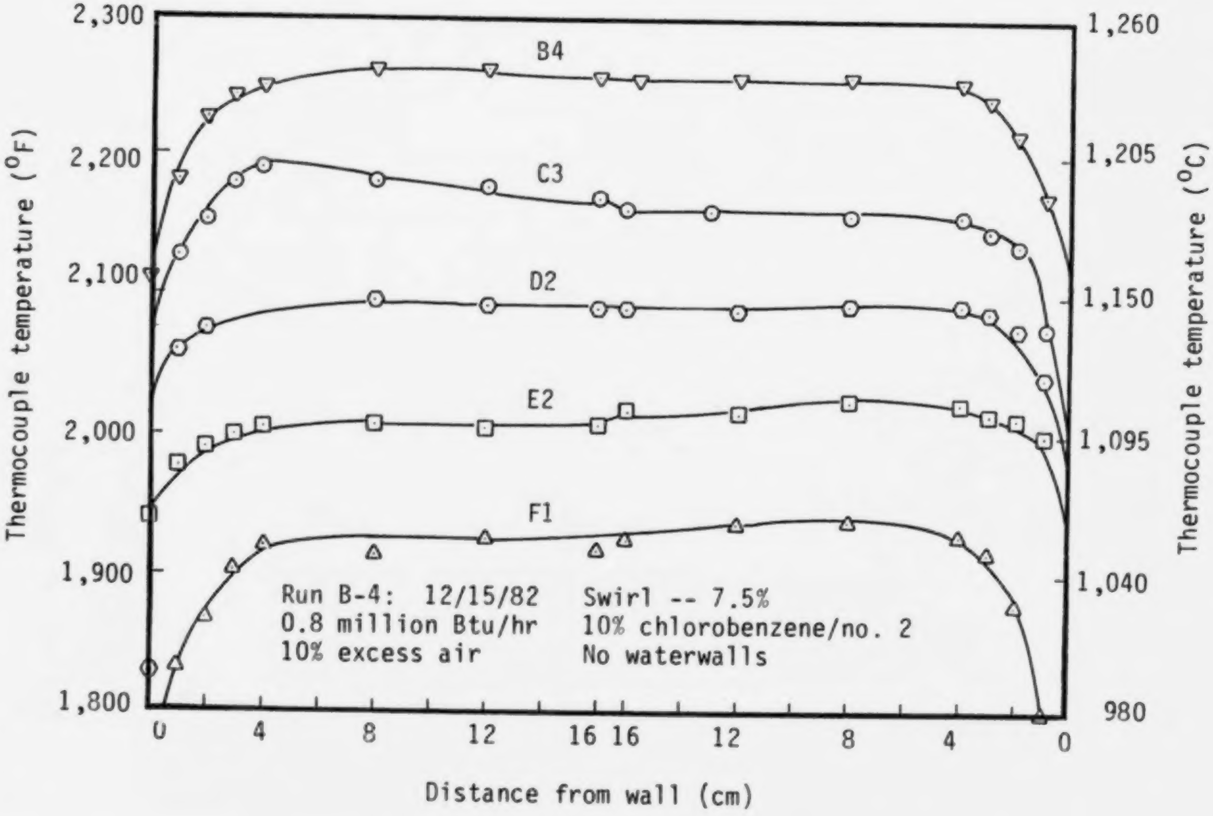

Figure 5. A typical set of cross sectional temperature profiles (Condition Ia, Run A-4).

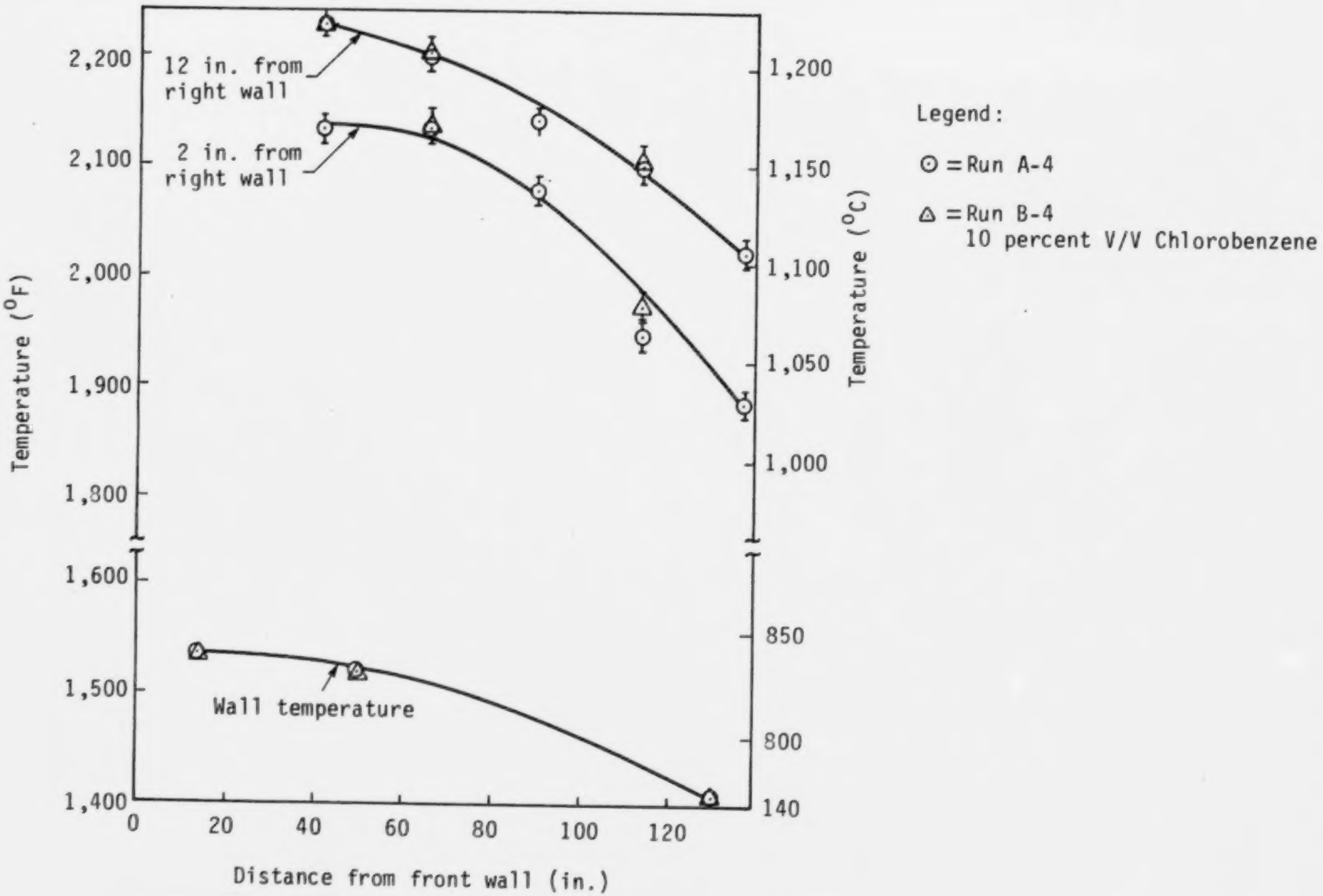

Figure 6. Axial temperature profiles are various radial distances from centerline including refractory wall temperatures.

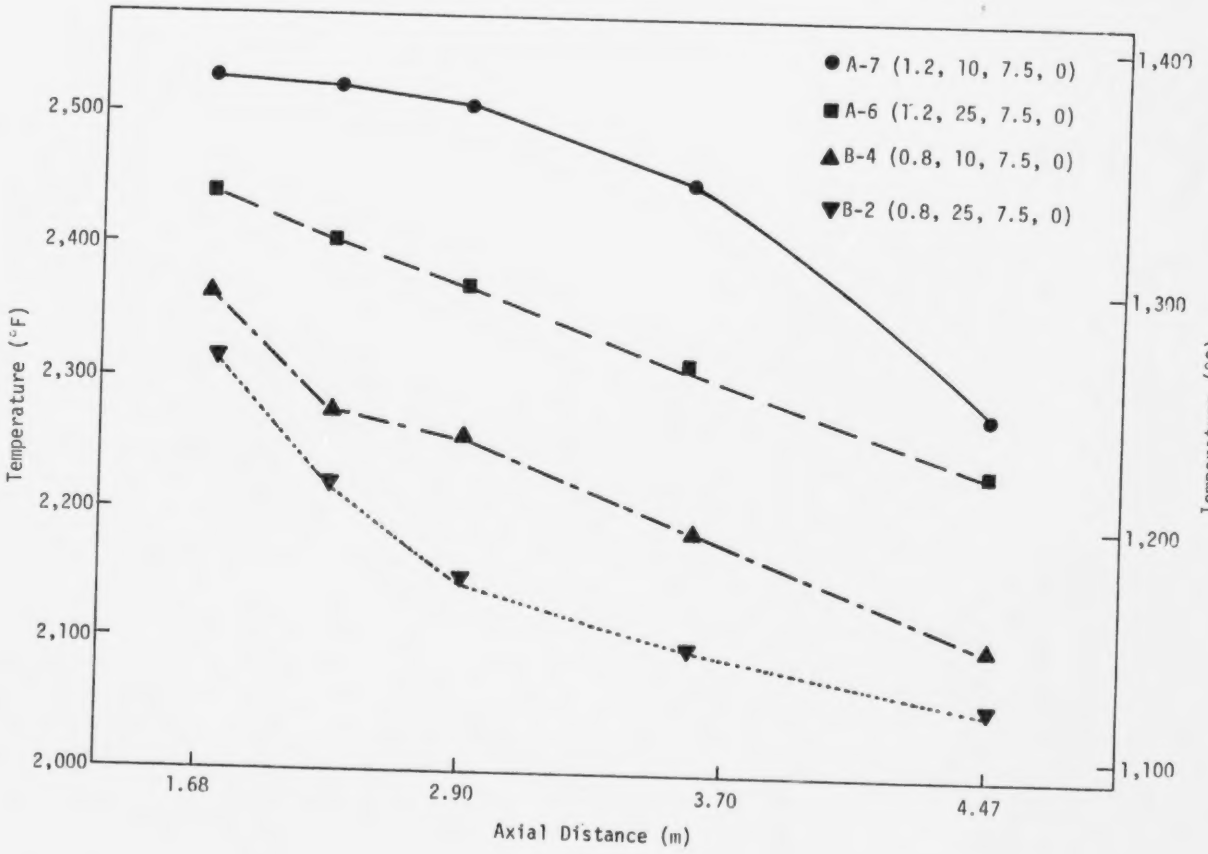

Figure 7. Centerline axial temperature profiles for four firing conditions without waterwalls. The numbers in parentheses are (million Btu/hr being fired, percent excess air, swirl setting, percent water walls).

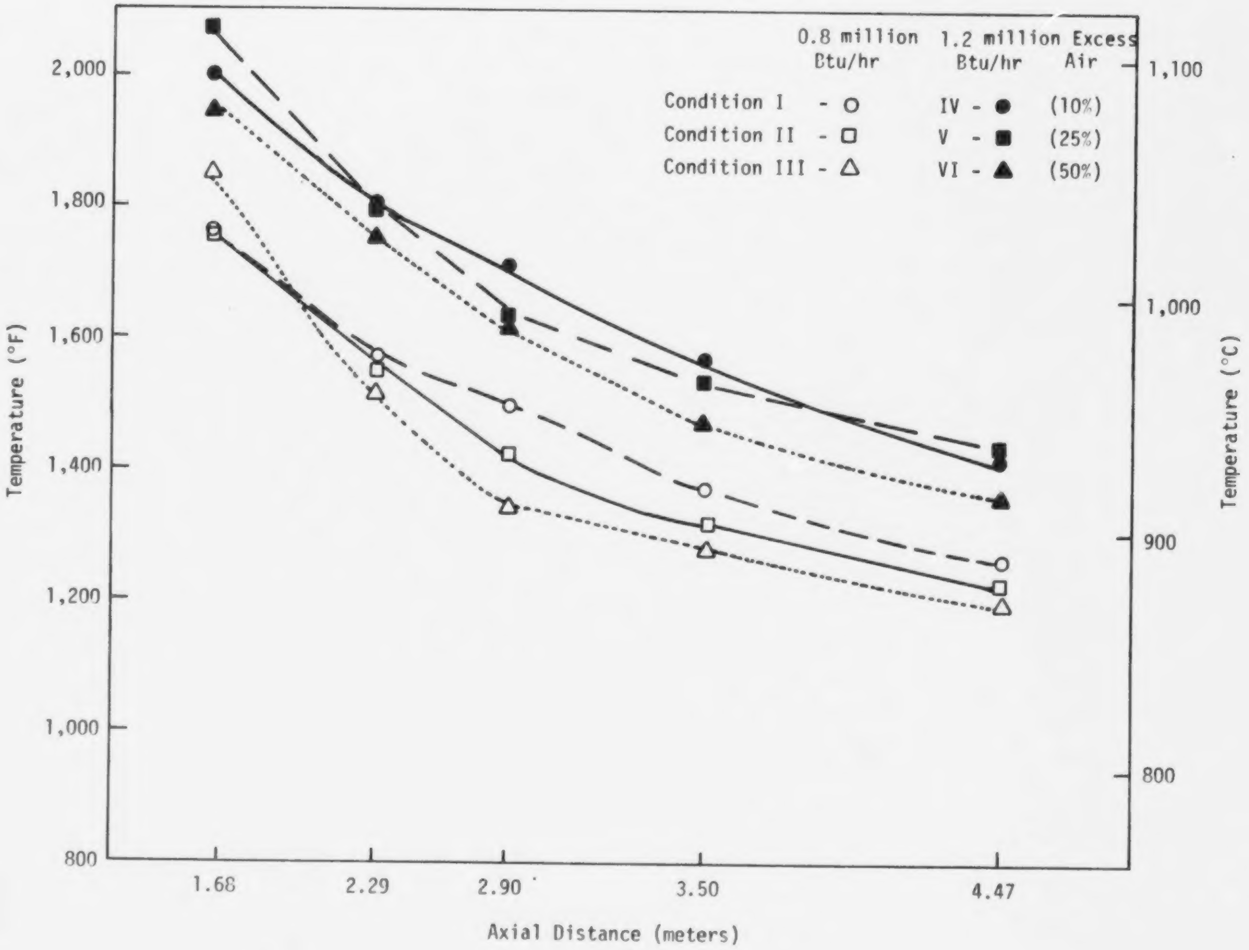

Figure 8. Centerline axial temperature profiles for six firing conditions with waterwalls.

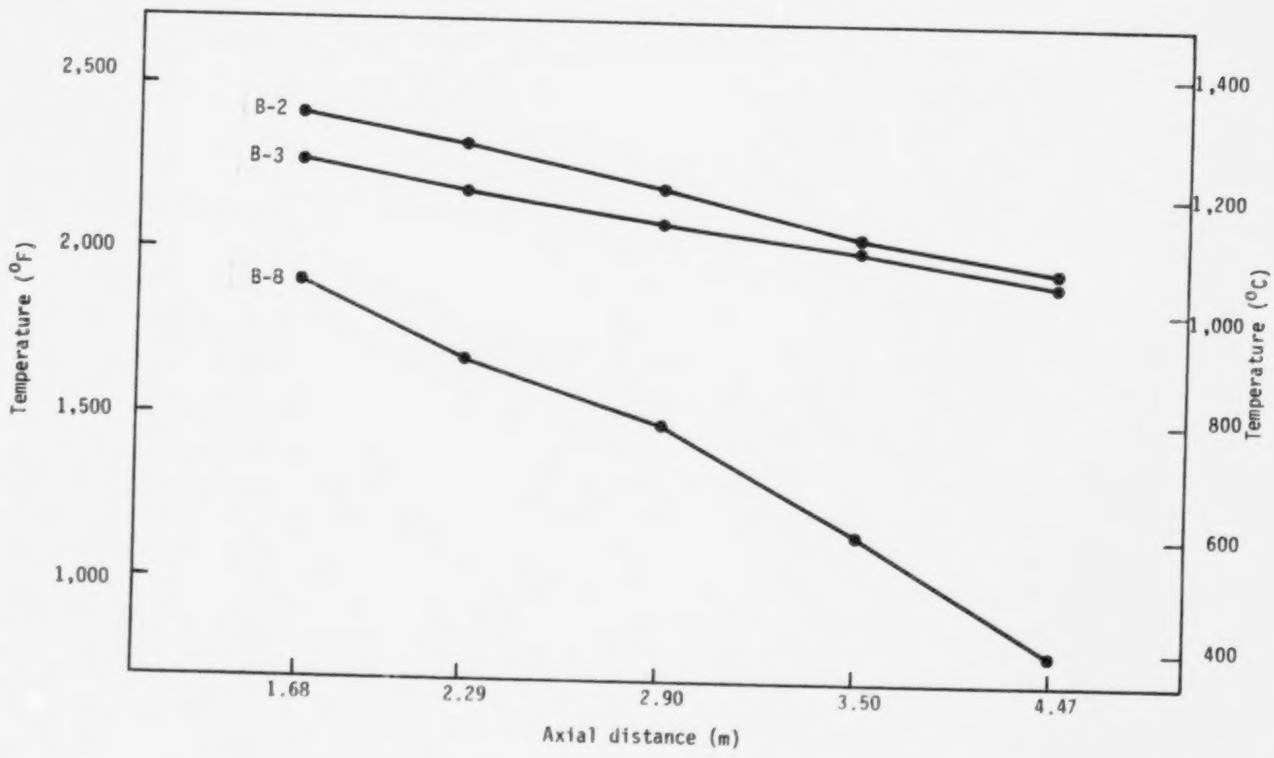

Figure 9. Centerline temperature profiles with (Run B-8) and without waterwalls (Runs B-2 and B-3). Normal conditions were 0.8 million Btu/hr, 25% Excess Air, and Swirl Setting 7.5.

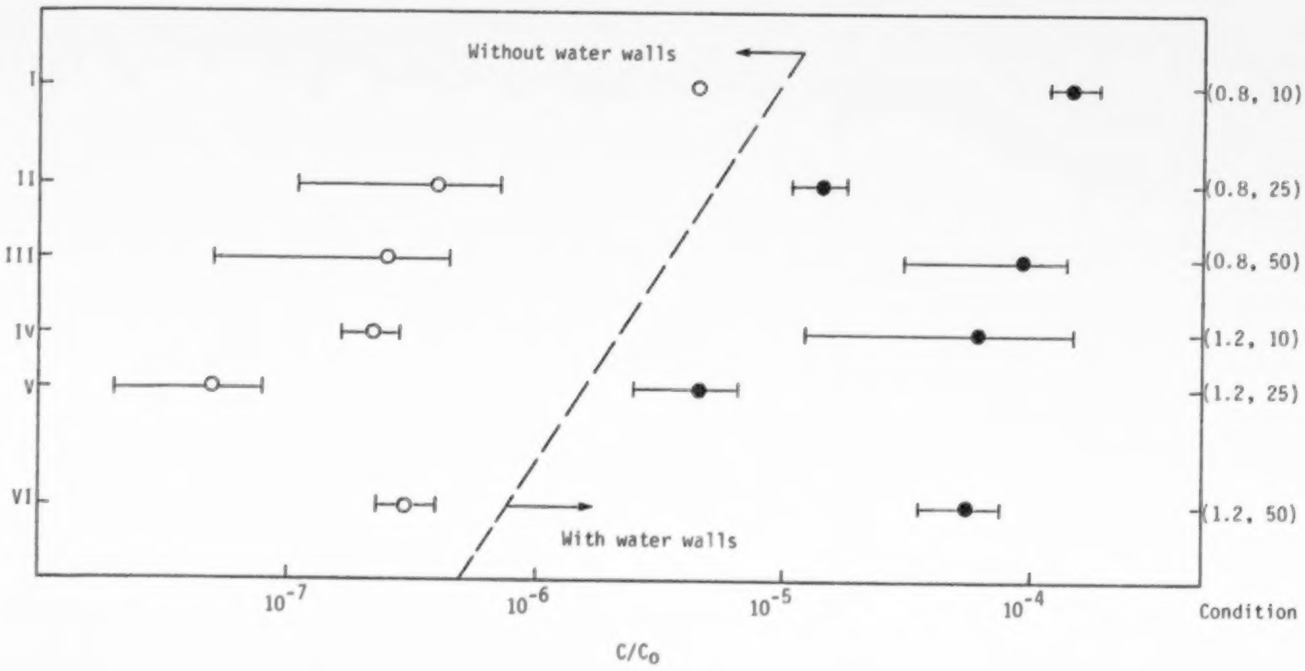

Figure 10. Plot of fractional breakthrough of chlorobenzene versus firing conditions. The numbers in parentheses are (million Btu/hr being fired, percent excess air).

since the waterwalls decreased the corresponding temperature profiles 220 to 280°C (400° to 500°F). Not surprisingly, the magnitude of the effect is within the range predicted by theory. Using the Arrenius expression for a rate constant, $k = A_{exp}\ (-E_a/RT)$, and algebraically manipulating the kinetic expressions to present the ratio of breakthrough fractions for a given waste under two different temperatures, one obtains

$$C_1/C_2 = \exp\ [E_a\ (T_1 - T_2)/RT_1T_2]$$

$C_1$ and $C_2$ are the breakthrough quantities at two different run temperatures (assuming the same feedrate in), $E_a$ is the empirical pseudo first order energy of activation for the disappearance of the waste, R is the appropriate gas constant, and $T_1$ and $T_2$ are the effective temperatures. Using effective temperatures of 1,100 and 1,380K, an activation energy of 50 kilocalories per gram mole, and a gas constant of 1.982 calories per gram mole °K, the calculated ratio of breakthrough quantities is 100.

### 4.3.3 Effect of Excess Air on Temperature Profiles

The effects of excess air on temperature profiles followed expectation. A comparison of Figures 7 and 8 shows effects of excess air on centerline axial temperature profiles for different firing rates. An alternate demonstration is given in Figure 11. Here, radial temperature profiles at two positions are shown for three excess air levels at a nominal 0.8 million Btu/hr firing rate. All three conditions are without waterwalls. On the centerline, gas temperatures vary as much as 140°C (250°F) at cross section C-3 (approximately 80 in. from the burner face) but only approximately 40°C (70°F) at position E-2 (114 in. from the face). The equivalent temperature difference at the higher firing rate of 1.2 million Btu/hr are on the order of 80°C and 25°C (150° and 50°)F), respectively. The lower difference at the higher firing rate is caused by radiative effects from the hotter flame zone radiating into the cooler postflame zone.

Qualitatively these excess air results will have opposing effects on destruction efficiencies. At the higher excess air level the increased oxygen content will promote destruction while the decreased residence time and temperature will suppress destruction. In fact, there appears to be a peak destruction efficiency between excess air rates of 10 and 50 percent. This is shown graphically in Figure 12.

### 4.3.4 Effects of Firing Rates on Thermal Profiles and DRE's

As expected, increasing firing rates increase temperatures. This is clearly demonstrated in Figures 7 and 8. The effect is most clearly illustrated in Figure 8 where temperature profiles for each of two firing rates (0.8 and 1.2 million Btu/hr) are plotted. At cross section C-3 the temperature difference between the two firing rates for a particular excess air rate ranged over 110°C (200°F); near the exit the temperature range was on the order of 80°C (150°F).

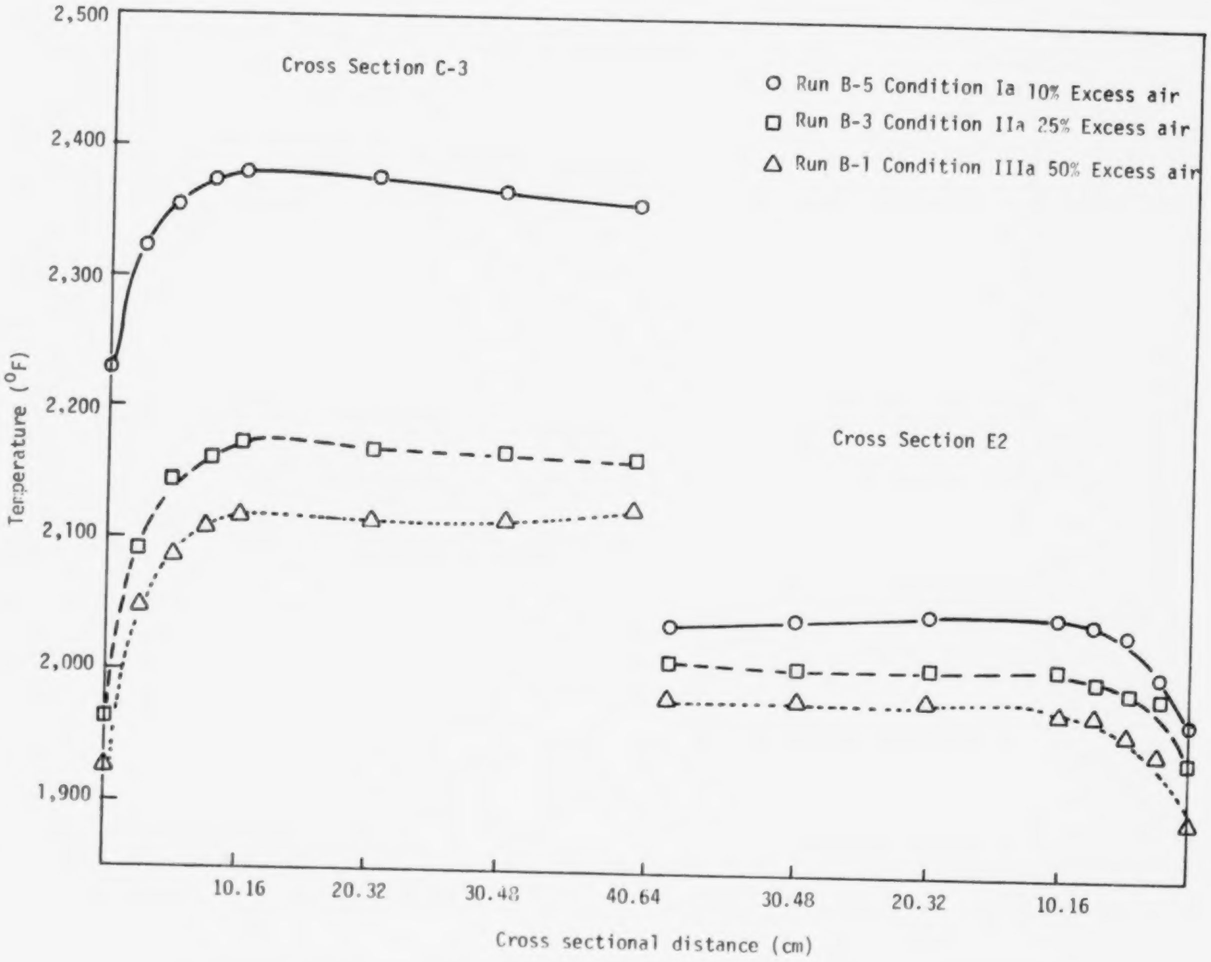

Figure 11. Effects of excess air on temperature for three firing conditions without waterwalls. Normal firing rate is 0.8 million Btu/hr.

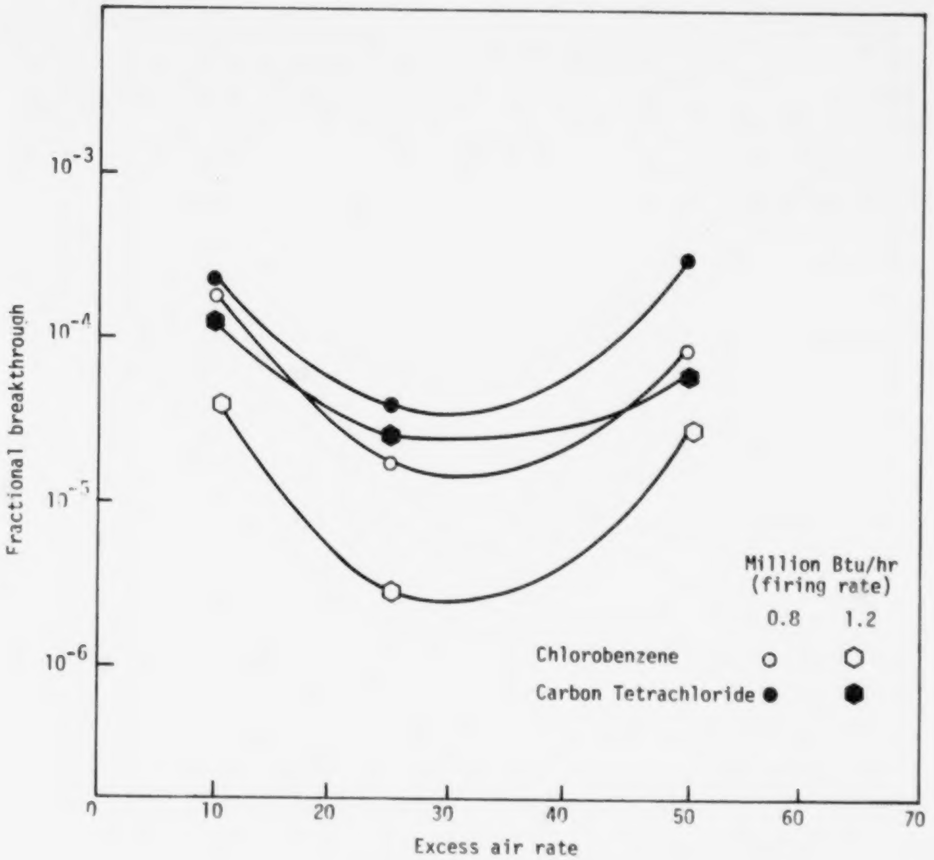

Figure 12. Effect of excess air on fractional breakthrough for carbon tetrachloride and chlorobenzene.

### 4.3.5 Effect of Swirl Setting on Thermal Profiles and DRE's

Burner swirl setting, a measure of the ratio of radial to axial air momentum, has a marked impact on flame shape but only a moderate impact on temperature profile. Figure 13 displays cross sectional temperature profiles for three firing conditions in which swirl was varied. The conditions are a firing rate of 0.8 million Btu/hr, an excess air rate of 25 percent, no waterwalls, and swirl settings of 7.5, 5.0, and 2.5. Swirl settings for this burner can range from 0 to 8. The swirl settings of 7.5 (condition IIa), 5.0 (condition VIIa), and 2.5 (condition VIIIa) represent a short, bushy flame, an intermediate flame, and a long, thin flame, respectively. The flame shape was estimated by visual inspection and empirical values for flame volume. Table 9 shows the visual estimates of flame length and diameter under condition IIa. The calculated flame length using the observed flame diameter for two different geometries is also shown. The flame length is estimated by calculation from the flame diameter because the observation port configuration allowed a much better visual estimate of flame diameter than flame length. The volume of a flame is empirically stated to be about 0.2 $m^3$/MW (11). For simplicity, the flame was approximated as a cylinder.

From the observed profiles in Figure 11, the effect of increased swirl is to increase the temperature gradient. However, the temperature changes only about 15°C (25°F) at the centerline. This is comparable to the measured temperature variance between runs (see Table 6), and is probably not significant.

There may be a significant variation in DRE with changes in swirl setting, but the data are difficult to interpret. No changes could be observed between settings 7.5 and 5.0 for any of the compounds. However, large differences in DRE for both carbon tetrachloride and chlorobenzene were seen between settings 5.0 and 2.0. (The setting 2.0 represents a long, thin flame). But the changes were in the opposite direction for the two compounds, showing increased DRE for chlorobenzene and decreased DRE for carbon tetrachloride.

### 4.3.6 Effect of Waste on Temperature Profiles and DRE's

For baseline condition IIa (nominal firing rate of 0.8 million Btu/hr, 25 percent excess air, swirl setting of 7.5, and no waterwalls) the effect of substituting 10 percent v/v chlorobenzene in the fuel on temperature appears to be within the experimental variance. This is illustrated by comparing the variance from Table 7 to the values in Table 10. This result is not surprising since the heat content of the fuel is 135,000 Btu/gal and that of chlorobenzene is 112,000 Btu/gal. A 10 percent v/v mixture will have a heating value only 1.7 percent less than an equivalent amount of fuel (no. 2 distillate). The accuracy of preparing the fuel/waste mixture is ±4 percent while the accuracy of measuring the feedrate is ±5 percent. The precision of the temperature measurement is 6°C (10°F). The conclusion is that 10 percent chlorobenzene does not significantly affect the thermal profile beyond the flame zone.

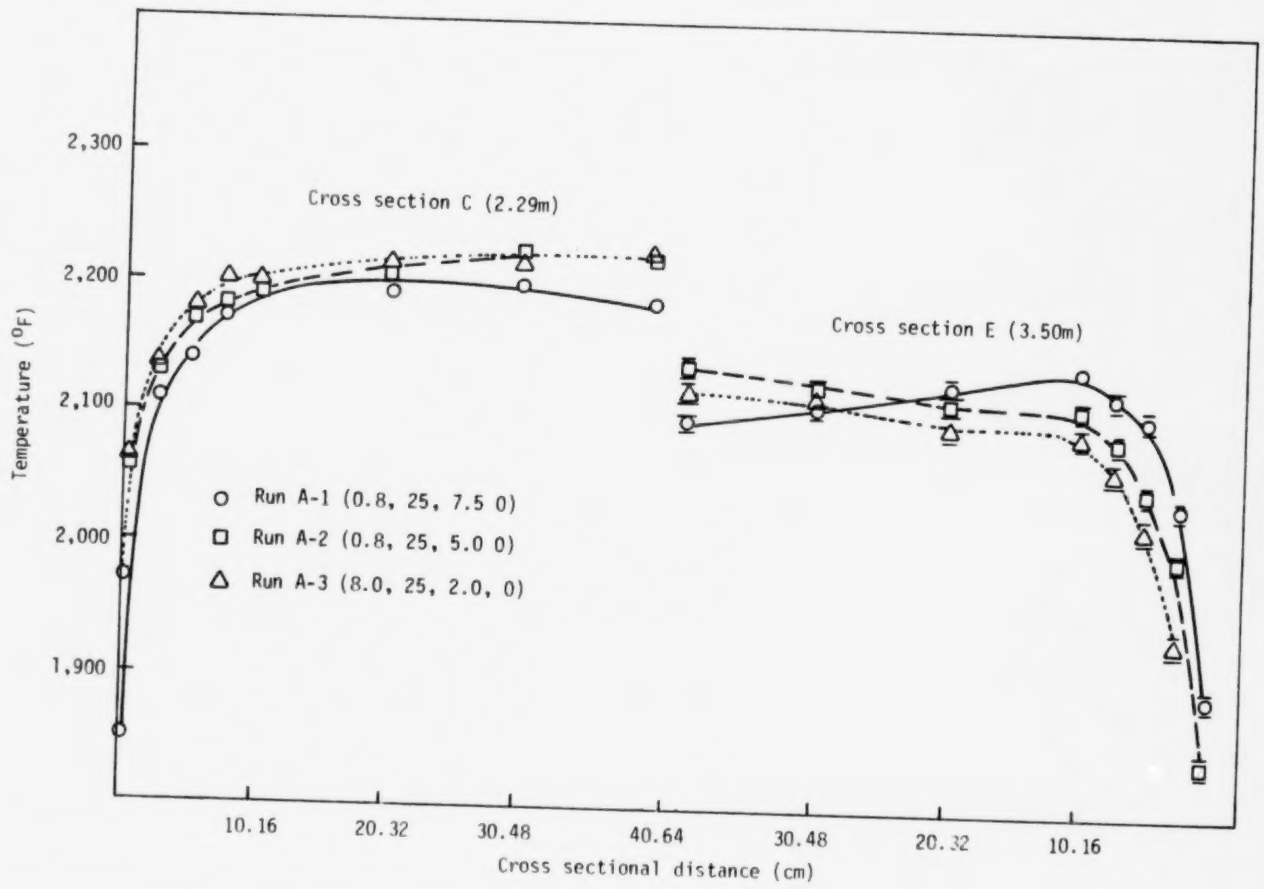

Figure 13. Effect of burner swirl setting on temperature profiles. The conditions are a firing rate of 0.8 million Btu/hr, an excess air rate of 25 percent, no waterwalls, and swirl settings of 7.5, 5.0, and 2.5.

TABLE 9. FLAME GEOMETRY ESTIMATION FOR BASELINE CONDITION IIa

| Swirl setting | Flame diameter (cm) (visual estimate) | Flame length (cm) (visual estimate) | Cylinder flame length (cm) (calculated)*,† | Frustrum flame length (cm) (calculated)*,‡ |
|---|---|---|---|---|
| 7.5 | 75 ± 7 | 16 ± 5 | 11 ± 2 | 18 ± 3 |
| 5 | 50 ± 7 | 50 ± 8 | 25 ± 7 | 43 ± 12 |
| 2.5 | 42 ± 7 | 66 ± 8 | 37 ± 12 | 63 ± 20 |

*Volume = (0.2 $m^3$/million watts) (0.29307 watts/Btu/hr)(0.8 million Btu/hr) = 0.0469 $m^3$.
†Length = $4V/\pi D^2$, where D = flame diameter.
‡Length = $48V/7\pi D^2$, for $D_1 = 2D_2$.

TABLE 10. EFFECT OF 10 PERCENT CHLOROBENZENE ON TEMPERATURE PROFILE FOR FIRING CONITION IV (1.2, 10, 7.5, 0)

| Distance from wall (in.) | Temperature (°F) | | | |
|---|---|---|---|---|
| | Cross-section B-8 | | Cross-section D-2 | |
| | Condition IV | Condition IV (10% waste) | Condition IV | Condition IV (10% waste) |
| 0 | 1,968 | 2,027 | 1,680 | 1,781 |
| 1 | 2,113 | 2,120 | 1,823 | 1,870 |
| 2 | 2,135 | 2,135 | 1,946 | 1,969 |
| 3 | 2,172 | 2,168 | 2,019 | 2,002 |
| 4 | 2,194 | 2,185 | 2,041 | 2,045 |
| 8 | 2,186 | 2,189 | 2,064 | 2,060 |
| 12 | 2,199 | 2,205 | 2,095 | 2,102 |

The same cannot be said for the more heavily chlorinated wastes. Table 11 shows the difference in bulk gas temperature during burning of the various chlorinated wastes. As is to be expected, carbon tetrachloride has a significant effect, depressing the temperature on the order of 25° to 45°C (50° to 80°F). It is interesting to note that there is a reversal in bulk gas temperature between cross sections B and D. This is consistent with a higher rate of heat extraction at higher temperatures resulting in a net lowering of temperature overall (see the modeling discussion in Section 5). The effect of the altered temperature profile on DRE is difficult and separate from the effect of compound structures. It is felt by the authors that compound composition does play a significant role in DRE independent of the effects on temperature profile. This is supported by the work of Dellinger, et al., of the University of Dayton Research Institute and of K. C. Lee of Union Carbide (12).

## 4.4 OTHER DRE CORRELATIONS

There are several other correlations for DRE's that can be examined. Among the most frequently discussed are CO and $NO_x$. It is felt that there should be some correlation between emissions of these species and destruction of POHC's. Since CO can be considered to be the last product of incomplete combustion (PIC), it would be expected that an increase in CO would accompany a decrease in DRE (an increase in POHC breakthrough). Conversely, an increase in $NO_x$ should herald a decrease in POHC breakthrough because nitrogen oxides are favored as temperature and residence time increases.

Attempts to correlate DRE to CO emissions in this test sequence were unsuccessful. The monitored CO levels did not vary significantly over the range of operating conditions achieved during this program. To change CO levels in this unit requires injecting air into the flame region, thus further cooling the furnace, or decreasing the excess air to near sub-stoichiometric levels. From the results previously discussed both procedures should decrease DRE (increase breakthrough fraction of POHC). The ratio $CO/CO_2$ should follow the same pattern, but perhaps be more sensitive. This is because an increase in CO for a given fuel must be at the expense of $CO_2$ formation.

The relationship between $NO_x$ emissions and fractional breakthrough of POHC is shown in Figure 14. There appears to be an upper limit on fractional breakthrough inversely proportional to $NO_x$ level. That is, for a given $NO_x$ level, the ratio of chlorobenzene emitted to the amount fired did not exceed a specified level. This behavior is consistent with theory. Because thermal $NO_x$ production increases exponentially with temperature, as $NO_x$ increases, POHC breakthrough should decrease, as observed.

## 4.5 PRODUCTS OF INCOMPLETE COMBUSTION

In order to maximize the number of variable data points, the analytical design for this program was simplified by not performing GC/MS analyses. This reduced the ability to identify and quantitate PIC's. Because the program was not directed toward PIC's, much raw data (such as the numerous

TABLE 11. EFFECT OF WASTE ON AVERAGE BULK GAS TEMPERATURES FOR FIRING CONDITION II (0.8 MILLION BTU/HR, 25 PERCENT EXCESS AIR, SWIRL SETTING 7.5)

| | | Temperature (°F) | | | |
|---|---|---|---|---|---|
| | | Section B-4 | | Section D-2 | |
| Waste | Run | Average | S.D.* | Average | S.D. |
| Chlorobenzene | B-8 | 1862 | 52 | 1445 | 33 |
| Carbon tetrachloride | C-3 | 1767 | 48 | 1545 | 23 |
| Chloroform | C-12 | 1842 | 48 | 1515 | 32 |
| 1,2 Dichloroethane | C-22 | 1840 | 42 | 1528 | 26 |

*S.D. = Standard deviation.

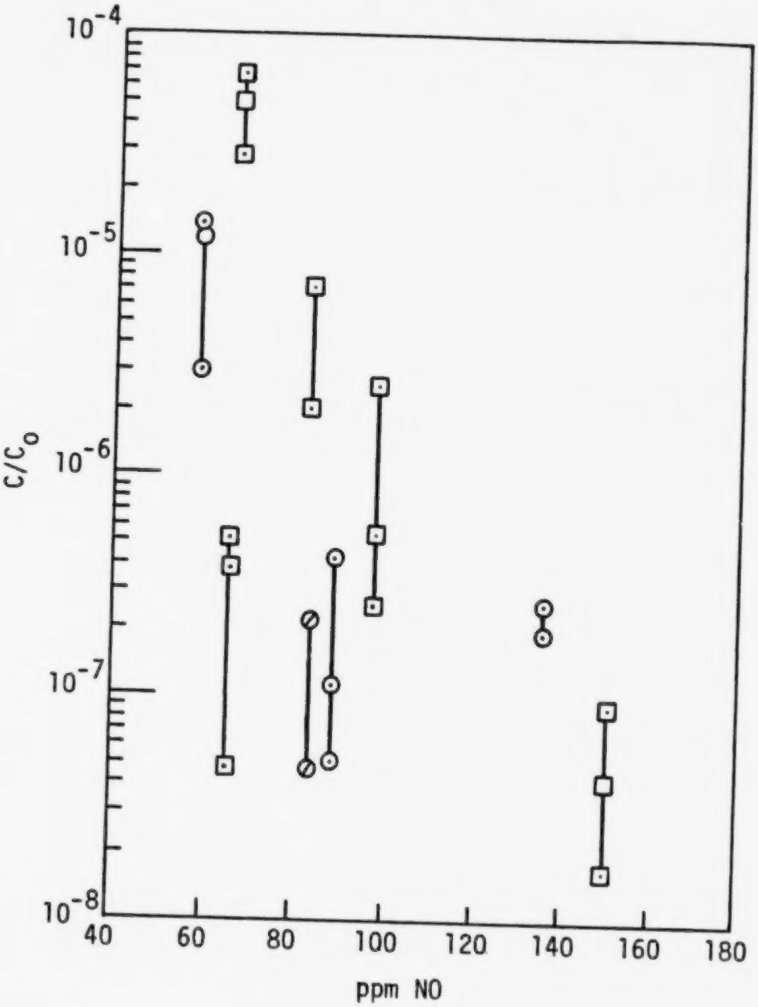

Figure 14. Correlation of NO emissions to fractional breakthrough of chlorobenzene.

chromatographic strips) that contains PIC information has not been reduced. However, even with limited examination of the data some important information is available. For example, in every run methylene chloride was observed at levels equal to or greater than the POHC of interest, even when it was not present as a POHC in the waste. Although some of this methylene chloride can be attributed to contamination, the levels were consistently higher than corresponding blank values. Peaks in the retention time range for methylene chloride were routinely off scale. Several other chlorinated organics not fired in the fuel have been identified as being in the emissions of one or more runs. These include such species as perchloroethylene, trichloroethylene, the trichloroethanes, the dichloroethylenes and ethanes, chloroform, and possibly chloromethane. An example is given in the summary Table 12. The significance of this finding is the following -- although DRE's for both POHC's (chlorobenzene and carbon tetrachloride) are greater than 99.99 percent, only 99.985 percent of all chlorinated organics being fired is destroyed or removed. Of the mass weight of chlorinated organics entering the combustor, 0.015 percent is being emitted. (Note that the compounds being emitted are not necessarily the same as those being fired).

## 4.6 COMPOUND COMPOSITION

As predicted by all the various methods, carbon tetrachloride was the most refractory material fired and chlorobenzene (6.6 Kcal/g) was the least refractory. However, in contrast to heats of combustion ranking, one of the easier compounds to destroy appeared to be 1,2-dichloroethane (3 Kcal/g). In addition, chloroform, with a heat of combustion only slightly greater than carbon tetrachloride (0.75 and 0.24 Kcal/gram respectively), appeared to have a destructibility on the order of chlorobenzene. This supports the laboratory scale findings of K. C. Lee (12) and of B. Dellinger (13).

## TABLE 12. SUMMARY OF RUN C-7

| | Chloro-benzene | Carbon tetrachloride | Chloroform[*] | Subtotal[†] | Other[‡] | Total[§] |
|---|---|---|---|---|---|---|
| Mass flow in[‖] | 17.34 | 9.72 | 0 | 27.05 | 0 | 27.05 |
| Mass flow out[**] | $1.48 \times 10^{-5}$ | $8.32 \times 10^{-4}$ | $1.22 \times 10^{-3}$ | $2.06 \times 10^{-3}$ | $2 \times 10^{-3}$ | $4 \times 10^{-3}$ |
| Out/in | $8.54 \times 10^{-7}$ | $8.56 \times 10^{-5}$ | N/A | $7.62 \times 10^{-5}$ | N/A | $1.48 \times 10^{-4}$ |
| Average DRE | 99.9999<br>±0.00016[††] | 99.9914<br>±0.0035 | N/A | 99.9924<br>±0.004 | N/A | 99.985<br>±0.020 |

[*] Major identified PIC.
[†] Includes POHC's plus chloroform.
[‡] Estimate of unidentified and/or unquantified PIC's.
[§] Estimate of total chlorinated organic species.
[‖] Estimate of total g/min.
[**] Average of three samples (g/min).
[††] Two standard deviation.

# SECTION 5

# MODEL DEVELOPMENT

The ultimate goal of the parametrics testing was to predict the destruction efficiency of a boiler for a given waste. To achieve this goal the information gathered on the pilot unit was extrapolated to full-scale boilers by a mathematical model. The model should take input information specific to the device being modeled and produce information that will predict the performance capabilities of that device with respect to those inputs. It should then be able to predict the performance of similar devices using the same process.

Although considerable efforts have gone into simple modeling of the chemistry that governs hazardous waste oxidation in idealized flow reactors, the physical and chemical processes which dominate destruction in real combustion devices have not been quantified. Destruction within such devices as incinerators, boilers, and kilns occurs in two separate regions, a flame zone and a postflame zone. A detailed, accurate model describing in-flame destruction events requires greater understanding and more data than are available. Figure 15 shows many of the phenomena affecting destruction within a turbulent spray flame. At least four of these are currently inadequately described. The chemical kinetics alone (the description of the reaction mechanism of chlorinated hydrocarbon combustion) is beyond the bounds of present knowledge. Although single burning fuel droplets have received some attention, there is no comprehensive description of burning fuel sprays. Particle loading can have a profound influence on radiative heat transfer, yet there does not presently exist a good model for soot formation in oil flames. Finally, there is great uncertainty in describing the flow patterns around the flame which govern the mixing of fuel and air. Figure 16 portrays processes that must be dealt with in a thermal destruction environment. Again, detailed accurate models of all of the processes do not exist. These represent only a few of the barriers to developing a detailed description of the thermal destruction of hazardous wastes in working combustors.

However, the detail described above may not be necessary to accomplish the prediction of destruction efficiency to the accuracy required by most potential users. That is, the use of global kinetics, or estimation of soot formation rates and radiosities among other items may not need to be modeled in detail to predict DRE. The detailed modeling of flame turbulence may be unnecessary to estimate the amount of material that must be destroyed by nonflame processes. The flight paths of individual moleculer or fuel pockets may not be required when the overall system performance is desired. Thus

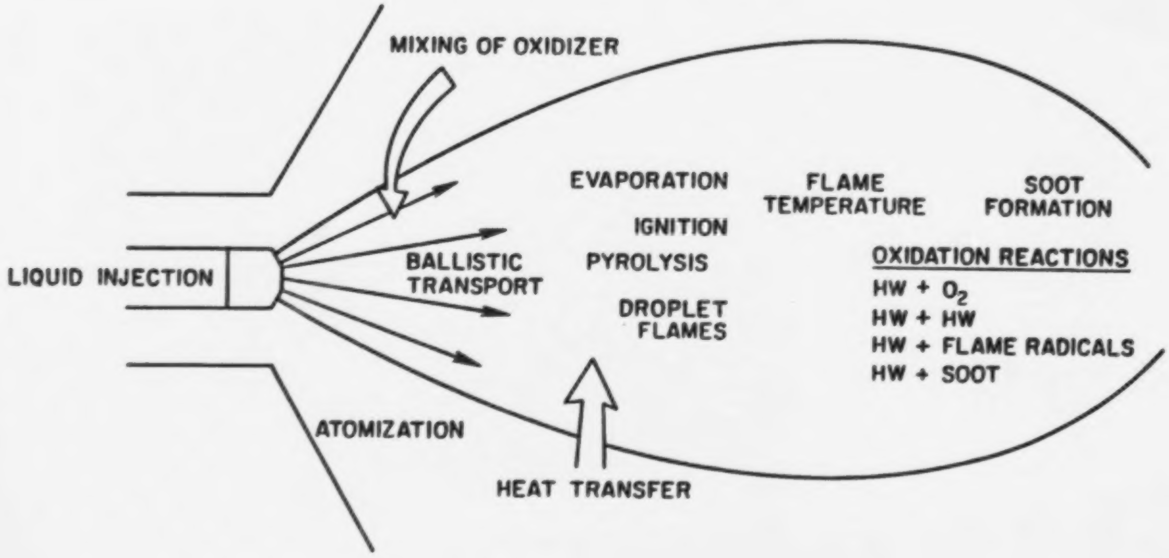
MIXING OF OXIDIZER
LIQUID INJECTION
BALLISTIC TRANSPORT
ATOMIZATION
EVAPORATION
IGNITION
PYROLYSIS
DROPLET FLAMES
HEAT TRANSFER
FLAME TEMPERATURE
SOOT FORMATION
OXIDATION REACTIONS
HW + $O_2$
HW + HW
HW + FLAME RADICALS
HW + SOOT

Figure 15. Turbulent spray flame processes affecting waste destruction efficiency (Reference 6-1).

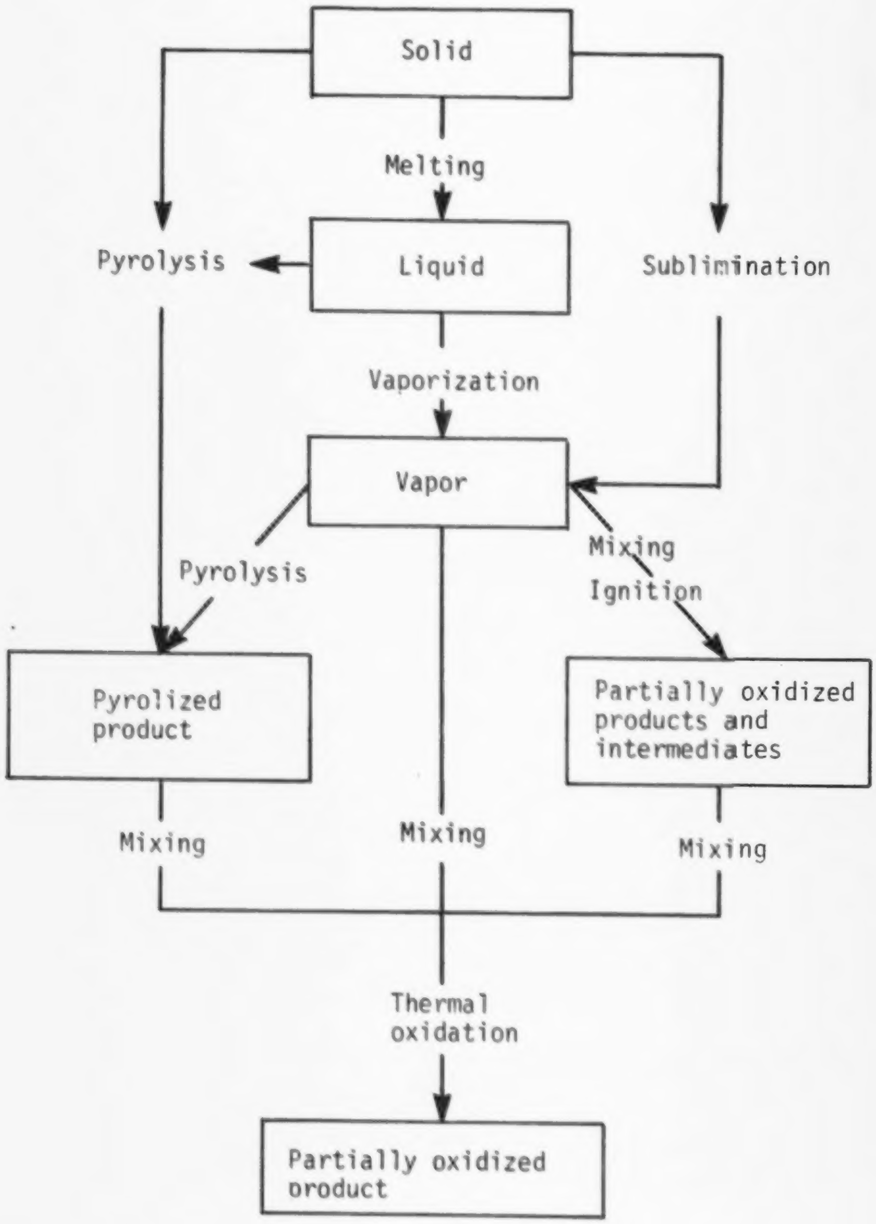
Solid
Melting
Pyrolysis
Liquid
Sublimination
Vaporization
Vapor
Pyrolysis
Mixing
Ignition
Pyrolized product
Partially oxidized products and intermediates
Mixing
Mixing
Mixing
Thermal oxidation
Partially oxidized product

Figure 16. Processes undergone by materials during thermal destruction (either within or outside a flame) (Figure courtesy Barry Dellinger, University of Dayton Research Institute).

this effort looked at the simpler, more global aspects of modeling, and compared the results to an actual thermal destruction system.

## 5.1 BACKGROUND

The intent of the modeling effort described in this report is to spark the development of furnace models which ultimately could aid: (1) the permitter, who must determine the suitability of a particular thermal device to adequately process a particular waste type; (2) the designer, who desires a quantitative description of the effects of furnace design parameters on waste destruction; and (3) the operator, who would like to optimize combustion and incineration efficiencies. The goals, the approach, and the design of this modeling effort have been primarily determined to support the permitter.

A destruction model would be helpful in assessing potential combustor performance. For example, a standard exists for incinerator requiring 99.99 percent destruction for any combination of waste and equipment. But all combinations cannot be tested. Furthermore, experience within this project indicates that flame destruction nominally achieves only 90 to 99.9 percent destruction. Thus, at least some destruction must be achieved in the postflame region if the 99.99 percent destruction goal is to be reached. Furthermore, the postflame region is not subject to the great complexity of physical and chemical interactions shown in Figure 15.

It was therefore decided to limit the model to a description of the postflame furnace environment. A postflame simulation can approach the needs of the user by providing a conservative estimate of waste destruction. For example, stack sampling results may reveal an overall DRE of 99.99 percent for chlorobenzene in a firetube boiler at optimum firing conditions. Suppose the contributions of fast in-flame destruction and long residence postflame destruction are divided evenly. Then 1 percent of the initial waste would break through the flame boundary, and 0.01 percent would remain at the furnace exit. The model simulation ignores the flame destruction, hence it predicts 1 percent breakthrough at the exit (99 percent DRE). The current model underestimates actual combustor efficiency by intent.

## 5.2 GOALS

The goals of the model development can be summarized as follows:

- Approach the ability to conservatively predict the DRE for a given device and waste combination
- Provide a tool to understand the operation and design parameters which dominate destruction efficiency
- Model a wide variety of furnace types, fuels, and operating conditions

In order to meet these goals, the model should accurately predict the bulk gas temperature-time history of the postflame gases because destruction efficiency is extremely sensitive to residence time and temperature. To eventually meet the needs of the three user groups, the model should also be simple and economical. That is, it should not require a large computer, it should have simple algorithms, and it should run rapidly.

The current model is discussed in the following sections.

## 5.3 APPROACH

The model program consists of two modules, as shown in Figure 17. The first module calculates a single average gas temperature, $T_j$, for each axial zone, j, into which the furnace is subdivided. An energy balance is performed on each zone. Figure 18 shows the principle energy flows into and out of a furnace zone. Radiative heat transfer dominates the heat losses from the gas phase. Separate radiative and convective terms describe the losses to the waterwall and refractory wall components of the firebox surface. The output bulk gas temperatures can be compared directly to the pilot-scale furnace measurements.

The second module uses as input the output from the first module. It extrapolates the single zone temperature to an axisymmetric radial temperature profile for the zone. The algorithm is based on an empirical description of the pilot-scale thermal boundary layers. Simple fluid mechanics of laminar and turbulent flows applied to the bulk flow properties and boundary layer temperatures produces a radial velocity profile for each zone. The residence time for a fluid particle which travels through an annulus i (always traveling parallel to the furnace wall) to reach a zone j, $\tau_{ij}$, follows directly. The concentration of the principal waste component, $C_{ij}$, can then be calculated by overlaying simple global kinetics on the axisymmetric temperature-time history.

Figure 19 shows the resulting set of mass breakthrough fractions for a typical model run. All of the waste escapes the flame region. At high centerline temperatures, essentially all ("ten nines") of the waste is destroyed. (In fact, thermodynamic equilibrium probably limits the destruction long before this point.) However, only 98.1 percent of the waste material which travels in the annulus nearest the wall is destroyed.

## 5.4 BULK GAS TEMPERATURE MODEL

The first goal of the model approach requires the prediction of a temperature profile of the combustion gases along the axis of bulk flow. There has been great interest in the past in developing heat transfer models to aid in the efficient design of industrial boilers (15 through 17). In the most advanced models, the furnace enclosure is divided into a number of three-dimensional zones. Each zone is considered to have uniform properties. A steady-state energy balance is determined for each zone, and the resulting set of nonlinear equations is solved for zone temperature and a set of radiant heat fluxes entering and leaving the zone. This model format allows

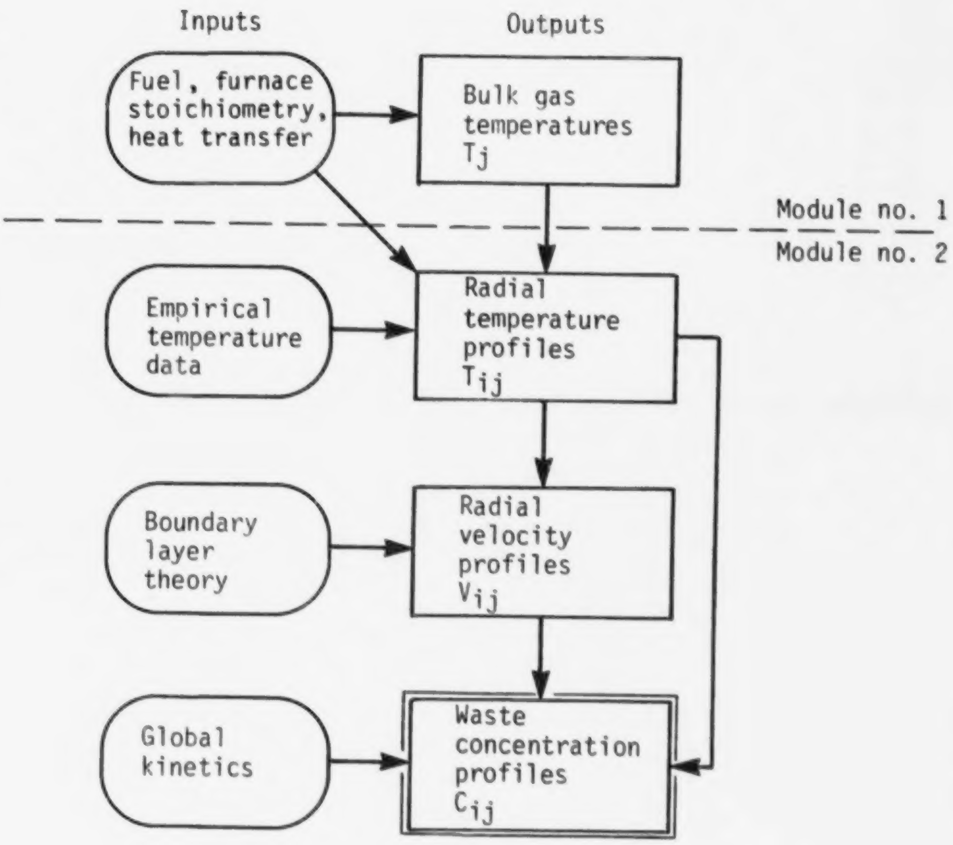
Inputs
Outputs
Fuel, furnace stoichiometry, heat transfer
Bulk gas temperatures $T_j$
Module no. 1
Module no. 2
Empirical temperature data
Radial temperature profiles $T_{ij}$
Boundary layer theory
Radial velocity profiles $V_{ij}$
Global kinetics
Waste concentration profiles $C_{ij}$

Figure 17. Furnace model flow diagram.

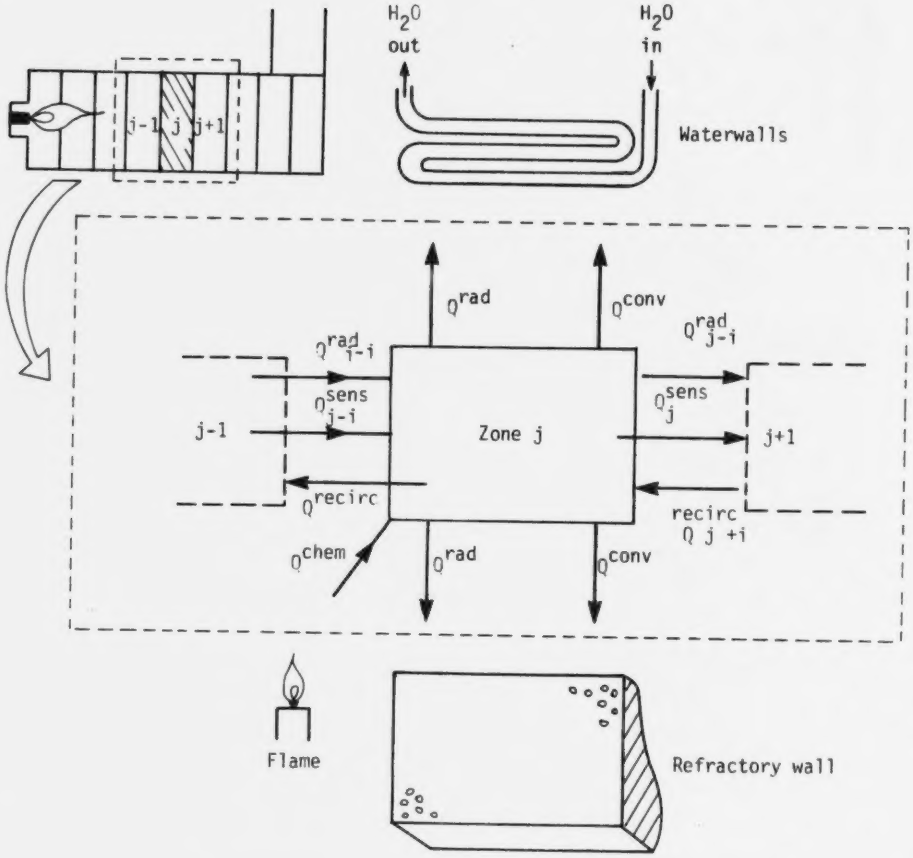
j-1
j
j+1
H₂O out
H₂O in
Waterwalls
Q rad
Q conv
Q rad j-i
Q rad j-i
Q sens j-i
Q sens j
j-1
Zone j
j+1
Q recirc
recirc Q j +i
Q chem
Q rad
Q conv
Flame
Refractory wall

Figure 18. Bulk temperature module zone energy balance.

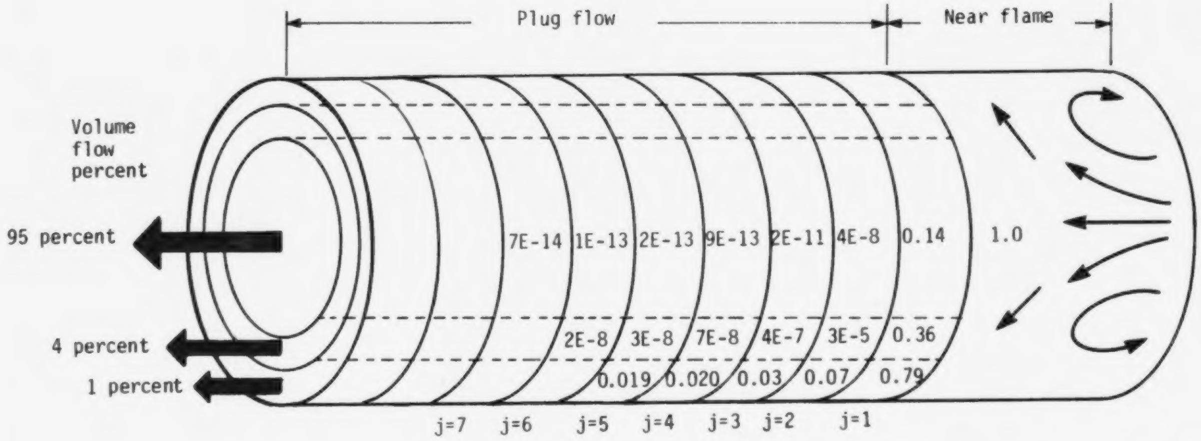
Plug flow
Near flame
Volume flow percent
95 percent
4 percent
1 percent
7E-14
1E-13
2E-13
9E-13
2E-11
4E-8
0.14
1.0
2E-8
3E-8
7E-8
4E-7
3E-5
0.36
0.019
0.020
0.03
0.07
0.79
j=7
j=6
j=5
j=4
j=3
j=2
j=1

Waste: Dichlorobenzene
Excess air: 25 percent
Firing rate: 0.8 million Btu/hr
Run 19

Annuli: 0, 1/8, 1/4 radius

Figure 19. Sample boundary layer module prediction of axisymmetric mass breakthrough fractions.

highly detailed three-dimensional views of temperature gradients and heat flow patterns. Unfortunately, as the number of zones increases, the computational burden increases geometrically. Further size and complexity can be added by analyzing the detailed aerodynamic flow patterns of a complicated fuel injection geometry.

A simpler furnace model can meet the goals of this study. The model can be limited to the case of long tubular combustor with essentially a plug flow of combustion gases, but for simple one-dimensional recirculation superimposed on the bulk flow. This simplification is quite adequate for describing a large variety of combustor types and for understanding the parameters that influence waste incineration.

Figure 20 shows how the axial zone model might be applied to a single burner, watertube boiler. Zones 1 through 6 represent regions of high temperature where destruction of waste fuels takes place; temperatures in the downstream zones are lowered by convective heat transfer to the water tubes to the extent that no further destruction occurs. A control volume is drawn around each zone and the energy flows summed and set equal to zero. Separate flows are considered for heat losses to water-cooled combustor surfaces and refractory (insulating brick) surfaces. The zone heat balance model is discussed in detail in the following subsections.

### 5.4.1 Zone Heat Balance

Figure 21a shows the simplest formulation of the control volume heat balance, Case I, in which wall heat losses are accounted for by four heat fluxes:

| | |
|---|---|
| $Q_{ww}^{rad}$ | Radiative transfer from zone to adjacent waterwall surfaces |
| $Q_{ref}^{rad}$ | Radiative transfer from zone to adjacent refractory wall surfaces |
| $Q_{ww}^{conv}$ | Convective transfer from zone to waterwall |
| $Q_{ref}^{conv}$ | Convective transfer from zone to refractory |
| $Q_{chem}$ | Chemical heat release from fuel consumption within zone |
| $mh_j$ | Sensible energy carried out of the zone, specified by the zone temperature |
| $mh_{j-1}$ | Sensible energy entering the zone from the zone immediately upstream |

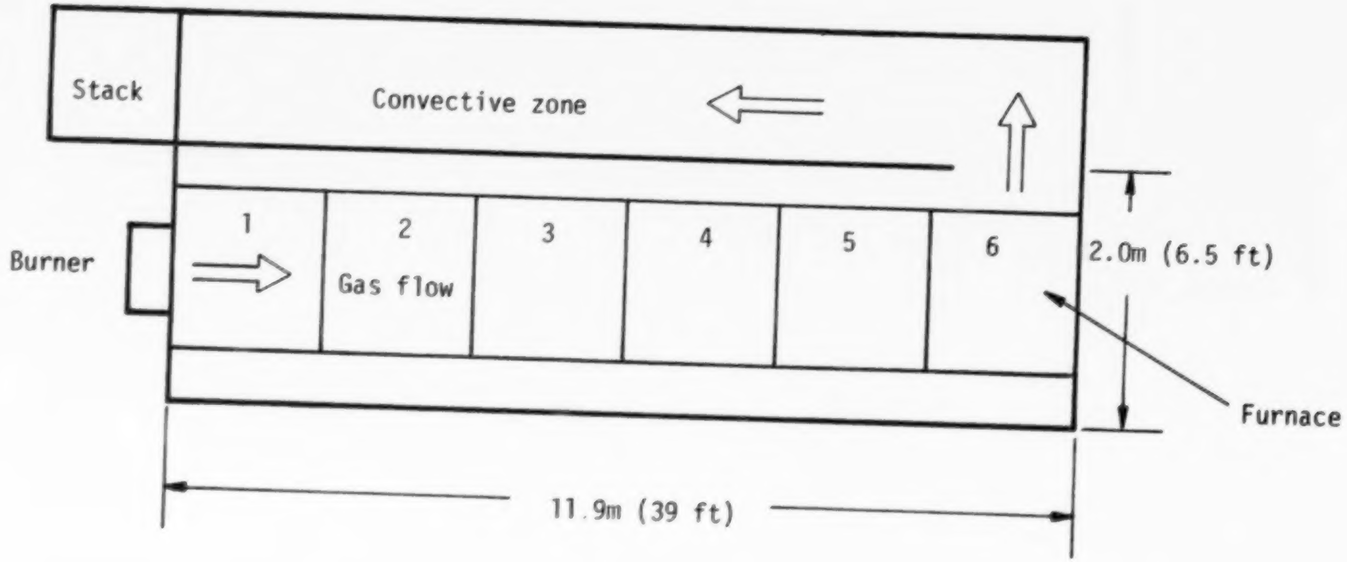
Stack
Convective zone
Burner
1
2
Gas flow
3
4
5
6
2.0m (6.5 ft)
Furnace
11.9m (39 ft)

Figure 20. Plan view schematic of package watertube boiler with 44 MW (150 million Btu/hr) capacity; furnace height = 2.7m (9 ft).

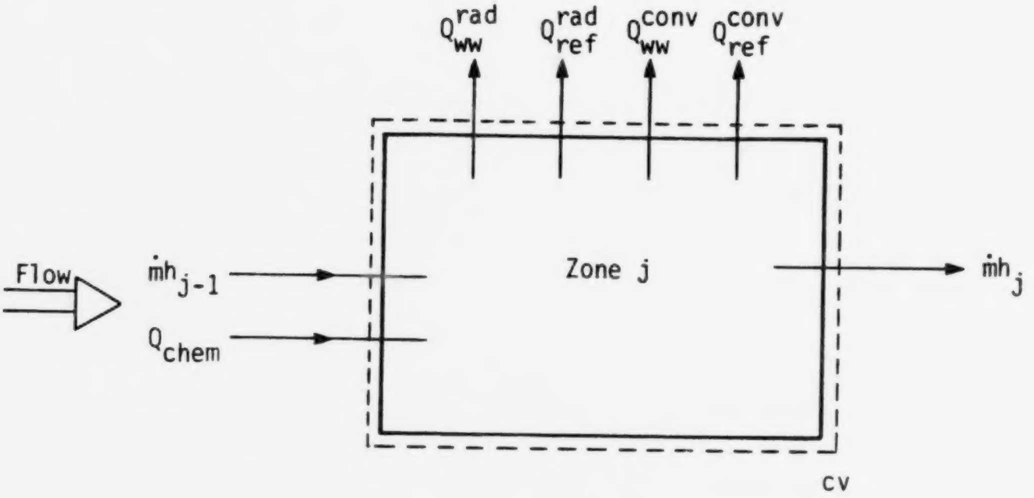

$Q_{ww}^{rad}$
$Q_{ref}^{rad}$
$Q_{ww}^{conv}$
$Q_{ref}^{conv}$
Flow
$\dot{m}h_{j-1}$
$Q_{chem}$
Zone j
$\dot{m}h_j$
cv

Figure 21a. Case I zone energy balance without interaction between zones.

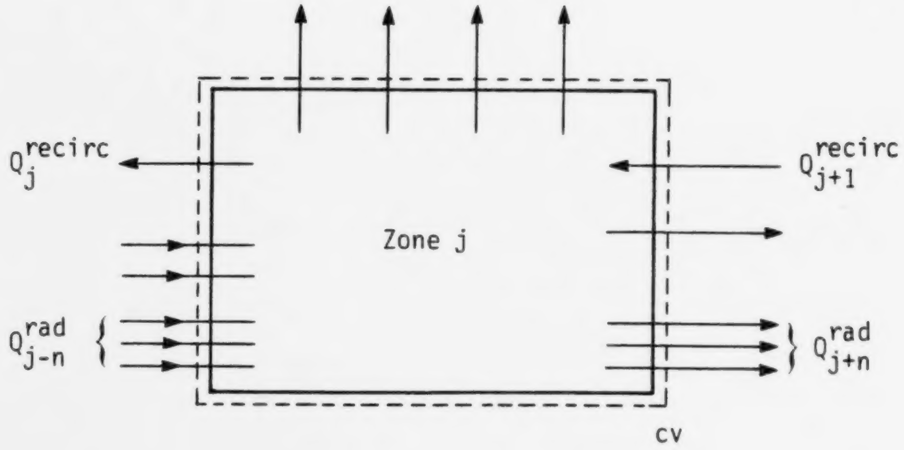

$Q_j^{recirc}$
$Q_{j+1}^{recirc}$
Zone j
$Q_{j-n}^{rad}$
$Q_{j+n}^{rad}$
cv

Figure 21b. Case II zone energy balance including recirculation and radiative transfer between zones.

In Case II, Figure 21b, additional detail is added in the form of recirculation flows and radiative transfer between zones. These new fluxes are described by:

| | |
|---|---|
| $Q^{recirc}_{j}$ | Heat carried from zone to the zone upstream of it by recirculation |
| $Q^{recirc}_{j+1}$ | Heat carried into zone by recirculation from the zone immediately downstream |
| $Q^{rad}_{j-n}$ | Gas-to-gas net radiative contribution to the zone from surrounding zones ($n = \pm 1, \pm 2, \pm 3$) |

Thus for Case I, the steady state energy balance is given by:

$$\sum Q_I = \dot{m}h_j - \dot{m}h_{j-1} + Q_{chem} - Q^{rad}_{ww} - Q^{rad}_{ref} - Q^{conv}_{ww} - Q^{conv}_{ref} = 0 \qquad (1)$$

And for Case II it is:

$$\sum Q_{II} = Q_I + Q^{recirc}_{j} - Q^{recirc}_{j-1} + \sum_{n=-3}^{3} Q^{rad}_{j+n} = 0 \qquad (2)$$

The solution algorithm will require in each case that the energy flow terms are all cast in terms of one unknown -- the effective temperature of the zone.

### 5.4.2 Wall/Gas Radiative Equilibrium

First the radiative losses from the combustion gas to both the waterwall and refractory wall components of the furnace surface are evaluated. Significant complexity results because of reradiation and reflection from the walls and absorption in the gas. The radiation fluxes at a surface are shown schematically in Figure 22, where G represents the incident radiation. A certain fraction is absorbed and the balance, R, is reflected diffusely. Assuming the surface can be approximated as a grey body, the quantity $\epsilon E$ represents the total re-emitted flux, where $\epsilon$ is the emissivity and E the black body emissive power. The total radiation returning to the furnace enclosure, or radiosity, J, is given by:

$$J = \epsilon E + \rho G \qquad (3)$$

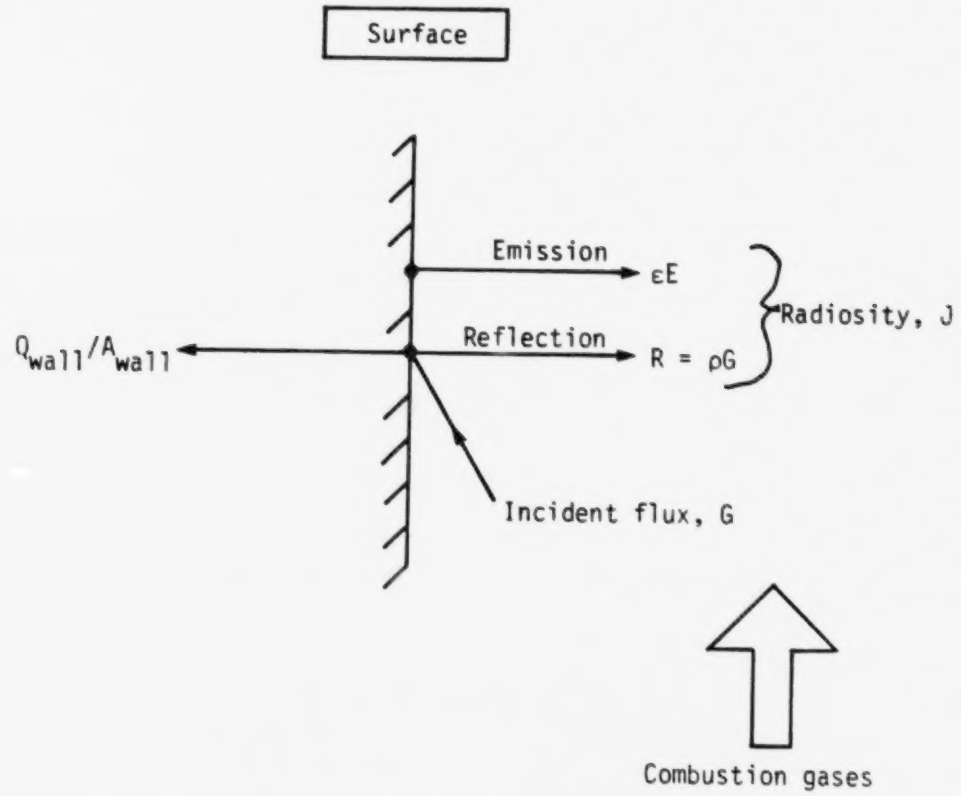
Surface
Emission
$\varepsilon E$
Radiosity, J
Reflection
$R = \rho G$
$Q_{wall}/A_{wall}$
Incident flux, G
Combustion gases

Figure 22. Surface radiation fluxes.

where $\rho$ is the reflectivity, or $1-\varepsilon$ for an opaque surface. The net heat loss to the wall is the difference between the incident flux and radiosity, or:

$$Q_{wall} = A\ (G - J) \tag{4}$$

where A is the surface area. Solving equation (6-3) for G and substituting:

$$Q_{wall} = A\varepsilon\ (J - E)/(1 - \varepsilon) \tag{5}$$

This represents the net heat absorbed through a waterwall or refractory wall surface that is irretrievably lost from the gas stream.

Consider radiation interchange between the two wall types. The fraction of the total radiation leaving the refractory and arriving at the waterwall is given by $J_w A_w F_{wr} \tau_G$, where $F_{wr}$ is the view factor and $\tau_G$ the transmissivity of the gas. Similarly, the total radiation to waterwall from refractory is $J_w A_w F_{wr} \tau_G$. The net transfer rate between the two is thus:

$$Q^{rad}_{rw} = A_w F_{wr}\ (1 - \varepsilon_G)\ (J_r - J_w) \tag{6}$$

It is assumed that the grey gas medium absorbs and transmits, but scattering and reflection of radiant energy by particles is negligible; $\tau_G$ is replaced by $1-\varepsilon_G$.

The expression for the heat transfer between the gas and refractory surface or gas and waterwall can be developed in a similar fashion. The fraction of the total radiation emitted by the gas which reaches the waterwall surface is $A_w \varepsilon_G E_G$ (the view factor is unity). The radiation leaving the wall and absorbed by the gas is $J_w A_w \alpha_G$ where $\alpha_G$ is the gas absorptivity. Since the gas is assumed to be a grey body and in equilibrium, $\alpha_G = \varepsilon_G$ and:

$$Q^{rad}_{ww} = A_w \varepsilon_G\ (E_G - J_w) \tag{7}$$

By analogy, the net transfer between the gas stream and refractory is given by:

$$Q^{rad}_{ref} = A_r \varepsilon_G\ (E_G - J_r) \tag{8}$$

Equations (5 through 8) are in a form that suggests recasting the set of nonlinear equations as an electrical network problem. The schematic for such a network is shown in Figure 23. The radiosities and blackbody emissive powers are represented by node potentials, while heat transfer rates are analogous to electrical currents. The conductance associated with each resistor in the circuit is specified by the appropriate equation (5 through 8). Summing the currents into each node produces three independent equations. If all but three parameters are specified, an exact solution exists. Solving for the radiosities $J_w$ and $J_r$ results in:

$$J_w = \frac{(E_G C_{Gr} + E_w C_w)(C_{Gw} + C_{rw} + C_r) + (E_G C_{Gr} + E_r C_r) C_{rw}}{(C_{Gw} + C_{rw} + C_w)(C_{Gw} + C_{rw} + C_r) - C_{rw}^2} \qquad (9)$$

and

$$J_r = \frac{(E_G C_{Gw} + E_r C_r)(C_{Gr} + C_{rw} + C_w) + (E_G C_{Gw} + E_w C_w) C_{rw}}{(C_{Gr} + C_{rw} + C_G)(C_{Gr} + C_{rw} + C_w) - C_{rw}^2} \qquad (10)$$

The conductances ($C_{xx}$), shown in Figure 23 are functions of the emissivities $\varepsilon_G$, $\varepsilon_w$, and $\varepsilon_r$; the surface areas $A_w$ and $A_r$; and the shape factor $F_{wr}$. The blackbody emissive powers are completely specified by the wall temperatures and the gas temperature. Therefore if the furnace geometry is well characterized and the emissivities known as a function of temperature, the radiative fluxes are completely determined by the gas temperature.

Previous models have typically assumed, as a first approximation, that refractory walls are perfectly insulating (18). The gas stream loses no heat through the refractory wall via radiative transfer. In terms of the circuit analog, the resistance between $J_r$ and $E_r$ becomes infinitely large. In practice, significant losses may occur through the refractory which are far larger than can be predicted from convective transfer alone (19). Yet refractory materials of reasonably low thermal conductivity (5 to 10 Btu-in./hr-ft$^2$-°R) do not behave like perfect sinks either. In order to create an adequate compromise, an empirical factor, $K_r$, has been introduced to account for the "semi-adiabatic" nature of refractory walls. The value of $C_r$, when multiplied by a $K_r$ on the order of 0.05, gives a conductance characteristic of the insulation types in question. The resulting overall heat loss coefficient agrees well with previous approaches to quantify imperfect heat loss through refractories (20). The approach differs from Reference 6-7 in that we started with the assumption that the wall is a perfect sink and made the appropriate empirical correction. The alternative is to assume a perfectly adiabatic wall and correct from the other direction.

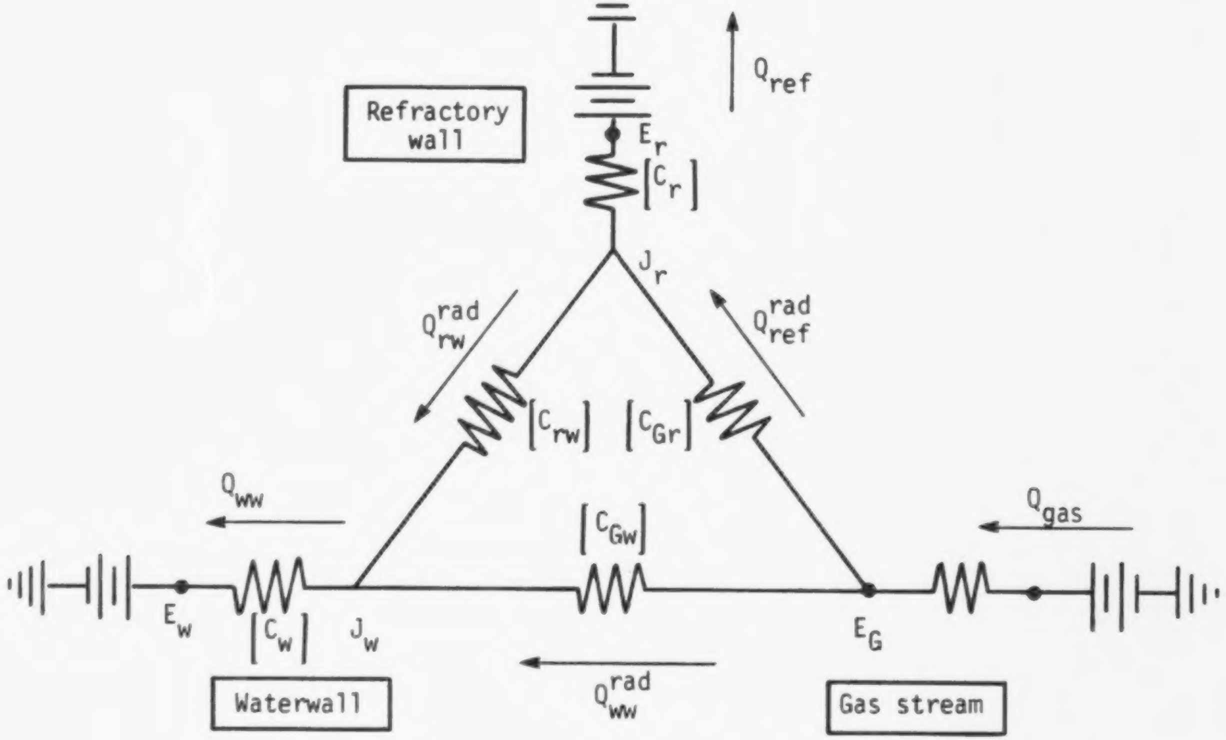
Refractory wall
$E_r$
$[C_r]$
$Q_{ref}$
$J_r$
$Q_{rw}^{rad}$
$Q_{ref}^{rad}$
$[C_{rw}]$
$[C_{Gr}]$
$Q_{ww}$
$[C_{Gw}]$
$Q_{gas}$
$E_w$
$[C_w]$
$J_w$
$E_G$
$Q_{ww}^{rad}$
Waterwall
Gas stream

Figure 23. Circuit analog for radiative equilibrium between a nonadiabatic refractory, waterwall sink, and an absorbing gas.

The calculation of the view factor $F_{wr}$ (the fraction of radiation leaving the waterwall and intercepted by the refractory) can be tedious for even the simplest geometries. Fortunately, an approximation has been developed by Hottel (21). The view factor can be expressed as a function of the "speckledness," S, of the furnace. A cylindrical enclosure with a great patchwork of intermingled cold and hot walls would have a high S-value, close to unity. A furnace with the refractory wall in a single plane would have an S-value of zero. The estimation of S within ±0.2 is perfectly adequate for the accuracy of the model.

### 5.4.3 Gas Emissivity

Traditionally, flame heat transfer models have relied on the well-known Hottel charts (22) for an engineering approximation to emissivity. Of the equilibrium combustion products, only carbon dioxide and water molecules radiate significantly; the emissivity value is a function of their concentrations and the mean beam length characteristic of the zone volume. Mean beam lengths are tabulated in Reference 23. Additional charts permit correction for overlap of absorption bands in a common wavelength region. The curve fits of the Hottel charts are adequate for regions well downstream of the initial heat release regions where $CO_2$ and $H_2O$ have approached equilibrium levels. In the luminous flame zone, however, the presence of radiating transient species (e.g., OH, CO, CH, etc.) and especially particulates can raise the overall emissivity appreciably. This is particularly true in flames of distillate oil cofired with chlorinated hydrocarbons. Such wastes as carbon tetrachloride, chloroform, and chlorobenzene have been observed to enhance distillate sooting tendency by an order of magnitude or more (24). In sooting oil flames, as well as particulate-laden coal flames, the effective emissivity is much closer to blackbody than the Hottel charts would suggest.

Following the approach of Beer (25) the emissivity of sooty clouds is approximated by considering the contributions of both soot and gas in three discrete spectral regions. Thus in the $n^{th}$ region, an overall absorption coefficient is given by:

$$K_n = K_{s,n} C + K_{g,n} (p_c + p_w) \tag{11}$$

where $K_{s,n}$ and $K_{g,n}$, the absorption coefficients for soot and gas respectively, are developed by empirical means; $p_c$ and $p_w$ are the partial pressures of carbon dioxide and water; and C is the mass loading of soot. The emissivity is derived by modifying Beer's Law to give:

$$\varepsilon = a_{g,n} (1-\exp(-K_n L)) \tag{12}$$

where L is the mean beam length for the zone and the $a_{g,n}$ are temperature-dependent weighting factors for the wavelength region. Linear correlations with gas temperature have been developed for the $a_{g,n}$.

The greatest uncertainty of this engineering approach is in the estimation of the soot mass per unit volume. Soot formation in oil sprays is a very poorly quantified phenomenon that depends on fuel type, oxygen contact, flame shape, velocity, and atomization. For example, mass loading can be varied over three orders of magnitude simply by doubling the oil pressure upstream of the atomizing nozzle (26).

### 5.4.4 Flame Volume

The fraction of each zone occupied by the luminous flame is important from two standpoints, the application of the sooting emissivity correction and the release of chemical energy associated with conversion to stable combustion products. Thus, an estimate of the flame volume and either the flame length or flame diameter is needed. Volume and diameter are used in this model allowing calculation of flame length. Once the flame length has been established, the chemical heat release is apportioned amongst the appropriate zones according to the fraction of the flame occupying the zone. Flame volumes in shell boilers have been estimated to be 0.2 $m^3$/megawatt (2.07 $ft^3$/million Btu/hr) with a corresponding carbon particle concentration of 8 $g/m^3$ for light oils (27). Flame shapes have been approximated by both cylinders and cones. This model uses a truncated frustrum. The volume of a frustrum is given by:

$$V = \pi L (r_1^2 + r_1 r_2 + r_2^2)/3 \qquad (13)$$

with $r_1$ and $r_2$ representing the minimum and maximum radii of the frustrum and L the length. Assuming a constant volumetric heat release within the flame zone, the flame length L is calculated from equation (13) to be:

$$L = \frac{3Fv_f}{\pi (r_1^2 + r_1 r_2 + r_2^2)} \qquad (14)$$

where F is the firing rate and $v_f$ is the flame volume per unit firing rate. Once the flame length is determined, the fraction of the flame volume in each zone can be calculated. The flame length L is first divided by the zone length $l_J$ to determine the number of zones over which the flame reaches. The fraction of the flame volume in each zone is then found using equation (13) where V is now $V_J$, L is $l_J$, and the radii are found iteratively beginning with the minimum flame diameter (at the nozzle end) and ending with the maximum flame diameter.

### 5.4.5 Convection

Typically convective heat transfer to furnace walls is overwhelmed by radiation in the high-temperature region where organics are destroyed. Estimating the convective flux to within 20 to 30 percent is generally sufficient for the model as the radiative flux is as much as an order of magnitude larger. The expression for turbulent flow in long pipes is suitable for most combustor types:

$$Nu = (0.023)Re^{0.8}Pr^{0.33} \tag{15}$$

The Nusselt, Reynolds, and Prandtl numbers are all evaluated at the bulk gas temperature. Free convection is negligible.

### 6.4.6 Recirculation

The sensible energy leaving a zone j and entering the zone immediately downstream is determined by (in Case I):

$$mh_j = \sum_{i=1}^{4} \dot{m}_i \quad {}_{T_{ref}}^{T_j} (C_p)_{ij} dT \tag{16}$$

This is the sum of the contributions from the four major fuel-lean species -- $CO_2$, $H_2O$, $O_2$, and $N_2$. The $(C_p)_{ij}$, the heat capacity of each species in zone j is calculated from a polynomial curve fit with the bulk gas temperature $T_j$. The polynomial coefficients are derived from standard tables (28). The reference state is that used for the fuel heating value, usually 77°F.

To account for gas flow from zone j returning upstream to zone j-1, a certain fraction of the sensible energy output $\dot{m}h_j$ becomes an input to zone j-1. The magnitude is a function of zone location, combustor geometry, and extent of burner swirl. For the near burner region of small industrial boilers, nearly half of the combustion gases may recirculate across zone boundaries. Several diameters downstream of the fuel nozzle the recirculation fraction tends to zero. Estimation of the values for each zone is made based on the knowledge of aerodynamics for each individual furnace configuration.

### 6.4.7 Gas/Gas Radiation

Radiation transfer in the gas phase is calculated after the method of Field, et al. (29). The energy, $q_{ij}$, absorbed into zone i which is emitted from zone j is given by:

$$q_{ij} = f_{vv} 4k_j B^3 \sim T_j^4 \qquad (17)$$

where the dimensionless factor $f_{vv}$ depends on ${}^{\wedge}{}_j$, the fraction of the radiant energy produced in zone j which escapes from it; the fractional absorption en route, and the fractional absorption by zone i. B is the zone length and $K_j$ is the absorption coefficient of zone j. The rate of radiant emission from zone i is:

$$q_i = \Phi_i 4k_i B^3 \sigma T_i^4 \qquad (18)$$

Values for escape factors $\Phi$ and reception factors $f_{vv}$ are taken from Field's plots.

Because $f_{vv}$ and k are variable from zone to zone in the system under study, average values for these factors must be used. Thus equation (6-17) is modified to

$$q_{ij} = 4(f_{vv})_k (\bar{k}_i k_j/\bar{k}) B^3 \sigma T_j^4 \qquad (19)$$

Each zone sees only the three zones immediately adjacent to it; i has the values ±1, ±2, and ±3. The effect of this gas-to-gas radiation calculation is to lower the temperature in the hotter zones and to raise the temperature in the cooler zones relative to Case I.

## 5.5 BOUNDARY LAYER DESTRUCTION MODEL

Given the bulk gas and wall temperatures as input, the second leg in the model calculates axisymmetric radial temperature and velocity profiles for each zone. The furnace is further partitioned into an appropriate number of concentric annular slices. Figure 24 shows typical profiles for a zone well downstream of injection. Typically the spacing between slices is smaller near the boundaries because of the steeper thermal and velocity gradients at the wall. To quantify the effect of wall quenching on thermal destruction, a time-temperature history is developed for each slice, and a simple chemical kinetic expression applied to each time-temperature path. Hence, the program calculates a set of concentrated profiles, one for each slice. The profile closest to the wall will represent an upper bound of the breakthrough poetential of the compound of interest for the given furnace geometry. The centerline slice result describes a lower bound, the best possible postflame destruction. The sum of the concentration paths, weighted by the volume flow rate through the slice, crudely approximates a single destruction efficiency for well-mixed stack gases.

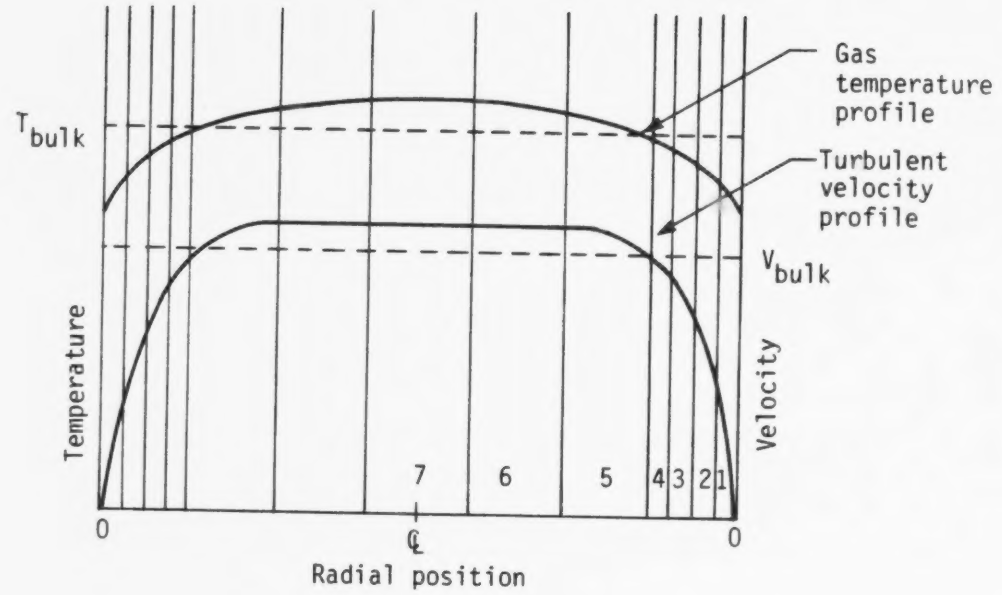
Gas temperature profile
Turbulent velocity profile
T_bulk
V_bulk
Temperature
Velocity
7
6
5
4
3
2
1
0
℄
0
Radial position

Figure 24. Typical radial temperature and velocity profiles for a zone showing slices.

### 6.5.1 Velocity Boundary Layer

As a first approximation the model is restricted to the case of fully developed flow in a cylindrical tube. In the laminar flow case, the parabolic radial velocity profile is easily derived as:

$$u(r) = \frac{\Delta P}{4L\mu}\,(r^2 - r_0^2) \tag{20}$$

where ΔP is the pressure drop across the axial distance L, $\mu$ is the gas viscosity, $r_0$ is the radius of the cylinder, and $u(r)$ the velocity at the distance r from the centerline. Therefore the average velocity in the slice between $r_1$ and $r_2$ is:

$$\bar{u}_{12} = \frac{\int_{r_1}^{r_2} \frac{\Delta P}{4L\mu}\,(r^2 - r_0^2)\,r\,dr}{\int_0^{r_0} r\,dr} \tag{21}$$

The bulk flow velocity, $\bar{u}_b$, integrated across the entire radius, is derived from the input mass flow and calculated density. Thus the velocity through a slice (at a given zone temperature) can be calculated independent of pressure drop and viscosity. Integrating equation (21) gives

$$\frac{\bar{u}_{12}}{\bar{u}_b} = 2\left[\left(\frac{r_2}{r_0}\right)^2 - \left(\frac{r_1}{r_0}\right)^2\right] - \left[\left(\frac{r_2}{r_0}\right)^4 - \left(\frac{r_1}{r_0}\right)^4\right] \tag{22}$$

Note that the variation in viscosity with temperature across the radius has been ignored.

For the fully turbulent case, the approach is similar, except that the boundary layer profile is expressed empirically in terms of the centerline velocity temperature, $u_m$, by the "1/7th law":

$$u(r) = u_m\left(1 - \frac{r}{r_0}\right)^{1/7} \tag{23}$$

First the bulk velocity $u_b$ is related to the maximum velocity $u_m$ by solving the integral

$$u_b = \frac{\int_0^{r_0} r\, u(r) dr}{\int_0^{r_0} r\, dr} = \frac{14}{15} u_m \tag{24}$$

Then calculating the average slice velocity between $r_1$ and $r_2$ in the same manner as the laminar case gives:

$$\frac{\bar{u}_{12}}{u_b} = \frac{\left(\frac{r_2}{r_0}\right)^{15/7} - \left(\frac{r_1}{r_0}\right)^{15/7}}{\left(\frac{r_2}{r_0}\right)^{2} - \left(\frac{r_1}{r_0}\right)^{2}} \tag{25}$$

Having calculated the velocity through each zone, and knowing the length of each zone, a mean residence time profile for a molecule traveling down a single slice follows.

### 5.5.2 Temperature Boundary Layer

Extending the bulk gas temperatures to full radial temperature profiles requires, in the purest sense, solution of the equation of radiative transport. For the purposes of this work, and within the calculation time/storage limits imposed by the computation approach, an empirical fit to the radial profile is adequate. The empirical method provides excellent accuracy for furnaces whose thermal environment is well characterized.

The radial temperature profile is divided into two regimes, the boundary layer and the bulk gas. The user specifies a boundary layer thickness (the dividing line) and the program applies a polynomial curve of up to sixth order to each regime. In the simplest version the bulk temperature is constant across the radius and the boundary layer temperature varies linearly between the bulk gas and the wall temperature. If data are available (from experiment or from three-dimensional modeling), more detail in the form of a polynomial curve can be added.

### 5.5.3 Global Chemical Kinetic Model

The destruction of organic wastes can be arbitrarily separated into two processes: in-flame oxidation and pyrolysis and postflame oxidation and pyrolysis (cf. Section 3.2). The flame region is characterized by very high temperatures, high free radical concentrations, very short residence times, and turbulent mixing. Additionally, soot formation, atomization, and nozzle design play a very large role in determining the conversion rates. Practical experience (supported by data obtained in this study) suggests that from 90 to 99.9 percent destruction is common. Although the better part of destruction may occur within the flame region, the current combustion knowledge is not sufficient to quantify the complex interactions in real combustors. The complexity of chemical and physical processes within the flame forces consideration only of the oxidation and pyrolysis in the postflame region. Therefore the model will tend to over estimate the actual waste output for furnaces with highly efficient burners and atomizers.

Even in the postflame gas phase, the chemical mechanism at the molecular level for typical large waste molecules is not well known. An alternative engineering approach is to describe the reaction scheme in terms of a small set of semi-global reaction rates of the Arrhenius form:

$$\frac{dC_i}{dt} = A_i C_i^a C_{O_2}^b \exp(-E_i/RT) \quad i=1,n \tag{26}$$

where $E_i$, the activation energy; $A_i$, the pre-exponential factor; and the exponents a and b are empirically determined (for pseudo-first-order rates a and b equal unity). $C_{O_2}$ is the local oxygen concentration, R is the universal gas constant, T is the local temperature, and $C_i$ is the component concentration in question. This modeling approach has been shown to offer great promise for coupled fluid mechanic/chemical kinetic problems (30).

## 5.6 BULK GAS TEMPERATURE MODEL RESULTS

The first module of the program predicts the distribution of heat flows lost through the furnace walls and a single axial gas temperature profile. The energy balance model is quite successful in predicting bulk gas temperatures over a range of firing conditions and furnace configurations. An effort was made to limit the required number of inputs and computational time and still achieve accurate postflame predictions. The following section describes the computational approach and model inputs used to describe the pilot-scale parametric tests.

### 5.6.1 Solution Approach

Two energy balances were described in Section 5.4.1. Case I essentially ignores any interaction between zones. Case II is more comprehensive in that it describes recirculation of gases from downstream to upstream zones and radiation interchange between zones. Case II increases the computational time five-fold, yet for a broad range of cases provides little additional accuracy. For a single-burner front-wall-fired furnace, for example, the bulk gas temperature decreases uniformly beyond the flame zone, and the extra modeling complexity is not required. This is not the case, say, for an opposed-wall-fired utility steam generator in which recirculation patterns dominate a large fraction of the firebox and large temperature gradients exist both above and below the burner levels. Since the immediate requirement of this model is to simulate the physical processes governing hazardous waste destruction in the Acurex Pilot-Scale Furnace, the discussion will be restricted to the Case I energy balance. Highest accuracy is sacrificed in favor of rapid computation. The major source of error results from the fact that the waterwalls one and two zones downstream of zone j do not receive any radiation from j, in spite of any view factor considerations.

Figure 25 shows a flowchart with the salient bulk temperature computation features. The data input section includes furnace dimensions, zone wall fractions occupied by waterwall, and operating conditions. The input data is retrieved from floppy disk files or can be manually input. The user selects one of three additional input sets: (1) refractory wall temperatures, (2) water wall steam heat losses, or (3) bulk gas temperature/refractory wall temperature differences. In essence, the choice determines the boundary condition for each zone that governs the radiative transfer solution. The first two input options, though giving greatest accuracy, are the hardest to specify in practice. A typical furnace operator could not assess with great certainty the distribution of refractory wall temperatures or waterwall heat losses along the firebox center (although they are measured in this study). The third option is far simpler to use; at a minimum one need only specify a single average difference between the expected bulk temperature and refractory wall temperature, averaged over the entire furnace length.

The program fixes the zone length at one-quarter the hydraulic diameter of the furnace. The following parameters are calculated for each zone: mass fractions of $CO_2$, $H_2O$, $O_2$, and $N_2$; surface areas of refractory and waterwall; volume fraction occupied by luminous flame; and chemical heat release within the zone.

The solution to the zone energy balances (Equation 1) follows. The algorithm is a modification of the ZEROIN FORTRAN code developed in 1973 (31). It solves a nonlinear equation by combining three different standard techniques: the bisection method, the secant method, and inverse quadratic interpolation.

Incorporating bisection guarantees that a root of the equation $f(T) = \Sigma Q_I = 0$, where T is the bulk gas temperature, will be found irrespective of the function behavior, if it exists in the chosen interval. Two abcissas (temperatures), $T_A$ and $T_B$, are selected initially which are known to bound the solution. Typically the program uses 1,000° and 4,000°R to cover the range of conceivable firebox temperatures. The function $f(T_A)$ and $f(T_B)$ are calculated. In terms of the heat balance, this means:

- Calculating the gas emissivity (at $T_A$ and $T_B$), which depends on soot loading and gas composition

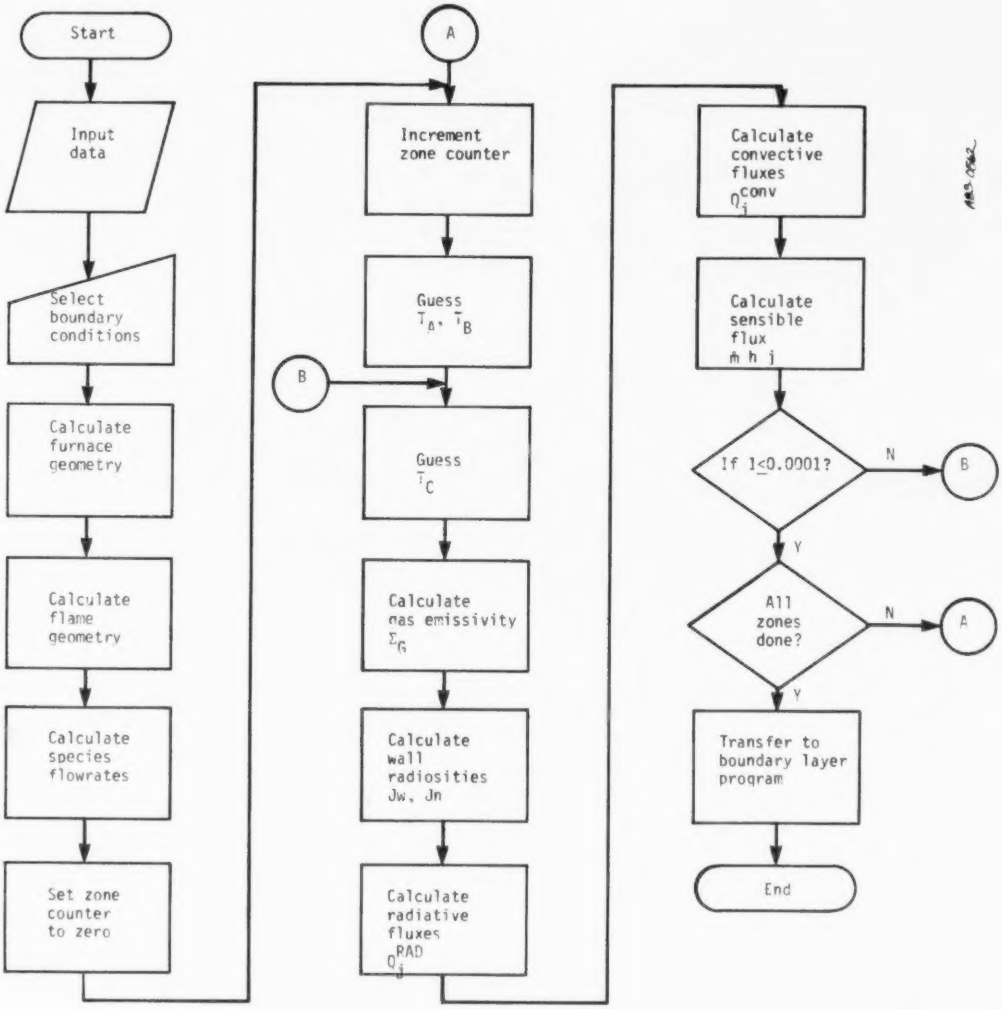
Start
Input data
Select boundary conditions
Calculate furnace geometry
Calculate flame geometry
Calculate species flowrates
Set zone counter to zero
A
Increment zone counter
Guess $T_A$, $T_B$
B
Guess $T_C$
Calculate gas emissivity $\Sigma_G$
Calculate wall radiosities Jw, Jn
Calculate radiative fluxes $Q_j^{RAD}$
Calculate convective fluxes $Q_j^{conv}$
Calculate sensible flux $\dot{m}$ h j
If $1 \leq 0.0001$?
N
B
Y
All zones done?
N
A
Y
Transfer to boundary layer program
End

Figure 25. Program flow chart for Case I bulk gas temperature model.

- Calculating the radiosities $J_W$ and $J_R$ at the walls, which depend on the gas emissivity, wall emissivities, wall surface areas, refractory insulation factor $K_R$, furnace "speckledness," and wall temperatures
- Calculating the radiative transfer terms, which depend on the radiosities
- Calculating the convective transfer terms and sensible energy leaving the zone
- Summing the energy flows into and out of the zone to get $f(T_A)$ and $f(T_B)$

Then $f(T_C)$ is calculated, where $T_C$ is the average of $T_A$ and $T_B$. If $f(T_A)$ and and $f(T_B)$ have the same sign, then $T_C$ replaces $T_A$, and the process is repeated. Otherwise $T_C$ replaces $T_B$.

Linear interpolation (the secant method) is considerably faster than bisection when the function evaluation approaches the root. The new guess, $T_C$, is found from the previous two guesses as the unique zero of the linear function that has the value $f(T_B)$ at $T_B$ and the value $f(T_A)$ at $T_A$. It is easily shown that:

$$T_C = T_B - \frac{f(T_B)}{(f(T_A) - f(T_B))/(T_A - T_B)} \tag{27}$$

$T_C$ replaces $T_B$, $T_B$ replaces $T_A$, and iteration is continued until the convergence criterion is met.

When f(T) has been evaluated at more than two temperatures, the convergence can be accelerated further by calculating the zero associated with a higher order function than a line. Inverse quadratic interpolation is analagous to linear interpolation in that the new guess, $T_D$, is calculated from the zero of the quadratic unique to the last three guesses: $T_A$, $T_B$, and $T_C$. The expression for $T_D$, however, can only be evaluated if $f(T_A)$, $f(T_B)$, and $f(T_C)$ are distinct. Also, the algorithm behavior can be extremely erratic far away from the function root.

The approach used here chooses the next iterate from two candidates -- one given by bisection and one by interpolation. Inverse quadratic interpolation is used when the three previous evaluations are distinct and linear interpolation is used when they are not. The interpolation answer is chosen only if it is within the current interval and is "reasonably" far from the endpoints; otherwise the bisection guess is carried over. In this way, the interval length is guaranteed to decrease at each step.

The number of function evaluations (energy balances) per zone is no greater than $\log_2 [(T_B - T_A)/(1/2\ \varepsilon + 2\ \varepsilon_M|T_B|)]$, where $\varepsilon$ is the convergence tolerance and $\varepsilon_M$ is the relative machine precision. The value of $\varepsilon$ was set to $1.0 \times 10^{-4}$; i.e., the net energy flux into a zone is zero to four decimal places. For the Apple II+ computer, $\varepsilon_M$ equals $1.0 \times 10^{-11}$. With the initial guesses $T_B$ and $T_A$ set to 4,000° and 1,000°R, the actual number of function evaluations required is usually between six and nine. The real time requirements is only on the order of several seconds, even using a slow BASIC interpreter.

Once the calculation is completed for each zone, the bulk gas temperatures and refractory wall temperatures are passed to a disk file which is used as input to the boundary layer program module.

### 5.6.2 Parameter Sensitivity Analysis

Postflame thermal oxidation kinetics of hazardous wastes are extremely sensitive to temperature. It is therefore instructive to characterize the effect on temperature history of the furnace configuration and primary fuel firing conditions. The model provides a tool for quantifying these effects. The principle parameters of interest have been varied individually to simply rank their impact on the axial temperature profile and test the model behavior. The baseline inputs, typical of firing distillate oil in the Acurex Pilot-Scale Furnace are summarized in Table 13.

Figure 26 shows two pages of computer printout for the baseline case. The first includes the essential inputs to the program; the second is the calculated energy flows and temperatures at each zone. Column 1 of page 2 shows the axial distribution of chemical energy released into the zone. The nonzero values indicate the presence of the luminous flame within the zone. The sum of the zone contributions equals the firing rate, the product of mass feed rate of fuel, and its higher heating value. The ratio is in proportion to the flame volumes occupying the zones. Column 2 shows the net radiation loss from the zone to other zones. In Case I, gas/gas radiative transfer is not considered so all entries are zero. Column 3 shows the radiative loss from the gas stream to the waterwalls, $Q_{WW}^{RAD}$; Column 4 shows the radiative interchange from the gas stream to the refractory walls, $Q_{REF}^{RAD}$ in Equation (6-1). Note that the transfer to the refractory is much greater than to the waterwall, roughly in proportion to the refractory/waterwall surface area ratio (10:1). Columns 5 and 6 are the analagous flows due to convective transfer. Because convective transfer goes as the gas/wall temperature difference, the heat flux (per unit area) to the cold waterwall is much higher than to the hot refractory wall. The heat flows are thus very close even with the relatively small waterwall area. Note that the total convective transfer only approaches the radiant transfer at the low temperatures near the firebox exit. Column 7 shows the sensible energy carried out of the zone, $\dot{m}h_j$. The first row ("zone 0") shows the energy carried in with the preheated air, generally between 5 and 10 percent of the firing rate. As a check on the energy balance, the sum of the sensible energy leaving the final zone and the total convective and radiative losses from the gas stream should equal the sum of the combustion air sensible energy and the total chemical energy. Columns 8 and 9 contain the total heat loss through the refractory and waterwall, $Q_{REF}$ and $Q_{WW}$. The values include

TABLE 13. BASELINE BULK TEMPERATURE MODEL INPUTS

| Parameter | Baseline value |
|---|---|
| Operating inputs | |
| Firing rate | 1.0 million Btu/hr |
| Excess air | 25 percent |
| Fuel heat of combustion | 19,200 Btu/lb |
| Fuel C:H mass ratio | 6.74 |
| Air preheat | 350°F |
| Fuel moisture fraction | 0 |
| Furnace design variables | |
| Waterwall temperature | 170°F |
| Refractory/bulk gas temperature differential | 200°F |
| Waterwall emissivity | 0.95 |
| Refractory emissivity | 0.44 |
| Refractory conductivity factor | 0.032 |
| Wall "speckledness" | 0.95 |
| Waterwall surface fraction | 0.10 |
| Furnace hydraulic diameter | 2.75 ft |
| Flame parameters | |
| Soot mass loading | $5 \times 10^{-4}$ g/g |
| Maximum flame diameter | 2.75 ft |

```
***** INPUTS *****


FURNACE WIDTH (DIAM) (FT):     2.75      FURNACE LENGTH (FT)          11
GEOMETRY NUMBER (1-2):         2         MAX FLAME DIAM (FT)          2
WATER WALL TEMP (DEG R):       630       EXIT TEMP (DEG R)            1250
FUEL TEMP (DEG R):             540       AIR TEMP (DEG R)             810
HEAT INPUT RATE (MBTU/HR):     1         FUEL HEAT CAPACITY:          .045
REFR EMISSIVITY:               .44       W-WALL EMISSIVITY:           .95
REFR INSUL FACTOR:             .032      SPECKLEDNESS:                .95
SOOT MASS LOADING:             5E-04


SPECIES MASS FLOW RATES (LB/HR)

                         COMBUSTION AIR      FLUE GAS
         NITROGEN        709.18              708.4
         OXYGEN          215.56              42.93
         CARBON DIOXIDE  0                   164.9
         WATER           0                   59.52
         TOTAL           924.74              975.75


FURNACE WALL GEOMETRY

ZONE        W-WALL FRAC     W-WALL AREA (SQ FT) REFR AREA (SQ FT)   ZONE CENTER (FT)
==========================================================================================
  1          .1              .594                11.285              .344
  2          .1              .594                5.346               1.031
  3          .1              .594                5.346               1.719
  4          .1              .594                5.346               2.406
  5          .1              .594                5.346               3.094
  6          .1              .594                5.346               3.781
  7          .1              .594                5.346               4.469
  8          .1              .594                5.346               5.156
  9          .1              .594                5.346               5.844
  10         .1              .594                5.346               6.531
  11         .1              .594                5.346               7.219
  12         .1              .594                5.346               7.906
  13         .1              .594                5.346               8.594
  14         .1              .594                5.346               9.281
  15         .1              .594                5.346               9.969
  16         .1              .594                5.346               10.656
```

Figure 26a. Baseline bulk temperature model major inputs printout.

```
          $$$$$ ENERGY FLOWS (MBTU/HR) $$$$$                                                        $$$ TEMPS (F) $$$
FROM                              GAS       GAS       GAS       GAS       GAS
-------------------------------------------------------------------------------------------------------------------
TO                  GAS     GAS   WW        REFRAC    WW        REFRAC              REFRAC    WW
-------------------------------------------------------------------------------------------------------------------
MODE                CHEM    RAD   RAD       RAD       CONV      CONV      SENS      TOT       TOT
-------------------------------------------------------------------------------------------------------------------
ZONE
                                                                                                      BULK GAS  REF WALL
===================================================================================================================
0      0            1       0     0         0         0         0         .0613     0         0         0         0
1      0            .7581   0     .0158     .2494     2.3E-03   4.5E-03   .5474     .1177     .1543     2093      1893
2      0            .242    0     .0241     .1463     2.6E-03   2.1E-03   .6143     .042      .1331     2318      2118
3      0            0       0     3.4E-03   .0296     2.4E-03   2.1E-03   .5766     2.2E-03   .0354     2192      1992
4      0            0       0     3.2E-03   .027      2.3E-03   2.1E-03   .542      2.8E-03   .0318     2075      1875
5      0            0       0     2.9E-03   .0245     2.1E-03   2.1E-03   .5104     3.2E-03   .0284     1967      1767
6      0            0       0     2.6E-03   .0221     2E-03     2.1E-03   .4816     3.4E-03   .0254     1868      1668
7      0            0       0     2.3E-03   .0199     1.9E-03   2.1E-03   .4554     3.6E-03   .0227     1777      1577
8      0            0       0     2.1E-03   .0179     1.8E-03   2.1E-03   .4314     3.6E-03   .0203     1694      1494
9      0            0       0     1.9E-03   .0161     1.7E-03   2.1E-03   .4095     3.6E-03   .0183     1617      1417
10     0            0       0     1.7E-03   .0145     1.6E-03   2.1E-03   .3895     3.6E-03   .0165     1547      1347
11     0            0       0     1.6E-03   .0132     1.6E-03   2.1E-03   .3711     3.5E-03   .0149     1481      1281
12     0            0       0     1.4E-03   .0119     1.5E-03   2.1E-03   .3542     3.5E-03   .0135     1421      1221
13     0            0       0     1.3E-03   .0108     1.4E-03   2.1E-03   .3385     3.4E-03   .0123     1365      1165
14     0            0       0     1.2E-03   9.9E-03   1.4E-03   2.1E-03   .324      3.4E-03   .0112     1312      1113
15     0            0       0     1.1E-03   9E-03     1.3E-03   2.1E-03   .3105     3.3E-03   .0102     1264      1064
16     0            0       0     1E-03     8.2E-03   1.2E-03   2.1E-03   .2979     3.2E-03   9.4E-03   1218      1018
-------------------------------------------------------------------------------------------------------------------
TOTAL  0            1.0001  0     .0676     .6304     .0291     .0366     6.9545    .206      .5577
```

Figure 26b. Baseline bulk temperature model outputs printout.

the contributions of both convection and radiation. The radiative loss to the refractory, $Q_{REF}$, is equal to $Q_{REF}^{RAD}$, the net radiation from the gas stream to the refractory, minus $Q_{RW}^{RAD}$, the sum of the reradiated and reflected components which are transmitted to the waterwall. The total waterwall heat loss, summed over the furnace length, is approximately three times the loss through the refractory. The final two columns show the calculated bulk gas temperatures and refractory wall temperatures. The difference in each zone has been fixed at 200°F for the baseline case.

The results of varying the inputs are summarized in Table 14. Four key temperatures, from Zones 2, 4, 10, and 16 are listed. Most of the inputs were varied by 20 percent of their absolute values in the direction of increasing flame temperature. Several parameters were varied more widely to cover a likely range of operation. In most cases the new temperatures are higher than the baseline temperatures along the entire furnace length.

For two cases, however, decreasing the excess air level and decreasing the flame diameter, the exit temperature decreased as the flame temperature increased. Decreasing the excess air level at a fixed firing rate has two consequences. The flame temperature is higher without the additional air because energy is exhausted in heating up excess nitrogen and oxygen. The exit temperatures are lower because of the loss in sensible energy associated with the decreased total mass flowrate. The slope of the temperature curve changes with flame diameter because of the redistribution of radiative transfer from the zones occupied by the flame. Recall the flame shape is assumed to be a cone frustum. At a fixed firing rate, decreasing the large diameter is equivalent to stretching the cone, because of the assumption of uniform volumetric chemical heat release. The first zone is cooler, because a smaller fraction of the heat is released there (less flame volume). The second zone is hotter, because more chemical heat is released there. The total radiative loss to the walls will be greater from the stretched flame cone, because its effective surface area is greater. Thus, the sensible energy entering the postflame region will be lower.

Table 15 shows a gross rating of parameter effects on the temperature-position profile of the baseline furnace configuration. The inputs are divided into three categories according to their potential for influencing the postflame thermal environment. One caveat is appropriate: the model inputs can be varied independently of one another. In actual operation, this may not be possible. For example, the carbon:hydrogen ratio of the fuel, inasmuch as it effects the equilibrium $CO_2:H_2O$ ratio and consequently the gas emissivity and enthalpy, has little effect on the heat loss rate. In practice, however, two fuels with different hydrocarbon compositions may have remarkably different heating values. The difference in furnace temperature history will be dramatic.

### 5.6.3 Comparison With Pilot-Scale Experiments

The model was run with inputs corresponding to a range of firing conditions in the experimental test matrix. Furnace diameter, furnace length, waterwall temperature, refractory emissivity, waterwall emissivity,

Table 14. Bulk Gas Temperature Profile Sensitivity

| Variable | Value | Percent change from baseline | Temperatures (°F) | | | |
|---|---|---|---|---|---|---|
| | | | Zone 2 | Zone 4 | Zone 10 | Zone 16 |
| Baseline Case | | | 2,318 | 2,075 | 1,547 | 1,218 |
| Firing rate | 1.2 million Btu/hr | +20 | 2,394 | 2,279 | 1,749 | 1,400 |
| Excess air | 0 percent | -20 | 2,612 | 2,060 | 1,417 | 1,066 |
| Fuel heat of combustion | 23,040 Btu/lb | +20 | 2,312 | 2,337 | 1,706 | 1,320 |
| Fuel C:H ratio | 5.40 | -20 | 2,345 | 2,071 | 1,546 | 1,219 |
| Air preheat | 512°F | +20 | 2,219 | 2,099 | 1,561 | 1,227 |
| Fuel moisture fraction | 0.10 | -10 | 2,318 | 1,987 | 1,447 | 1,194 |
| Waterwall temperature | 296°F | +20 | 2,323 | 2,077 | 1,550 | 1,224 |
| Gas-refractory temperature difference | 100°F | -50 | 2,368 | 2,087 | 1,572 | 1,253 |
| Waterwall emissivity | 0.76 | -20 | 2,338 | 2,124 | 1,589 | 1,254 |
| Refractory emissivity | 0.34 | -20 | 2,374 | 2,092 | 1,558 | 1,226 |
| Refractory conductivity factor | 0.003 | -75 | 2,314 | 2,124 | 1,578 | 1,240 |
| Speckledness | 0.50 | -50 | 2,314 | 2,071 | 1,543 | 1,215 |
| Waterwall surface fraction | 0.08 | -20 | 2,355 | 2,109 | 1,574 | 1,239 |
| Furnace diameter | 2.20 ft | -20 | 2,673 | 2,296 | 1,909 | 1,612 |
| Soot mass loading | $4 \times 10^{-4}$ | -20 | 2,352 | 2,104 | 1,564 | 1,230 |
| Maximum flame diameter | 1.8 ft | -10 | 2,412 | 1,948 | 1,470 | 1,167 |

TABLE 15. SENSITIVITY RANKING OF BULK TEMPERATURE MODEL INPUTS

High Sensitivity Inputs

- Feed rate
- Excess air
- Fuel heating value
- Furnace surface area
- Flame shape
- Fuel moisture content

Medium Sensitivity Inputs

- Waterwall emissivity
- Refractory conductivity
- Soot loading
- Refractory temperature
- Air preheat

Low Sensitivity Inputs

- Waterwall temperature
- Refractory emissivity
- Speckledness
- Fuel C:H ratio

refractory conductivity factor, speckledness, and soot mass loading were the same for every model run. Firing rate, excess air, fuel composition, fuel moisture content, waterwall surface area, flame diameter, and refractory/gas temperature difference were matched to experimental observations.

Approximations were necessary for certain furnace design variables. For simplicity, the refractory/bulk gas temperature difference was fixed at ~110°C (200°F) over the length of the firebox for the case with all waterwalls present, and ~170°C (300°F) with no waterwalls. The average waterwall temperature was fixed at ~77°C (170°F) by solving an energy balance on a panel. Because of the dependence of radiant transfer on the difference in temperatures raised to the fourth power, however, this value is not crucial to the model. The waterwall emissivity was fixed at 0.81, the average normal emissivity of a steel sheet with a rough oxide coating (23). The emissivity of different refractory types varies widely. White refractory emissivity can be below 0.3 at 2,000°F, fire clay emissivity is above 0.7. An intermediate value of 0.44 was chosen. Again the waterwall model is not extremely sensitive to the choice. The greater the insulation value of the refractory, the less sensitive the heat transfer is to the refractory emissivity. The refractory conductivity factor, $K_R$, was chosen to agree with that of (6-7). The soot mass loading was arbitrarily fixed at $5 \times 10^{-4}$ g/g. Finally, the flame diameter was taken from visual observation to be 2.0 ft at an oil pressure of 45 psig, and 2.3 ft at 80 psig. The relationship was assumed to be linear in between.

Figure 27 shows a comparison between the model and several experimental results. The experimental bulk temperature values are calculated as the weighted average of seven radial measurements. There is good agreement for a range of postflame temperatures of ~900°C (1,600°F). The comparisons include several firing rates and stoichiometries, as well as tests with and without waterwalls in place. The experimental temperature measurements do not correspond to steady-state conditions. The zone energy balance has no time-dependent term. It would be expected, therefore, that the model predicts temperatures in excess of the measured values. This is indeed the case at the high-temperature conditions.

The model prediction of the relative heat loss through waterwalls and refractory walls also agrees well with data from the pilot-scale tests. Figure 28 compares the model to the experiment waterwall heat loss for a range of firing rates at the nominal 25 percent excess air condition.

## 5.7 BOUNDARY LAYER MODEL RESULTS

The second module of the program performs the following:

- Extends the single bulk gas temperature profile to a set of radial temperature profiles, one for each zone
- Calculates a set of radial velocity profiles, one for each zone

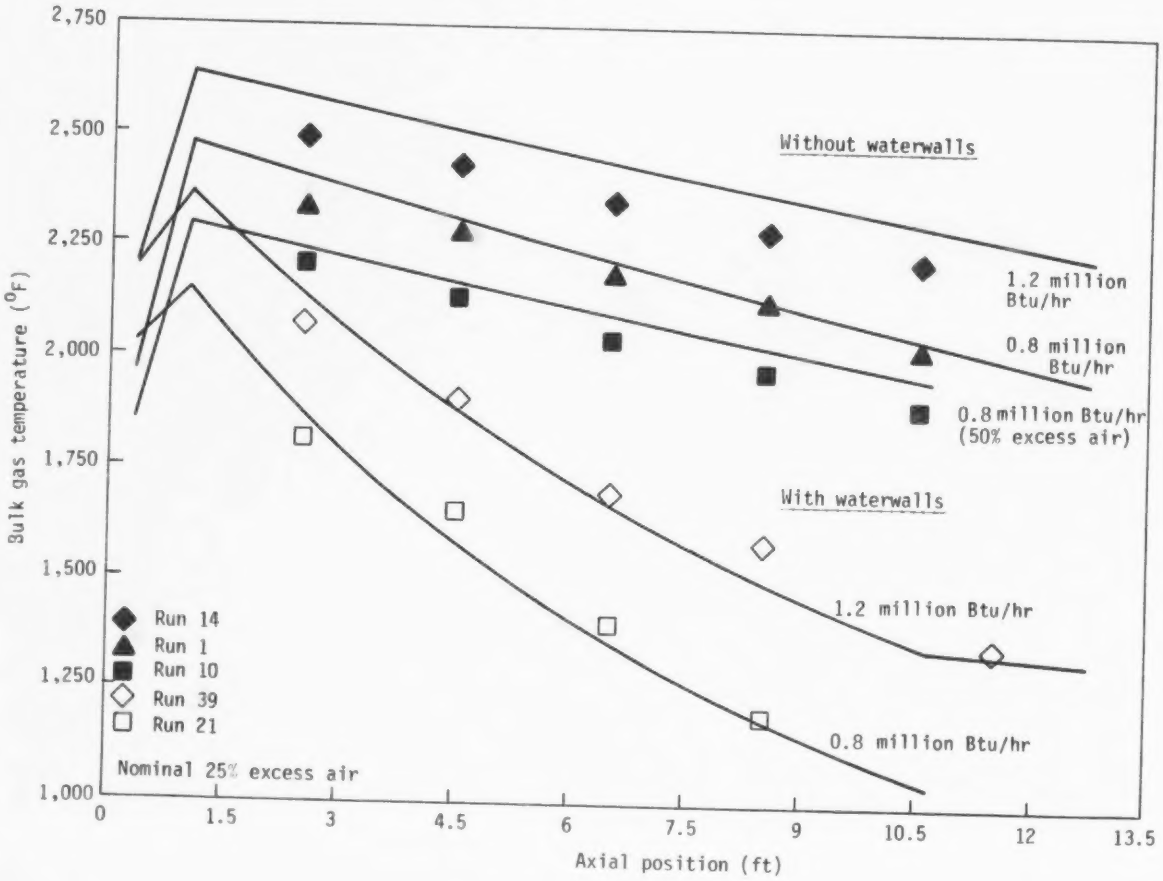

Figure 27. Comparison of model (solid line) to experimental bulk gas temperature data.

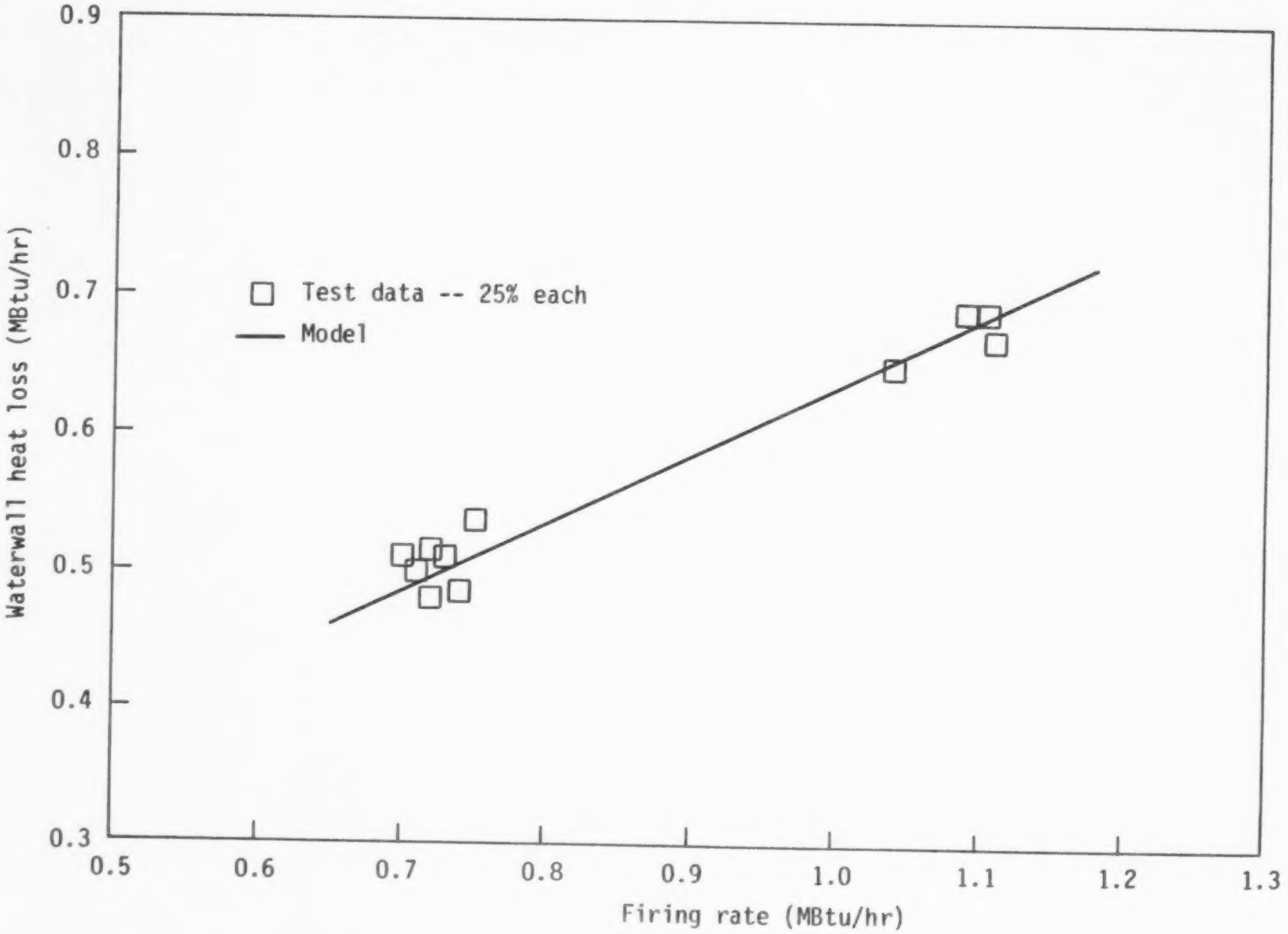

Figure 28. Comparison of model and experimental waterwall heat losses.

## 5.7 BOUNDARY LAYER MODEL RESULTS

The second module of the program performs the following:

- Extends the single bulk gas temperature profile to a set of radial temperature profiles, one for each zone
- Calculates a set of radial velocity profiles, one for each zone
- Calculates a set of axial waste concentration profiles, one for each annular slice
- Reduces the set of concentration profiles to a single, bulk gas, waste concentration profile

The following section describes the essential computational features and a set of trial runs.

### 5.7.1 Solution Approach

The solution of the velocity and temperature boundary layers are straightforward, as described in Section 5.5. The result is a set of axial time-temperature profiles, corresponding to concentric annular slices of the furnace. The program integrates the set of global kinetic expressions along each of the concentric paths.

For each annulus the following set of nonlinear first-order differential equations is solved:

$$f_1 = \frac{dT}{dt} = \sum_{i=1}^{5} iA_i t^{i-1} \qquad (28a)$$

$$f_j = \frac{dC_j}{dt} = -k_j(T,O_2)C_j^a \qquad j = 2, N \qquad (28b)$$

where the $A_i$ are the fifth-order polynomial least-squares coefficients that correlate temperature with residence time, and the $C_j$ are the set of N principal waste components. The polynomial curve fit is necessary to give a continuous temperature profile, because the time step for integration will necessarily be far smaller than the typical zone residence time.

The initial value problem is solved by a modification of the fourth-order Runge-Kutta technique. Let y be one of the dependent variables for which we are solving. The unmodified method approximates a Taylor Series expansion by:

$$y_{n+1} = y_n + \frac{1}{6}(m_0 + 2m_1 + 2m_2 + m_3) \qquad (29)$$

where $y_n$ is the nth evaluation of y, and

$m_0 \equiv hf(y_n, t_n)$

$m_1 \equiv hf(y_n + \alpha m_0, t_n + \beta h)$

$m_2 \equiv hf(y_n + \alpha m_1, t_n + \beta h)$

$m_3 \equiv hf(y_n + m_2, t_n + h)$

where h is the time step, f is the derivative function, and $\alpha$ and $\beta$ are constants whose values are chosen for best accuracy. The algorithm is "self-starting"; one need only specify the initial value, $y_0$, and time, $t_0$, to generate the solution profile. Note four function evaluations are necessary for every time step.

To solve the furnace problem, the initial time is zero, the initial waste concentration is unity (so that the solution represents fractional breakthrough $C/C_0$), and the initial temperature is given by the curve fit evaluation at the initial zone. The solution accuracy increases as the time step decreases. A time step of 0.005 sec was found to be sufficient for most model cases. With 16 zones and 3 annuli, the real computation time on the Apple II+ was between 15 and 20 min.

### 5.7.2 Baseline Parameter Effects

The baseline bulk temperature model conditions (Table 13) were applied to the boundary layer model. Several runs were made with carbon tetrachloride as the injected waste. The additional inputs required by the second module are summarized in Table 16.

The first five entries specify the calculation grid. "First zone" and "last zone" refer to the starting and ending zones for the integration; $C/C_0$ is set to unity at the center of the first zone. The calculation begins in the third zone, downstream of the zones occupied by the flame. The farther downstream of the flame, the more conservative the estimate of destruction efficiency.

The shape of the radial temperature profiles is specified by the boundary layer thickness and polynomial order. For simplicity, the temperature is assumed to be constant across the center of the furnace and to drop off linearly at one-quarter of a radius from the wall. This is a reasonable representation of the experimental temperature data (see Figure 5).

The furnace is divided into three concentric annuli whose borders are one-eighth and one-quarter of a radius from the wall. Computational time is saved by selecting a small number of annuli, at the expense of a conservative DRE prediction.

TABLE 16. BASELINE BOUNDARY LAYER MODEL INPUTS

| Parameter | Baseline value |
|---|---|
| Furnace Inputs | |
| First zone | 3 |
| Last zone | 10 |
| Temperature boundary layer thickness | 25 percent furnace radius |
| Temperature boundary layer polynomial order | 1 |
| Annuli locations | 0 percent<br>12.5 percent<br>25 percent<br>100 percent furnace radius |
| Chemical Kinetic Inputs | |
| Pre-exponential factor, $A_{21}$ | $2.75 \times 10^5$ $S^{-1}$ |
| Activation energy, $E_A$ | 25.5 Kcal/gmole |
| Oxygen factor, f | 0.229 |
| Waste exponent, b | 1 |

The pseudo first-order rate constants used for inputs to the model were taken from the literature (32, 33). They were derived from the fixed temperature oxidation of dilute vapors of hazardous waste in air in a quartz tube flame reactor. The rate constants are not well suited to the furnace model because they do not include an oxygen-dependent term; the available constants pertain only to a 21 percent oxygen level. The mole percent of oxygen in furnaces operating in the 10 to 50 percent excess air regime is well below 10 percent. The form of the rate constant, k, in equation (30) is:

$$k = A\, C_{O_2}^{b} \exp(-E/RT) \tag{30}$$

where A is a constant independent of oxygen concentration. We introduce a factor, f, defined by

$$f = \left(\frac{A_{21}}{A}\right) C_{O_2}^{\ b} = \left(\frac{C_{O_2}}{0.21}\right)^{b} \tag{31}$$

where $A_{21}$ is the pre-exponential factor determined experimentally at 21 percent oxygen, and $C_{O_2}$ is the equilibrium mole percent of oxygen in the postflame gases. $C_{O_2}$ is assumed constant over the entire combustor length. The rate becomes:

$$k = A_{21}\ f\ \exp(-E/RT) \tag{32}$$

In the absence of an established oxygen dependence, b was set equal to unity for the baseline condition. The values of $A_{21}$ and E correspond uniquely to carbon tetrachloride (34).

Table 17 shows the important components of the computer output for the baseline case. The four tables correspond to three annuli and the overall bulk flow results. Each table shows the cumulative residence time, temperature, and mass fraction waste breakthrough, $C/C_0$, at the center of each zone. Note DRE is related to $C/C_0$ by:

$$DRE = (1 - C/C_0)(100) \tag{33}$$

The overall fractional breakthrough, under the "bulk flow" heading, is simply the average of each annular contribution, weighted by the flowrate through the annulus. In this case, the postflame gases in the furnace center promote

## TABLE 17. BASELINE BOUNDARY LAYER MODEL OUTPUT FOR THREE ANNULI AND BULK CONDITIONS

```
ANNULUS #1          INTERVAL: 0 < R/RO < .125
                    VOL FLOW %: 1.16

ZONE       RES TIME  GAS TEMP  C/CO
            (SEC)      (F)
-------------------------------------------
1          .33       1950      0
2          .63       2175      0
3          .95       2049      .871872453
4          1.28      1932      .219421909
5          1.63      1824      .0763579507
6          1.99      1725      .0344029186
7          2.37      1634      .0194124566
8          2.76      1551      .0132512905
9          3.16      1474      .0103205832
10         3.59      1404      8.8540794E-03
11         4.01      1338      8.8540794E-03
12         4.46      1278      8.8540794E-03
13         4.92      1222      8.8540794E-03
14         5.4       1169      8.8540794E-03
15         5.88      1121      8.8540794E-03
16         6.38      1075      8.8540794E-03
```

```
ANNULUS #2          INTERVAL: .125 < R/RO < .25
                    VOL FLOW %: 3.97

ZONE       RES TIME  GAS TEMP  C/CO
            (SEC)      (F)
-------------------------------------------
1          .29       2064      0
2          .56       2289      0
3          .83       2163      .810777776
4          1.12      2046      .12423283
5          1.43      1938      .0283117855
6          1.75      1839      8.99552279E-03
7          2.08      1748      3.83390225E-03
8          2.42      1665      2.12458236E-03
9          2.78      1588      1.41113209E-03
10         3.14      1518      1.08800238E-03
11         3.52      1452      1.08800238E-03
12         3.92      1392      1.08800238E-03
13         4.32      1336      1.08800238E-03
14         4.74      1283      1.08800238E-03
15         5.17      1235      1.08800238E-03
16         5.61      1189      1.08800238E-03
```

```
ANNULUS #3          INTERVAL: .25 < R/RO < 1
                    VOL FLOW %: 94.87

ZONE       RES TIME  GAS TEMP  C/CO
            (SEC)      (F)
-------------------------------------------
1          .24       2121      0
2          .46       2346      0
3          .7        2220      .77404394
4          .94       2103      .115215436
5          1.19      1995      .0248640887
6          1.46      1896      7.25439314E-03
7          1.74      1805      2.99500088E-03
8          2.02      1722      1.54873923E-03
9          2.32      1645      9.82923458E-04
10         2.63      1575      7.25003158E-04
11         2.95      1509      7.25003158E-04
12         3.27      1449      7.25003158E-04
13         3.61      1393      7.25003158E-04
14         3.96      1340      7.25003158E-04
15         4.32      1292      7.25003158E-04
16         4.69      1246      7.25003158E-04
```

```
BULK FLOW CONDITIONS

ZONE      GAS TEMP  WALL TEMP RES TIME  REYN NO   VEL       WEIGHTED C/CO
            (F)       (F)      (SEC)              (FT/S)
------------------------------------------------------------------------------
1         2093      1893      .24       3654      2.81      0
2         2318      2118      .47       3654      3.06      0
3         2192      1992      .71       3654      2.92      .776635988
4         2075      1875      .95       3654      2.79      .116782428
5         1967      1767      1.21      3568      2.67      .0255984386
6         1868      1668      1.48      3568      2.56      7.6345546E-03
7         1777      1577      1.76      3568      2.46      3.21890254E-03
8         1694      1494      2.05      3568      2.37      1.70739267E-03
9         1617      1417      2.35      3569      2.29      1.10819094E-03
10        1547      1347      2.66      3568      2.21      8.33742966E-04
11        1481      1281      2.98      3361      2.14      8.33742966E-04
12        1421      1221      3.31      3361      2.07      8.33742966E-04
13        1365      1165      3.66      3361      2.01      8.33742966E-04
14        1312      1113      4.01      3361      1.95      8.33742966E-04
15        1264      1064      4.37      3361      1.9       8.33742966E-04
16        1218      1018      4.74      3361      1.85      8.33742966E-04
```

99.93 percent DRE at Zone 10 (6.875 ft from the front wall). However, the postflame gases along the wall promote only 99.12 percent DRE at Zone 10. The bulk flow table shows that the turbulent flow boundary layer shape was calculated for the baseline case, because the bulk Reynolds number exceeded 3,000.

Figure 29 shows the baseline concentration profiles at each annulus plotted against axial position. The graph shows clearly that the cold walls quench waste conversion reactions in the postflame gases in the outermost annulus. Destruction efficiency increases sharply at greater than one-eighth of a radius from the wall. In this case the weighted average profile is very close to the centerline profile. In cases where the walls are significantly cooler relative to the bulk gas, the weighted average can be more strongly influenced by the boundary layer profile.

The chemical model, in single-step form, is very sensitive to the pre-exponential factor and extremely sensitive to the activation energy. This is apparent in integrating Equation (28) at fixed temperature and for $b = 1$:

$$\frac{C}{C_0} = \exp\left[tA\, C_{O_2}^{a} \exp(-E_A/RT)\right] \qquad (34)$$

Mass fraction breakthrough varies as the exponent of the pre-exponential factor, and the exponent of the exponent of activation energy. Figure 30 shows waste concentration profiles under the baseline conditions with the activation energy and the pre-exponential factor alternately increased by 20 percent over the baseline carbon tetrachloride values. The graph emphasizes how slight deviations in the specification of activation energy in the single-step model can drastically alter the destruction prediction.

The effect of increasing firing rate can also be understood in terms of Equation (26). Breakthrough varies as the exponent of residence time and the exponent of the exponent of temperature. If the combustor volumetric heat release is such that increasing firing rate causes a reasonable temperature rise, the destruction efficiency should increase; the temperature effect dominates the residence time effect. Figure 31 compares the destruction profile at three annuli for the 1.2 million Btu/hr case to the baseline 1.0 million Btu/hr case. Each furnace region contributes to greater carbon tetrachloride destruction efficiency at the higher firing rate.

The effect of excess air on destruction efficiency is more complicated. At a fixed firing rate, increasing the excess air results in four effects, it:

- Increases the oxidation rate, according to the oxygen dependence in Equation (26)

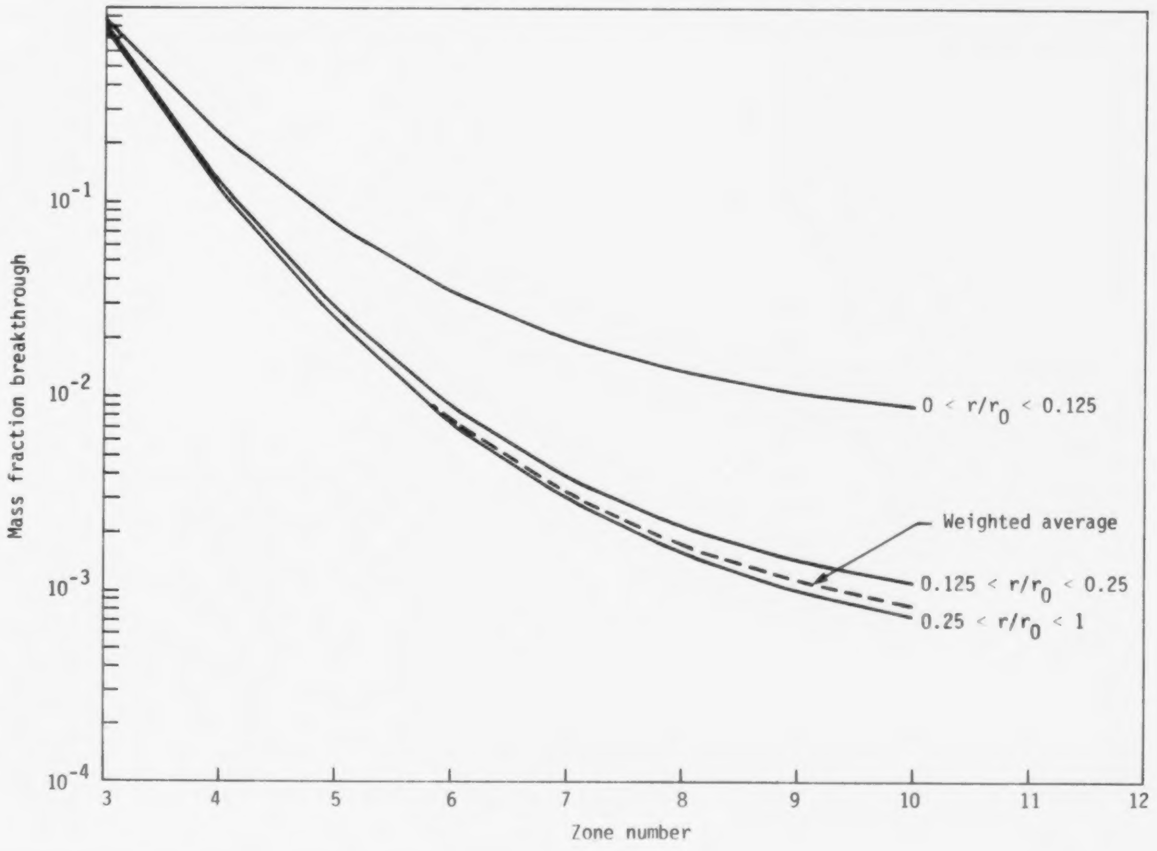

Figure 29. Baseline axial carbon tetrachloride concentration profiles.

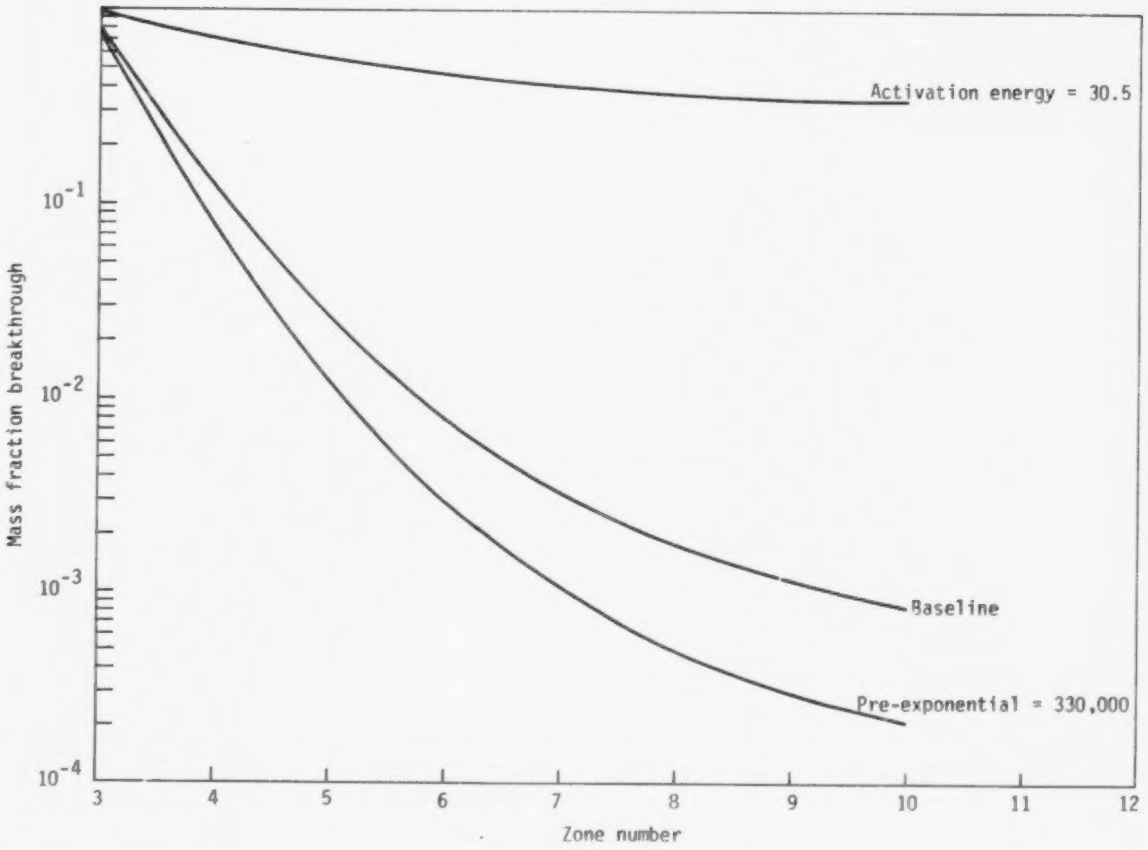

Figure 30. Effect of 20 percent increase in Arrhenius constants on baseline bulk concentration profiles.

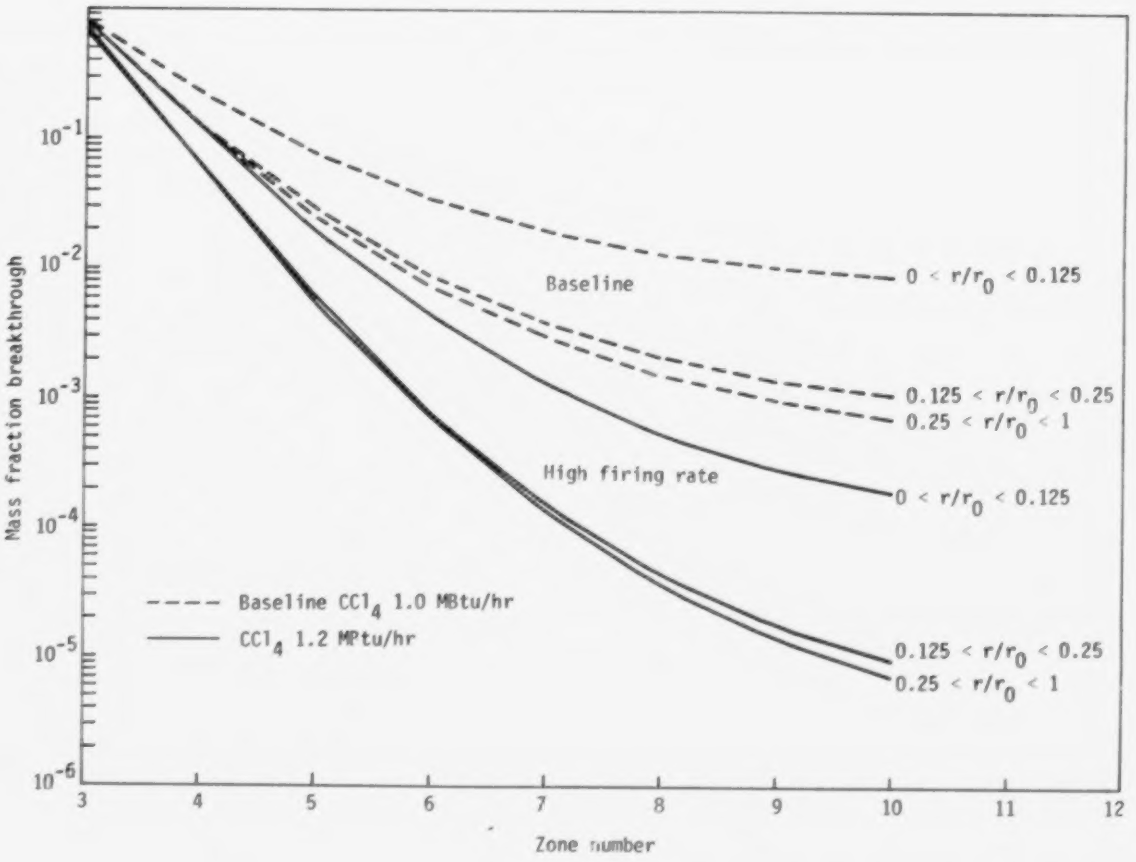

Figure 31. Effect of firing rate on three-annuli baseline $CCl_4$ destruction.

- Decreases the near-flame temperatures, because of the energy loss in heating the excess nitrogen

- Decreases the residence time, because of the higher mass flowrate

- Increases the near-exit temperatures, when the change in mass flowrate is proportionally greater than the change in wall heat loss. This is often the case with a large waterwall surface area.

The first and last effects tend to promote waste destruction, the second and third tend to inhibit it. Because of these competing effects, the result of increasing excess air for a given furnace type and operating regime is not at all obvious. Destruction efficiency can increase with excess air level, decrease with excess air level, or show a relative maximum depending on the input parameters. Figure 32 shows the weighted average, carbon tetrachloride breakthrough at 10 percent, 25 percent, and 50 percent excess air levels, with all other baseline conditions intact. In this case, the effect of oxygen availability dominates the destruction efficiency; the model predicts increasing destruction efficiency with increasing excess air level for this operating regime and furnace configuration. Particular care should be taken in not interpreting this trend as characteristic of all or even most waste types, furnace types, or firing conditions. The oxygen dependency in the kinetic expression has not been well defined by experiment. The oxygen exponent, a, for example, was randomly chosen to have the value of 1. An oxygen exponent of less than 1 would result in a prediction of greater destruction at every excess air level. However, it would also tend to decrease the variation of destruction with oxygen concentration, so that gas temperature and residence time would determine the shape of the curves in Figure 32.

Furthermore, for simplicity, a single term was selected to describe destruction, rather than separate, additive terms for oxidation and pyrolysis. Distinct oxidative and pyrolytic kinetic constants are not presently available for the waste compounds of interest. The simplified model therefore predicts no destruction at stoichiometric combustion conditions. In practice, local oxygen availability and pyrolysis will produce nonzero destruction.

Of the remaining operating parameters, most affect the model's destruction efficiency through their effect on temperature (recall in-flame destruction is ignored). Their ranking in influence on destruction is therefore the same as Table 14. The inputs which influence only gas temperature in the chemical model are:

- Fuel heating value

- Flame shape

- Waterwall emissivity

- Refractory conductivity

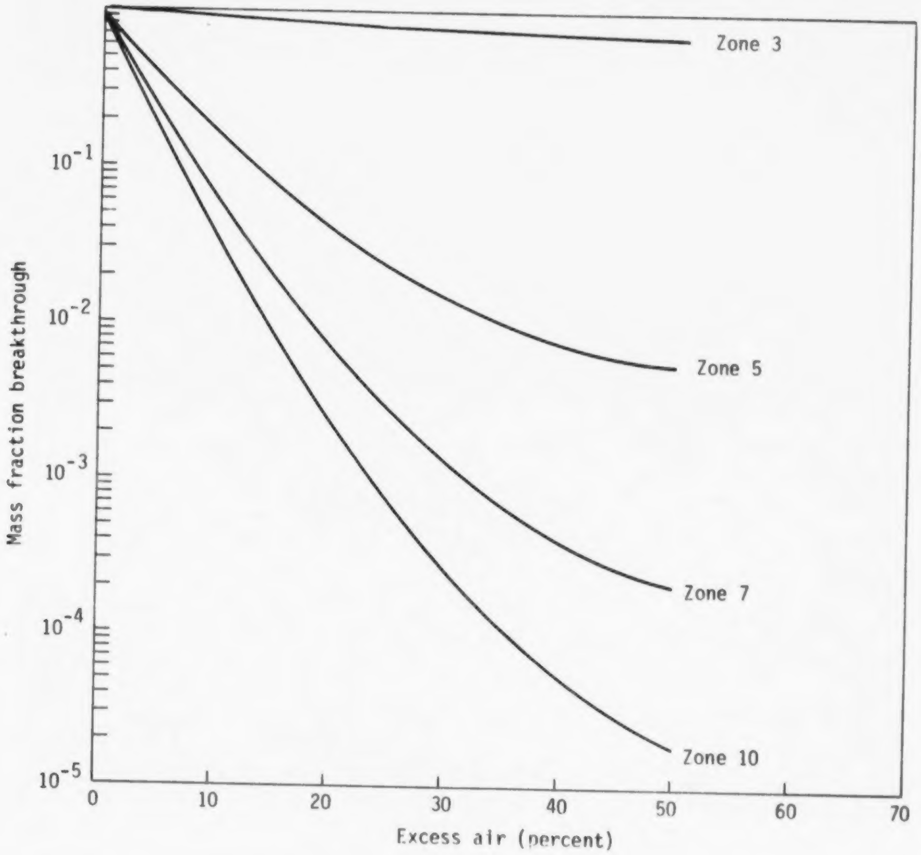

Figure 32. Effect of excess air level (0 to 50 percent) on baseline weighted average $CCl_4$ destruction at various axial furnace positions.

- Soot loading
- Refractory temperature
- Air preheat
- Waterwall temperature
- Refractory emissivity
- Speckledness

The following inputs influence not only temperature, but also residence time:

- Feed rate
- Excess air
- Furnace surface area

The following inputs influence not only temperature, but also oxygen concentration:

- Excess air
- Fuel moisture content
- Fuel C:H ratio

The latter two lists contain the parameters whose effects on destruction efficiency are most difficult to determine without benefit of a well-defined numerical model.

### 5.7.3 Comparison With Pilot-Scale Results

It would be very difficult to assess the accuracy of the destruction model simply by comparison to "input-output" furnace tests. The contribution of flame destruction processes to postflame oxidation of the waste stream can not be isolated. The model predicts only the destruction efficiency of the waste molecules which have survived the flame region; a real furnace converts the principal organic constituents to inorganic form both in the flame and beyond it. Detailed in-furnace sampling of the waste would be necessary to verify the model predictions.

Figure 33 shows a comparison between sample data from the Acurex pilot-scale furnace outlet and the model. Carbon tetrachloride is the waste component. The model weighted average $C/C_0$ is calculated at the two experimental firing rates over the range of 10 to 50 percent excess air. The preexponential factor was $2.75 \times 10^5$ $sec^{-1}$ and the activation energy was 25.5 Kcal/gmole (preliminary data (34)). The calculated bulk flow Reynolds

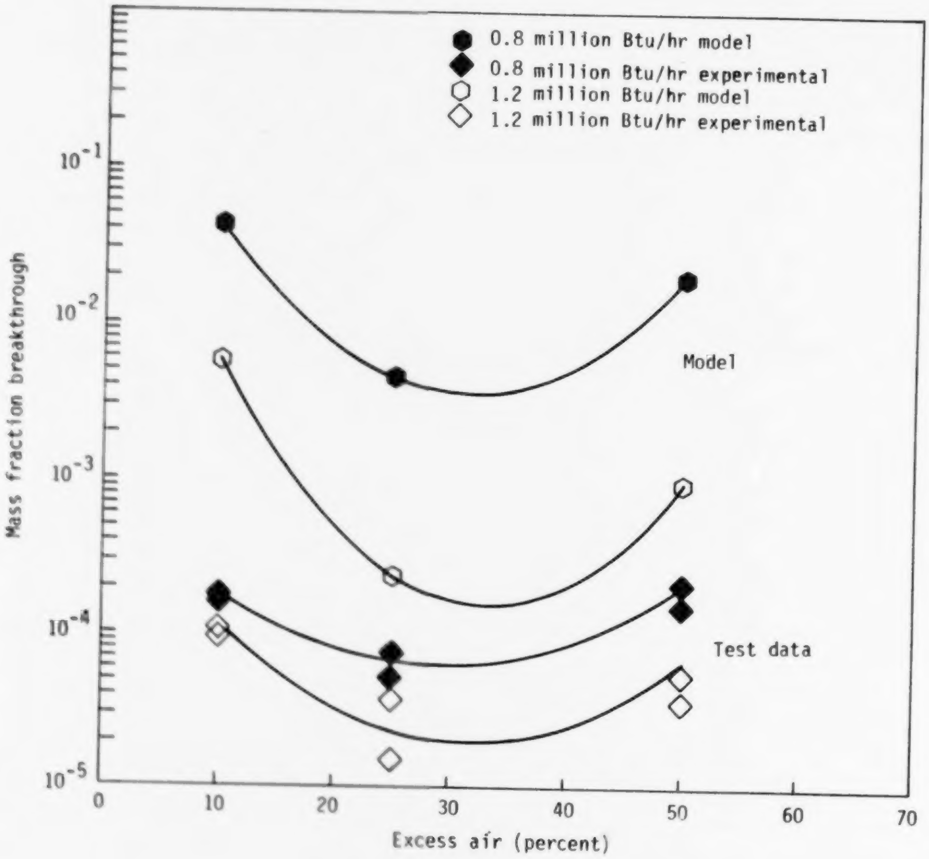

Figure 33. Comparison of weighted average model prediction and pilot-scale carbon tetrachloride destruction data at variable excess air.

number exceeded 3,000 in each case so that turbulent velocity profiles were calculated. A linear curve fit of the temperature boundary layer was selected.

Unlike the baseline case, the model prediction of mass breakthrough does not continually decrease with excess air over the range 10 to 50 percent. With the baseline furnace geometry and operating regime, the excess oxygen available for oxidation dominates the velocity and temperature changes as excess air is increased. The baseline destruction rate increases with excess air. However, in the pilot-scale tests with waterwalls, the decrease in flame temperature and residence time counterbalances the increase in oxygen availability and sensible energy input. Both the model and the experimental results show an optimum excess air level for destruction efficiency between 10 and 50 percent. This is true at both of the experimental firing rates. As in the baseline case, the temperature effect dominates the residence time effect as firing rate is varied, so that destruction efficiency increases as firing rate increases.

As expected, the model curves in Figure 33 lie above the experimental curves. The difference in the predicted and experimental mass fraction breakthroughs is about two orders of magnitude. If the model is accurately predicting the carbon tetrachloride destruction in the postflame gases, then the destruction efficiency due to flame processes alone is about 99 percent for these tests.

## 5.8 SUMMARY AND CONCLUSIONS

Model development has been initiated to aid in the design, operation, and permitting of liquid-fired hazardous waste combustors. The model can closely predict the bulk temperature measured in the pilot-scale tests. It revealed which operating and design variables strongly influence the temperature-time profile in the postflame region. The model further gave insights into those parameters which dominate postflame thermal oxidation of waste compounds cofired with distillate oil. The computer program, although limited by the size and speed of a microcomputer, has the potential to place conservative bounds on destruction efficiency in working combustors.

Several improvements should be made in the future. The foremost of these is based on the need for oxygen-dependent global rate expressions. When kinetic rate constants are available that describe oxidation and pyrolysis in furnaces at low excess air conditions (3 to 10 percent oxygen by volume), the model will be more likely to identify the optimum excess air level for destruction efficiency.

The boundary layer destruction model needs to be verified by comparison with experimental data from detailed furnace probing. It may be necessary to upgrade the model by inclusion of a more detailed aerodynamic and mixing description. To simulate a broader range of combustor types, the effects of multiple burner geometries should be included. Further improvement in the chemical kinetic description could be added by extending the single-step global model to set off several semi-global reaction steps, with potential products of incomplete combustion as intermediates. When the necessary additions and refinements have been made, it will be appropriate to compare the model results to emissions from a full-scale liquid-injection furnace.

# REFERENCES

1. Duvall, D. S. and Rubey, W. A. Laboratory Evaluation of High-Temperature Destruction of Kepone and Related Pesticides. EPA-600/2-76-209, U.S. Environmental Protection Agency Municipal Environmental Research Laboratory, Cincinnati, Ohio, December 1976.

2. Duvall, D. S. and Rubey, W. A. Laboratory Evaluation of High-Temperature Destruction of Polychlorinated Biphenyls and Related Compounds. EPA-600/2-77-228, U.S. Environmental Protection Agency Municipal Environmental Research Laboratory, Cincinnati, Ohio, December 1977.

3. Lee, K. C., Jalmes, H. J., and McCauley, D. C. Thermal Oxidation Kinetics of Selected Organic Compounds. J. Air Poll. Control Assoc., V. 29, 749, 1979.

4. Lee, K. C., Jalmes, H. J., and McCauley, D. C. Predictive Model of the Time-Temperature Requirements for Thermal Destruction of Dilute Organic Vapors. 72nd Annual Meeting of the Air Poll. Control Assoc., June 1979.

5. Proceedings of the Sixth Annual Research Symposium: Treatment of Hazardous Waste. EPA-600/9-80-001, U.S. Environmental Protection Agency, Municipal Environmental Research Laboratory, Cincinnati, Ohio, March 1980.

6. Proceedings of the Eighth Annual Research Symposium: Incineration and Treatment of Hazardous Waste. EPA-600/9-83-003, U.S. Environmental Protection Agency, Industrial Environmental Research Laboratory, Cincinnati, Ohio, April 1983.

7. Harrison, J. W., White, J. B., and King, W. J. Assess Hazard Potential From Combustion of Wastes in Industrial Boilers. EPA Contract No. 68-02-3170-21, October 1980.

8. Castaldini, C., Willard, H. K., Wolbach, C. D., and Waterland, L. R. A Technical Overview of the Concept of Disposing of Hazardous Wastes in Industrial Boilers. EPA Contract No. 68-03-2567, Task 4034 Report, June 1984.

9. Ibid., pp. 77ff.

10. McCormick, R., Merrill, R. C., Waterland, L. R., and Wolbach, C. D. Engineering Analysis of the Practice of Disposing of Hazardous Wastes in Industrial Boilers. EPA Contract No. 68-03-3043, Task SCA 04 Report, January 1982.

11. Lucas, D. M. and H. E. Toth, "The Calculation of Heat Transfer in the Fire Tubes of Shell Boilers," Journal of the Institute of Fuel, October 1972.

12. Lee, K. C., Jalmes, H. J., and McCauley, D. C. Predictive Model of the Time-Temperature Requirements for Thermal Destruction of Dilute Organic Vapors. 72nd Annual Meeting of the Air Poll. Control Assoc., June 1979.

13. Personal communication, B. Dellinger, U.D.R.I., May 1983.

14. Miller, D. L., W. A. Cundy, and R. A. Matula. Incinerability Characteristics of Selected Chlorinated Hydrocarbons. Paper presented at the Ninth Annual Research Symposium Land Disposal, Incineration and Treatment of Hazardous Waste, F. Mitchell, KY, 1983.

15. Hottel, H. C. and E. S. Cohen. Radiant Heat Exchange in a Gas-Filled Enclosure, Allowance for Non-Uniformity of Gas Temperature. A.I.Ch.E. J. 4:3, 1958.

16. Steward, F. R. and H. K. Guruz. Mathematical Simulation of an Industrial Boiler by the Zone Method of Analysis. In: N. H. Afgan and J. M. Beer (ed.), Heat Transfer in Flames. J. Wiley and Sons, New York, NY, 1974. p. 47.

17. Bueters, K. A., J. G. Cogoli, and W. W. Habelt. Performance Prediction of Tangentially Fired Utility Furnaces by Computer Model. In: Proceedings of the Fifteenth International Combustion Symposium, Tokyo, 1974.

18. Field, M. A., D. W. Gill, B. B. Morgan, and P. G. W. Hawksley. Combustion of Pulverized Coal. The British Coal Utilization Research Association, (2nd ed. by the Institute of Fuel, 1974), Leatherhead, 1976. p. 124.

19. Wolbach, C. D., C. Castaldini, A. R. Garman, and J. M. Kennedy. Subscale Parametric Studies on the Combustion of Hazardous Wastes. Paper presented at Ninth Annual Research Symposium Land Disposal, Incineration and Treatment of Hazardous Waste. Ft. Mitchell, KY, 1983.

20. Hottel, H. C., A. F. Sarofim, and I. H. Farag. Radiative Exchange in Combustion Chambers. In: H. B. Palmer and J. M. Beer (ed.), Combustion Technology: Some Modern Developments. Academic Press, New York, New York, 1974. p. 190-209.

21. Hottel, H. C. First Estimates of Industrial Furnace Performance. In: N. H. Afgan and J. M. Beer (ed.), Heat Transfer in Flames. J. Wiley and Sons, New York, NY, 1974. p. 5-28.

22. Hottel, H. C. and R. B. Egbert. Radiant Heat Transmission from Water Vapor. Trans. of A.I.Ch.E, June 1942, pp. 38,3.

23. Siegel, R. and J. R. Howell. Thermal Radiation Heat Transfer. McGraw-Hill, New York, NY, 1981.

24. Haynes, B. S. and H. G. Wagner. Soot Formation. Prog. Energy Combust. Sci., 7, 1981.

25. Beer, J. M. Methods for Calculating Radiative Heat Transfer From Flames in Combustors and Furnaces. In: N. H. Afgan. op.cit., pp 29-48.

26. Prado, G. P., M. L. Lee, R. A. Hites, D. P. Hoult, and J. B. Howard. Soot Formation in a Turbulent Diffusion Flame. In: Proceedings of the Sixteenth Symposium (International) on Combustion. The Combustion Institute, Pittsburgh, PA., 1977. p. 649-661.

27. Lucas, D. M. and A. A. Lockett. Mathematical Modeling of Heat Flux and Temperature Distribution in Shell Boilers. In: Proceedings of the Fourth Symposium on Flames and Industry: Predictive Methods for Industrial Flames. Imperial College, London, September, 1972. p. 161.

28. Maron, S. H. and C. F. Prutton. Principles of Physical Chemistry, 3rd ed. The Macmillan Co., New York, NY, 1958. p. 283.

29. Field, M. A. et al., op. cit., pp. 102-107.

30. Aronowitz, D., R. J. Santoro, F. L. Dryer, and I. Glassman. Kinetics of the Oxidation of Methanol: Experimental Results Semi-Global Modeling and Mechanistic Concepts. In: Proceedings of the Seventeenth Symposium (International) on Combustion. The Combustion Institute, Pittsburgh, PA., 1979. p. 633-644.

31. Brent, R. P. Algorithms for Minimization Without Derivatives. Precentice Hall, New York, NY, 1973.

32. Dellinger, B., et. al. Factors Affecting the Gas-Phase Thermal Decomposition of Chlorinated Aromatic Hydrocarbons.

33. Lee, K. C., et al. Revised Model for the Prediction of the Time-Temperature Requirements.

34. Personal communication, B. Dellinger, U.D.R.I., January 1983.

## APPENDIX A

## TEST FACILITY DETAILED DESCRIPTION

This section supplements Section 3.2 to provide additional information on the hardware, instrumentation, and ancillary systems of the Acurex Pilot-Scale Furnace. The discussion includes only the facility subsystems used in this study. The furnace, whose additional capabilities are listed in Table 18, was designed to handle a variety of fuels and simulate a range of burning configurations and combustor types. Previous studies have used synthetic coal-derived liquids, coal, gas, methanol, and oil-gas mixtures for fuel. Figure 34 presents a view of the facility showing the burner assembly mounted on the front wall, the horizontal radiant firebox, and the vertical convective cooling section.

### A.1 RADIANT SECTION

The horizontally oriented firebox is often referred to as the "radiant section" as radiation dominates the heat transfer to the walls. It is segmented into six subsections: a front wall with burner mount, four removable tunnel modules, and a 90° elbow. For this study all modules were installed, so that the total path length from front wall to back wall was 4.57m (15 ft) (see Figure 35). Figure 36 shows the firebox in cross section. The gas passed through an 84-cm (33-in.) diameter cylinder contained in a 145-cm (57-in.) square shell; the wall was 30.5 cm (12 in.) thick at its minimum. The wall was constructed of Harbison-Walker Lightweight 1,650°C (3,000°F) castable refractory with thermal conductivity of 65 $\text{watt}\cdot\text{cm}/\text{m}^2\cdot{}^\circ\text{C}$ (4.5 $\text{Btu}\cdot\text{in.}/\text{hr}\cdot\text{ft}^2\cdot{}^\circ\text{F}$) at an average temperature of 1,095°C (2,000°F). Five ports along the top and 23 on each side allowed sampling probe and thermocouple insertion, visual access, and radiant panel plumbing. Additional angled ports on the sides accommodated thermocouple probes to measure wall temperatures. Five sheathed Type K Chromel/Alumel thermocouples were positioned along the length of the radiant section to monitor the furnace transient heatup. The gas stream pressure in the furnace was monitored by a pressure tap at a port halfway between the front and back walls.

The refractory walls serve to insulate the gas stream from large radiative heat losses. Matching the temperatures of a full-scale combustor becomes increasingly difficult as combustor size increases. The volume of the firebox is associated with the firing rate; if the wall has a characteristic linear dimension X, then the nominal firing rate goes as $X^3$. The heat loss goes as the surface area, $X^2$. So decreasing the size of a

## TABLE A-18. ACUREX PILOT-SCALE FURNACE CAPABILITIES

| | |
|---|---|
| Combustion Chamber | • 33-in. I.D. x 15 ft long<br>• 2- and 3-ft sections<br>• Viewports<br>• 2-in. diameter access ports for sampling or air staging<br>• Refractory lined (3,000°F)<br>• Coal-fired 1 to 1.5 million Btu/hr<br>• Gas-fired 2.5 million Btu/hr<br>• Oil 2 million Btu/hr<br>• Horizontal orientation |
| Convective Section | • Removable heat exchange sections -- tailor flue temperature profile<br>• Oil cooled |
| Air Supply | • Preheated up to 600°F<br>• Nominal 4 psi supply<br>• Up to 150 percent excess air<br>• Measurement and control of air flow |
| Fuel Supply | • Pulverized solid screw feed<br>• Heat traced liquid supply |
| Burner | • Variable swirl research burner<br>-- Multiple fuel capability<br>-- Variable axial fuel tube location<br>-- Capability to change velocity<br>-- Capability to change quarl design |
| Flue | • I.D. Fan<br>• Baghouse |
| Emissions | • $O_2$, CO, $CO_2$, NO, UHC, $SO_2$ particulates<br>• Sampling probes for in-flame samples |

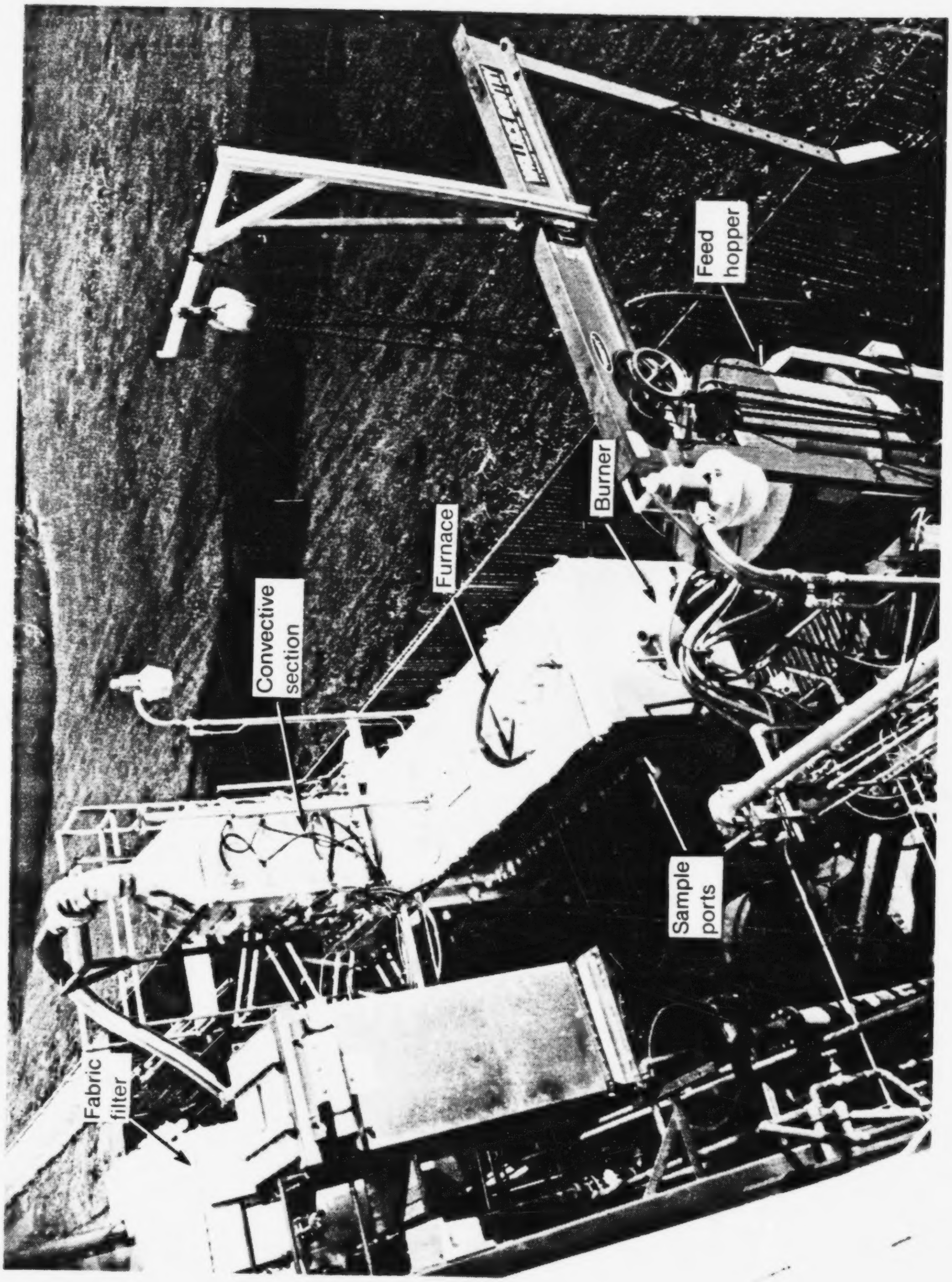
H-065
Fabric filter
Convective section
Furnace
Burner
Feed hopper
Sample ports

Figure 34. Acurex pilot-scale research furnace.

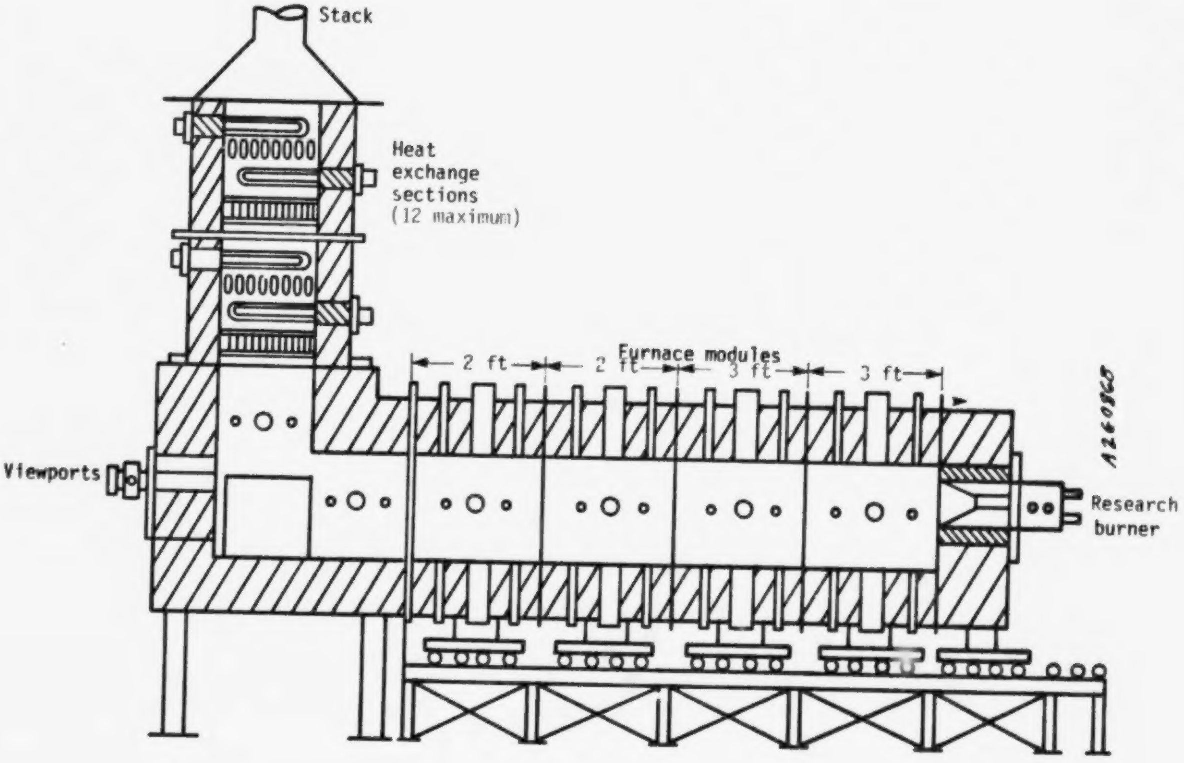
Stack
Heat exchange sections (12 maximum)
Furnace modules
2 ft
2 ft
3 ft
3 ft
A260868
Viewports
Research burner

Figure 35. Furnace schematic.

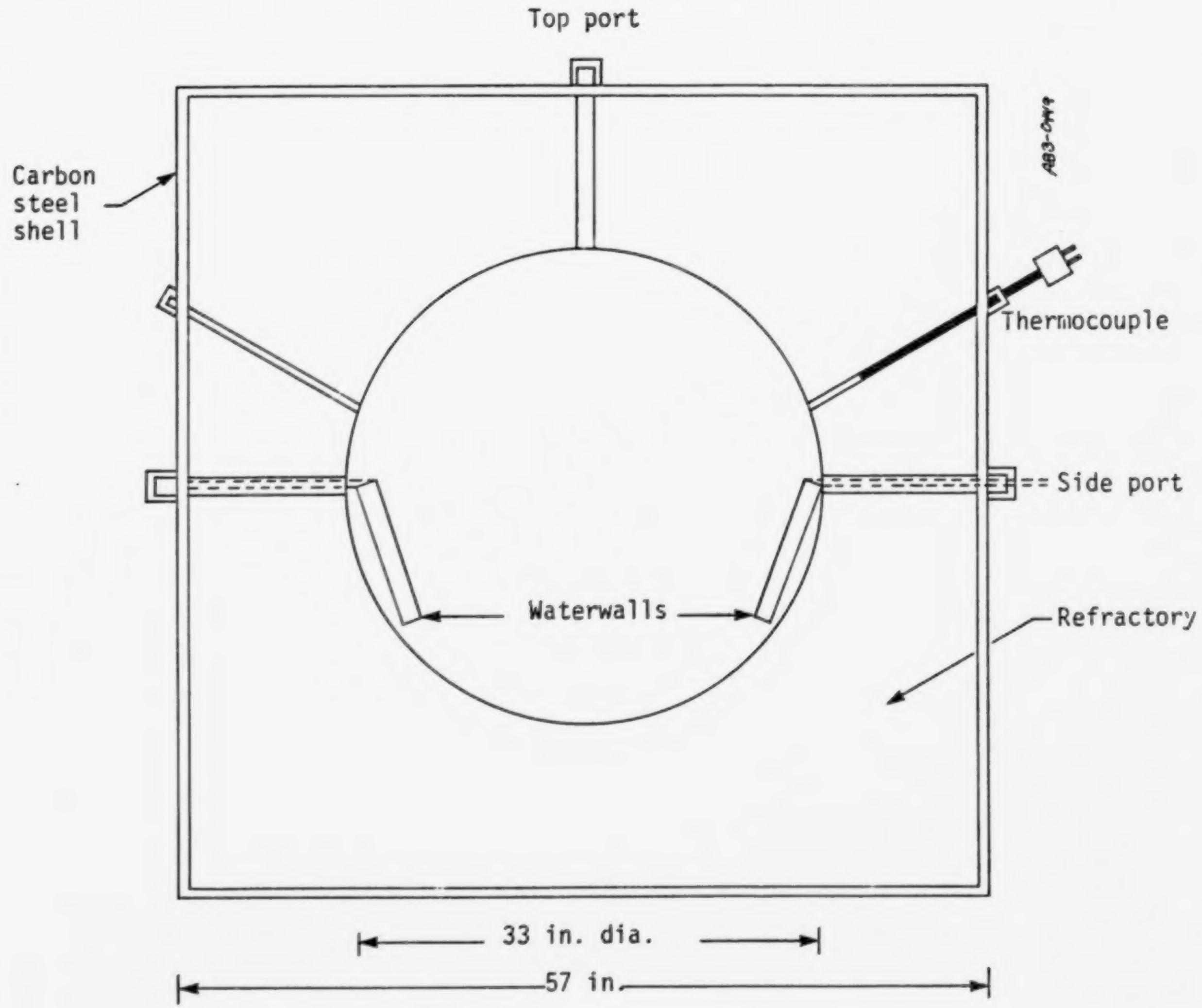
Top port
Carbon steel shell
AB3-0449
Thermocouple
Side port
Waterwalls
Refractory
33 in. dia.
57 in.

Figure 36. Firebox cross-section schematic.

combustor, that is, modeling a full-scale unit by a pilot-scale, necessarily increases the surface-to-volume ratio. Thus the heat loss per energy input is greater in the pilot-scale case, so better wall insulation is required to maintain the same gas temperature history.

Introducing the radiant panel waterwalls into the firebox brought the Acurex Pilot-Scale Furnace from the temperature regime of a 1,000-MW utility steam generator to that of a 50-MW packaged watertube boiler. The panels were constructed of three parallel 1-1/2 in. x 3/4 in. SS 304 rectangular tubes, as shown in Figure 37. The panels hung from the port tubes so that most of the surface area for heat transfer was below the tunnel centerline. Figure 38 shows the placement of each of the six panels within the firebox. The surface area exposed to the bulk gas represented 7.59 percent of the total refractory surface area.

To measure the energy removed with the water, Type K thermocouples were placed on the inlet and outlet side of each of the six panels, as close to the panel as physically possible to minimize error (±2°F). One Hedland No. 705-025 (2.0 to 25.0 gpm) flowmeter was mounted on the inlet manifold to each side of the furnace to measure water flow to ±5 percent uncertainty.

## A.2 CONVECTIVE SECTION

Downstream of the radiant section, the postflame gases make a 90° turn and enter the "convective section." Two refractive lined modules, each 32 in. high, contain up to 12 removable U-tube cooling drawer assemblies. Each drawer holds 20 1/2-in. diameter SS 304 tubes. A range of heat loads may be absorbed according to the number of drawers mounted; five were appropriate for the time-temperature requirements of this study.

Initially water was used as the cooling fluid. However, since the tube temperature was very low (below 140°F), flue gas moisture condensation problems resulted. Hydrochloric acid from the waste fuel caused undue corrosion. To remedy the situation, Therminol-66, a high-temperature organic oil, was substituted for water as a heat transfer fluid. The tube temperature (above 250°F) was raised above the acid dew point. A schematic of the Therminol supply system is shown in Figure 39.

## A.3 FUEL/AIR DELIVERY SYSTEMS

The combustion air supply system is shown schematically in Figure 40. Forced draft was provided by a Spencer turbine blower at delivery pressures to 8 in. W.C. Volume flowrate was measured to ±8 percent uncertainty with parallel Datametrics hot wire anemometers inserted in venturi tubes. A General Electric electric air heater with proportional controller allows air preheat up to 600°F, measured at the burner mixing plenum.

Natural gas was fired overnight to maintain the furnace close to operating temperature. The supply system is shown in Figure 41. A Fischer & Porter rotameter was used to meter gas flow to ±2 percent uncertainty.

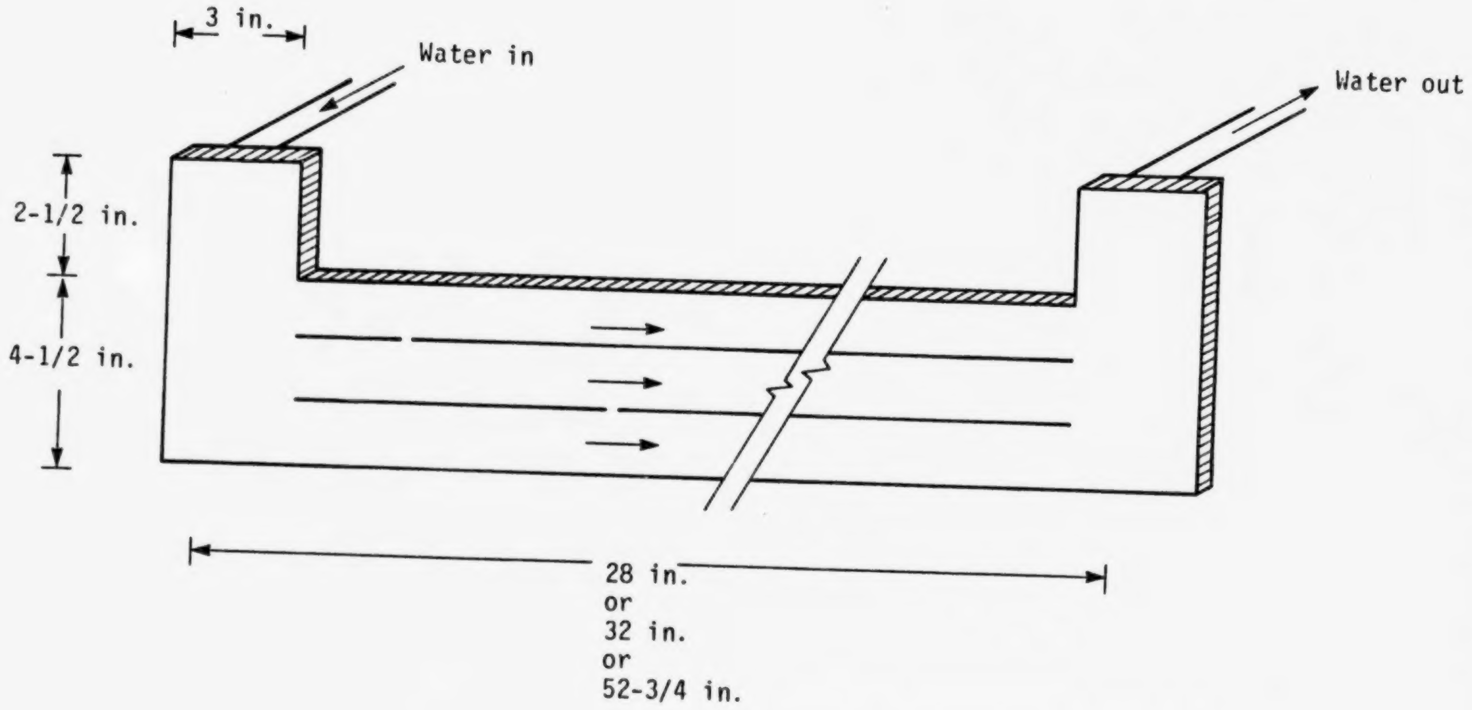
3 in.
Water in
Water out
2-1/2 in.
4-1/2 in.
28 in.
or
32 in.
or
52-3/4 in.

Figure 37. Single waterwall panel schematic.

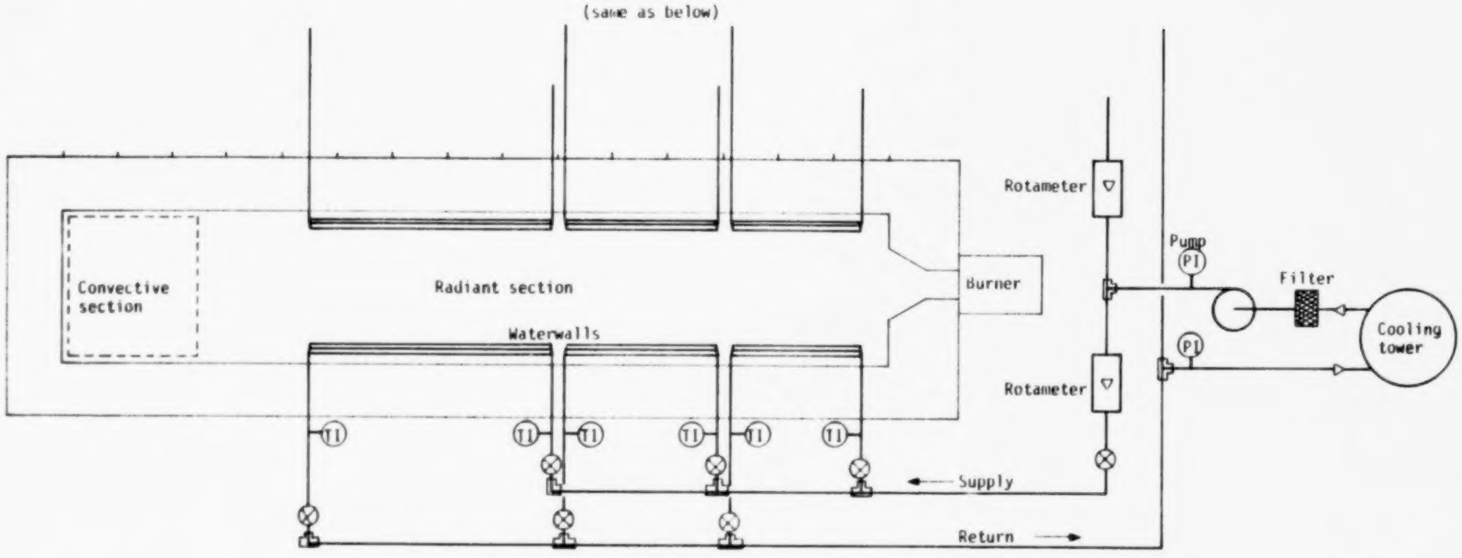
(same as below)
Rotameter
Pump
PI
Filter
Convective section
Radiant section
Burner
Cooling tower
Waterwalls
PI
Rotameter
TI
TI
TI
TI
TI
TI
Supply
Return

Figure 38. Waterwall cooling system showing radiant panel locations (plan view furnace to scale).

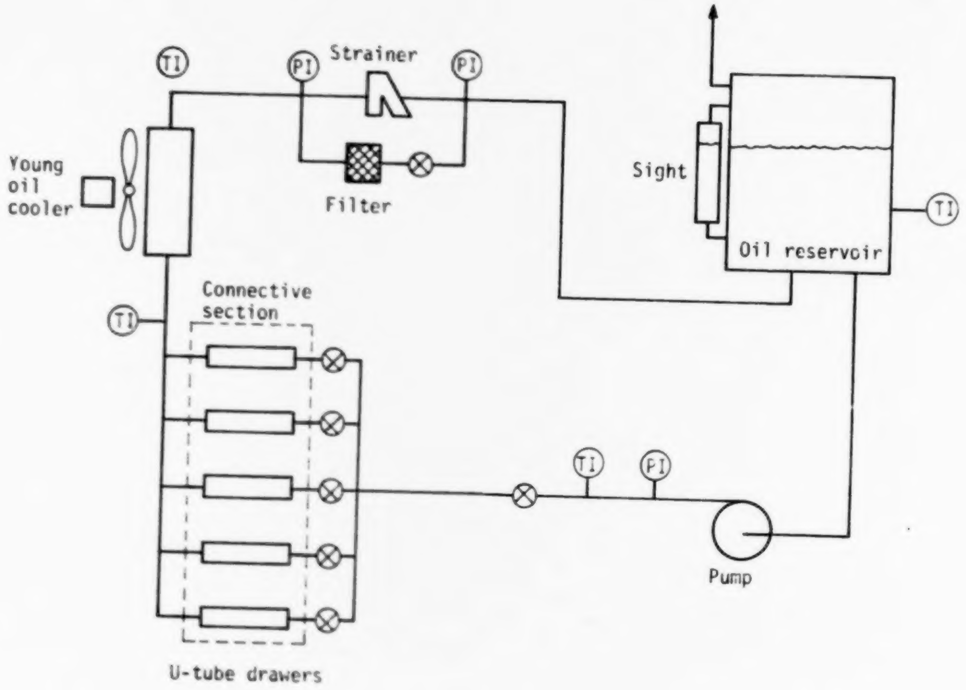
Strainer
TI
PI
PI
Young
oil
cooler
Filter
Sight
TI
Oil reservoir
Connective
section
TI
TI
PI
Pump
U-tube drawers

Figure 39. Convective section Therminol system schematic.

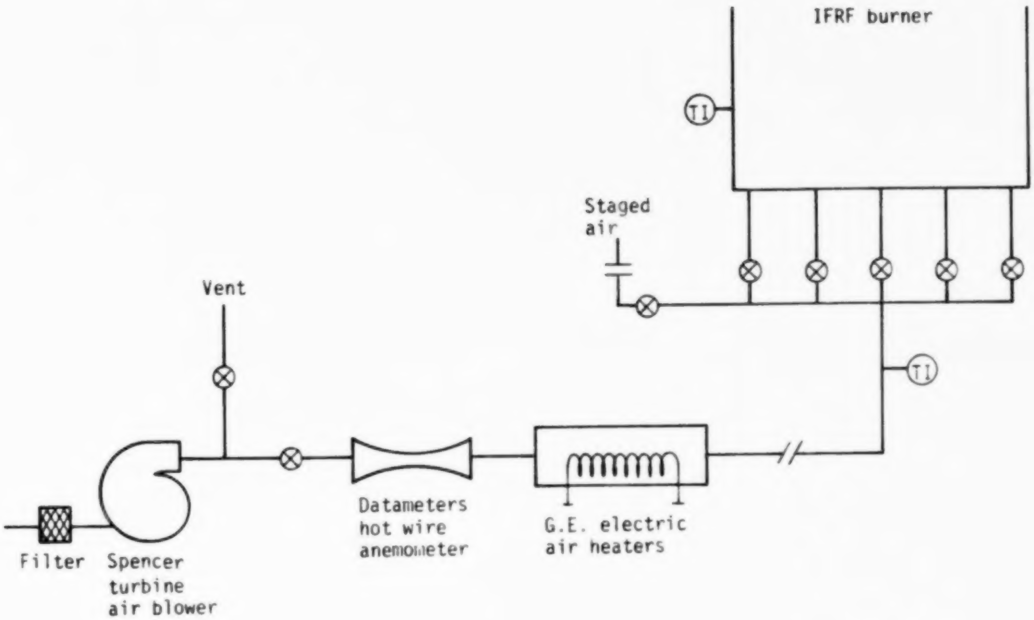
IFRF burner
TI
Staged air
Vent
TI
Filter
Spencer turbine air blower
Datameters hot wire anemometer
G.E. electric air heaters

Figure 40. Combustion air supply system.

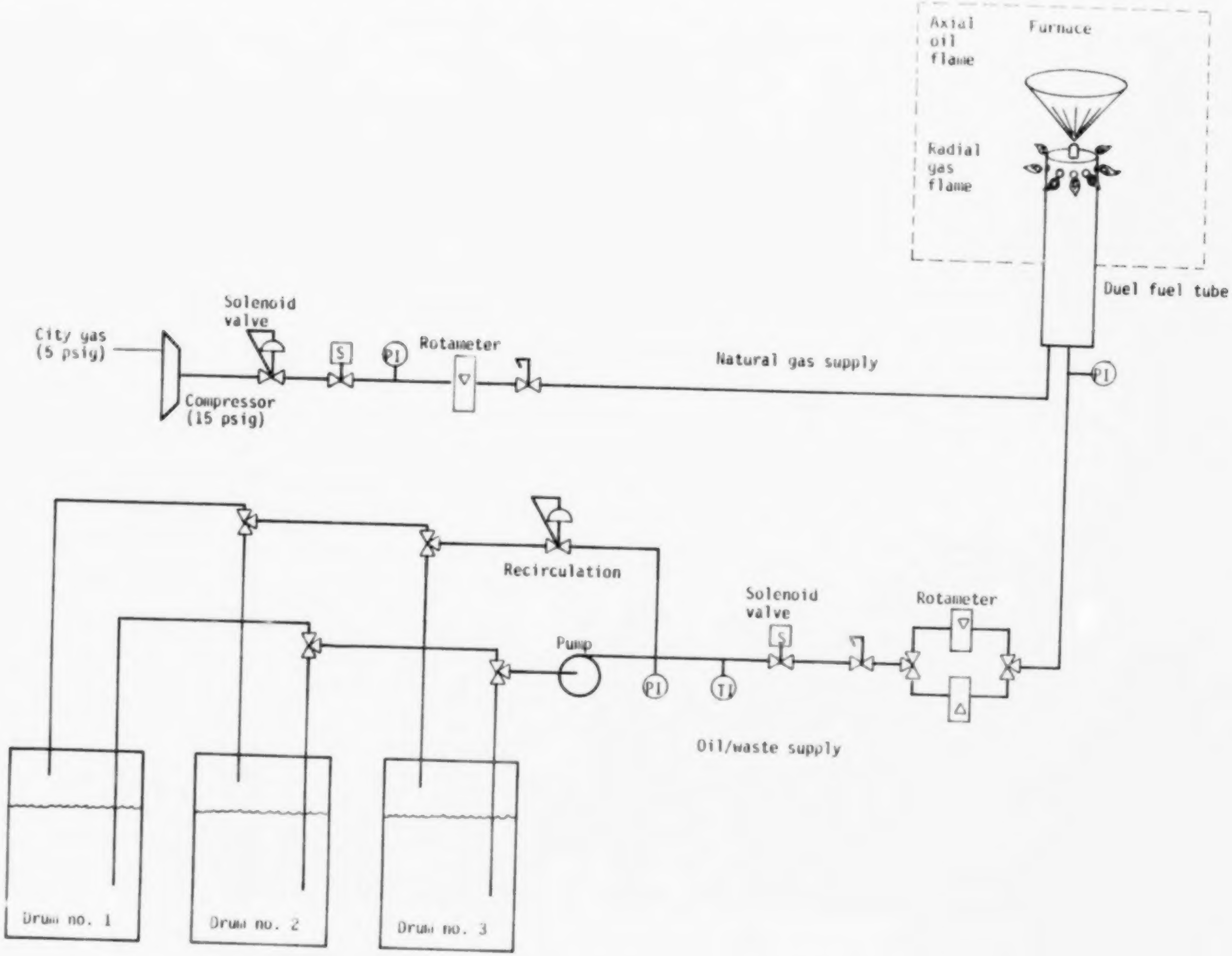
Axial oil flame
Furnace
Radial gas flame
Duel fuel tube
City gas (5 psig)
Solenoid valve
Compressor (15 psig)
S
PI
Rotameter
Natural gas supply
PI
Recirculation
Solenoid valve
Rotameter
Pump
PI
TI
S
Oil/waste supply
Drum no. 1
Drum no. 2
Drum no. 3

Figure 41. Fuel feed system schematic.

Figure 40 also shows the liquid fuel feed system. No. 2 fuel oil/hazardous waste mixtures was prepared in advance in three 55-gallon drums. A Viking FH-32 centrifugal pump could deliver up to 3 gpm. Typically over 90 percent of the flow was recirculated to the drum source. The balance was metered with a thermocouple and a Fischer & Porter rotameter to ±4 percent absolute accuracy. Most of the uncertainty was associated with the large viscosity change of no. 2 fuel oil over the operating temperature range (60° to 100°F) of the system. Two rotameters allowed highest accuracy of flowrate measurement between 0 and 27.0 gph water equivalent. The solenoid valve in the oil delivery line (as well as the natural gas line) interlocked with the furnace safeguard system. In the event that the flame was extinguished, a Honeywell ultraviolet flame detector automatically shut down the fuel system.

The fuel delivery tube used for this study is shown in Figure 42. Fuel oil and natural gas could be fired simultaneously. The gas was injected radially from the tube through 12 1/8-in. diameter holes. This mode provided good mixing with the combustion air passing through the annular space between the tube and the burner throat. The liquid fuel traveled down the central passage of the tube. The threaded end accommodated interchangeable atomizing nozzles.

The Delavan WDA pressure-atomizing nozzles are shown in Figure 43. Back pressure from the orifice determined the flowrate; the nominal rating of the nozzle was the flowrate at 100 psig of no. 2 fuel oil. Most tests were conducted with 10-gph nozzles. The nozzles operate over a range of 40 to 150 psig; the higher the pressure, the more the droplet size distribution was shifted towards smaller droplets. The Sauter mean diameter varied roughly as pressure to the -0.3 power. All nozzles used were of the hollow-cone spray type. The included angle of the cone was usually 70°.

## A.4 BURNER DESIGN

The burner used for the experimental test work on the wall-fired, pilot-scale furnace is shown in Figure 44. The burner was a single register, concentric jet burner with variable swirl intensity in the annular air supply. It was based on a design developed by the International Flame Research Foundation (IFRF). The burner could be fitted with gas, liquid, or solid fuel injectors. The fuel tube could be positioned at any axial location relative to the burner exit. The burner had a water-cooled quarl with a throat diameter of 5-3/4 in. opening to a diameter of 12-3/4 in.

The design values and operating parameter ranges of the IFRF research burner are listed in Table 19. Variable throat inserts ranging from 2 to 5 in. in diameter permit a wide range of secondary air velocities. For this study a 3-in. diameter throat and 300°F air preheat provided the appropriate air entrance velocity.

The swirl is produced by a moving block swirl generator (see Figure 44). The swirl register consists of two annular plates and two series of interlocking wedge-shaped blocks each attached to one of the plates. The

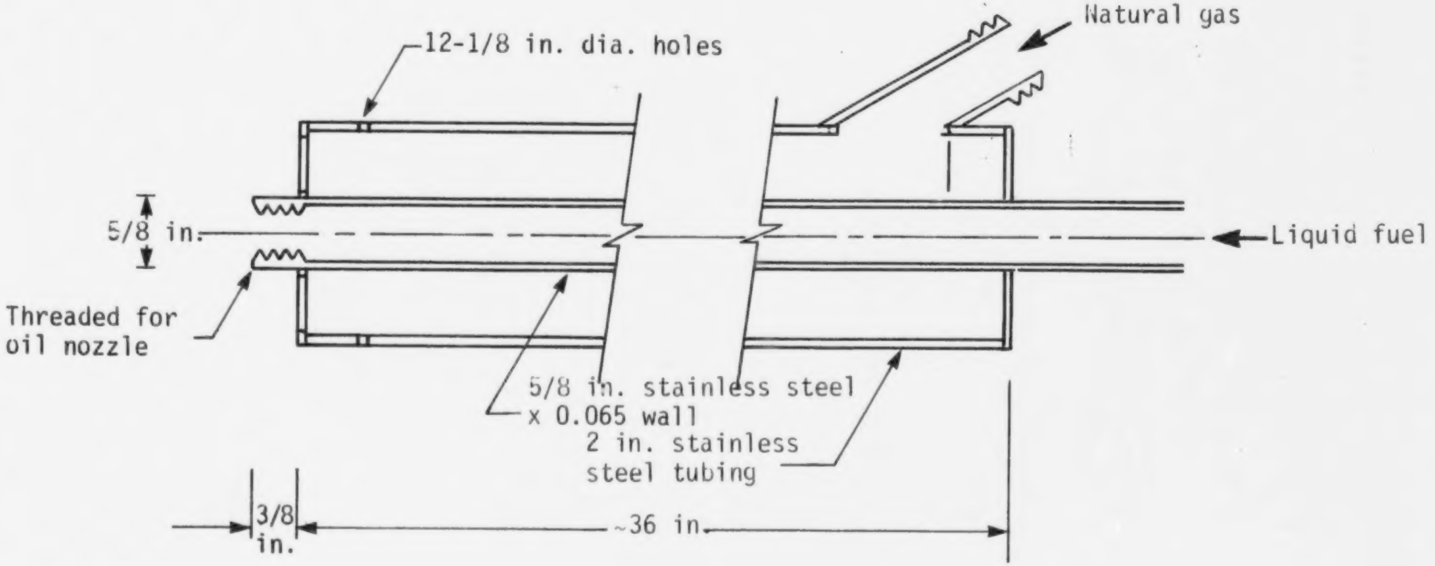
Natural gas
12-1/8 in. dia. holes
5/8 in.
Liquid fuel
Threaded for
oil nozzle
5/8 in. stainless steel
x 0.065 wall
2 in. stainless
steel tubing
3/8
in.
~36 in.

Figure 42. Fuel oil/natural gas dual fuel tube.

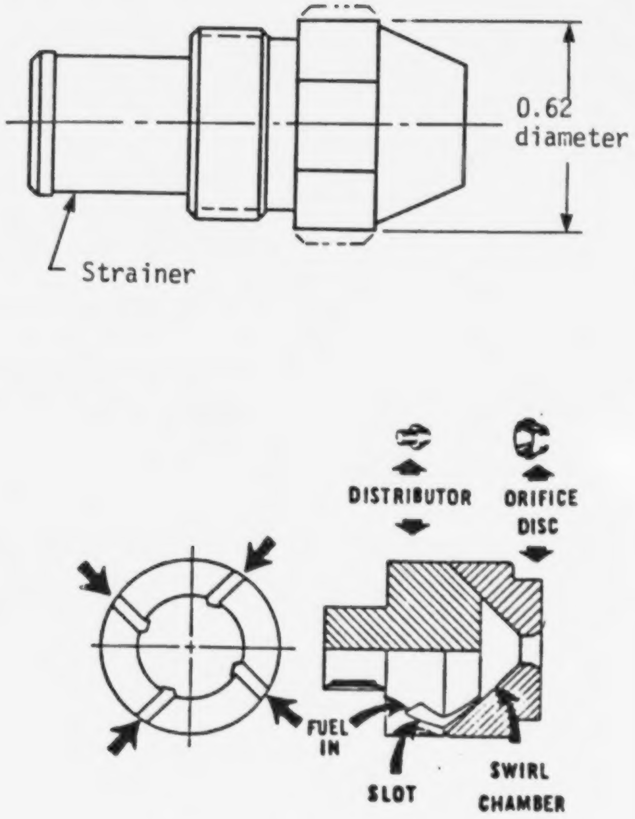
0.62
diameter
Strainer
DISTRIBUTOR
ORIFICE
DISC
FUEL
IN
SLOT
SWIRL
CHAMBER

Figure 43. Delavan Type WDA pressure-atomizing nozzle (hollow cone spray pattern).

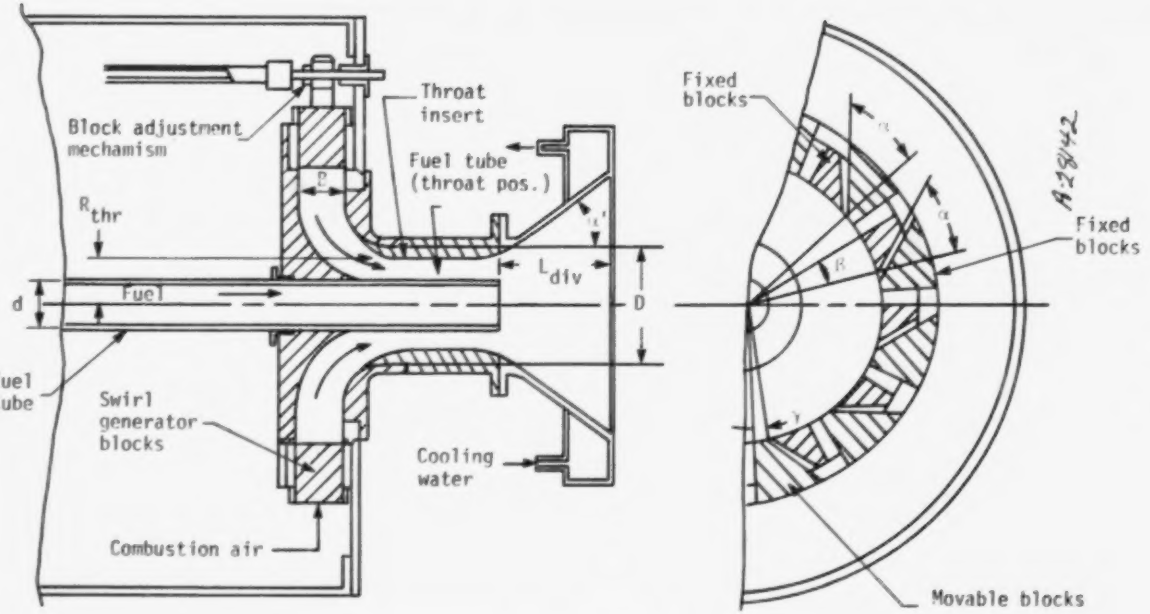
Block adjustment mechamism
Throat insert
Fuel tube (throat pos.)
β
$R_{thr}$
$L_{div}$
α'
d
Fuel
D
Fuel tube
Swirl generator blocks
Cooling water
Combustion air
Fixed blocks
α
α
A-28142
Fixed blocks
β
γ
Movable blocks

Figure 44. IFRF burner system.

TABLE 19. IFRF BURNER DESIGN PARAMETERS

| Parameter | Nominal design value | Operating range |
|---|---|---|
| Firing rate[a] (million Btu/hr) | 1.0 | 0.6 to 1.5 |
| Total air (lb/hr) | 900 | 540 to 1,350 |
| Excess air (percent of theoretical) | 20 | 0 to 50 |
| Primary air (percent of theoretical) | 15 | 10 to 25 |
| Secondary air preheat (°F) | 400 | 70 to 600 |
| Primary air velocity (fps) | 69 | 46 to 114 |
| Secondary air throat velocity[b] (fps) | 174 | 100 to 200 |
| Secondary air swirl no.[b] | 0.85 | 0 to 0.85 |
| Fuel tube axial position | Burner throat | Burner throat to quarl exit |

[a] For $\frac{\text{Higher Heating Value}}{\text{Theoretical Air}} = \frac{1,325\ \text{Btu}}{\text{lb (air)}}$

(Typical for solid and liquid fuels).

[b] For 3 in. diameter throat sleeve.

blocks form alternating radial and tangential air flow channels which interlock so that the air flow splits into radial and tangential streams which combine downstream from the swirl generator into one swirling air flow. Rotating the back plate clockwise (the front plate is fixed to the burner) progressively closes the radial channels and opens the tangential channels.

The relationship between swirl vane setting (on a scale of 0 to 8 as reported) and swirl number can be calculated from the definition of swirl number and the geometry of the swirl vanes. It can be shown that (reference A-1):

$$S = \frac{\sigma R}{2B}\left[1 - \frac{R_h}{R}\right]^2$$

where

$S$ = Swirl number

$R$ = Secondary flow radius

$R_h$ = Primary fuel tube radius

$B$ = Secondary flow inlet dimension

$\sigma$ = Ratio of the average tangential and radial velocity components at the swirler exit

Figure 44 shows where these dimensions are located. For the IFRF burner, $R = 1.5$ in., $R_h = 1.0$ in., and $B = 1.25$ in., thus, $S = 0.333\sigma$.

The coefficient $\sigma$ is found from:

$$\sigma = \frac{2\pi}{Z\varepsilon_m} \sin\alpha \frac{\cos\alpha\,[1 + \tan\alpha \tan\varepsilon/2]\,(\varepsilon/\varepsilon_m)}{\{1-[1-\cos\alpha\,(1 + \tan\alpha \tan\varepsilon/2)]\varepsilon/\varepsilon_m\}}$$

where

$\varepsilon_m$ = Maximum angle setting = 8°

$Z$ = Number of swirl blocks = 12

$\alpha$ = Block angle = 43° 23'

$\varepsilon$ = Actual angle setting

These angles are shown in Figure 45. Figure 46 is a graph of swirl number versus relative swirl setting. The swirl range of 0 to 0.85 provides enough variability to investigate swirl numbers high enough to produce recirculating

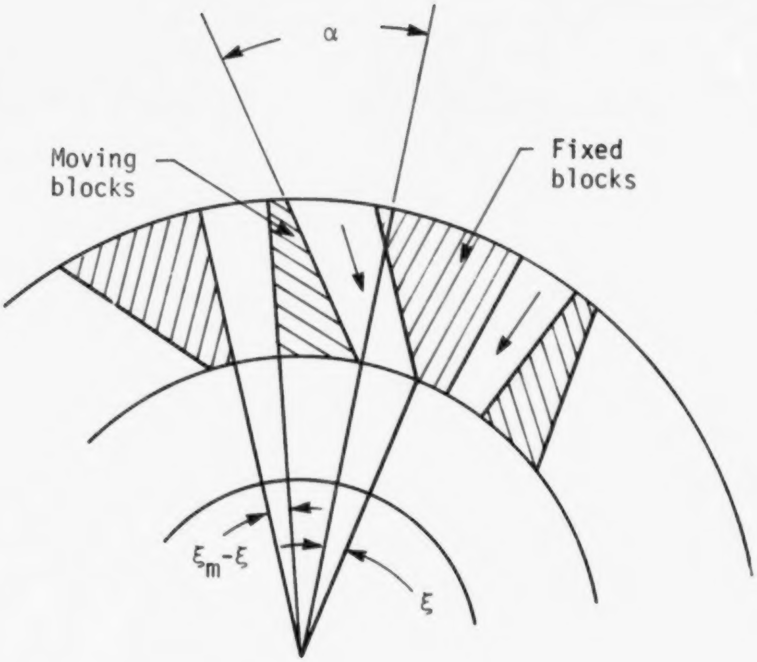
α
Moving blocks
Fixed blocks
$\xi_m-\xi$
$\xi$

$\xi_m = 8^{o}$

$\alpha = 43^{o}\ 23'$

Figure 45. Movable block type swirl generator.

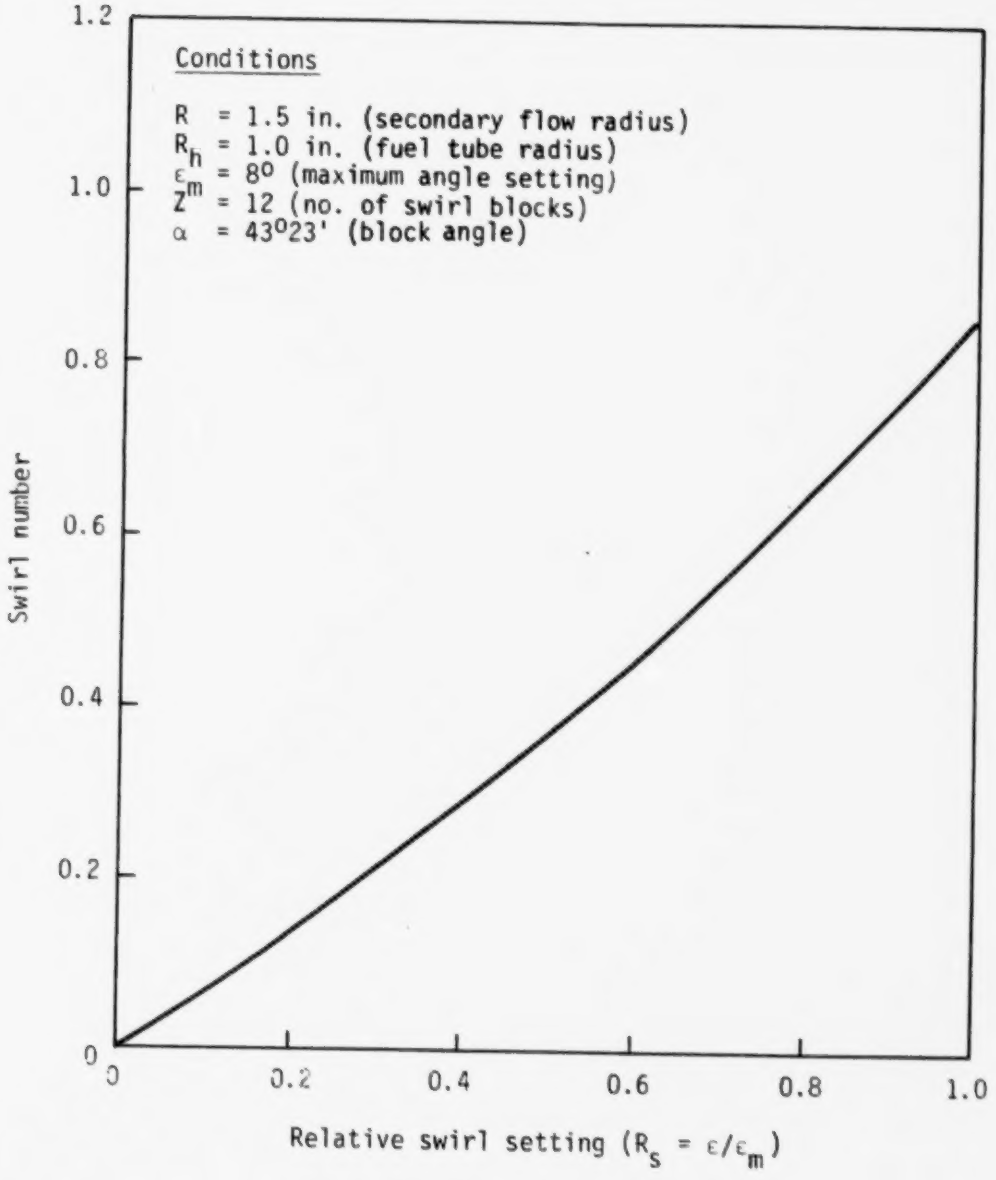

Figure 46. Calculated swirl no. for pilot-scale IFRF burner.

flow and low enough so that recirculating flow does not exist. Reference A-1 indicates that the critical swirl level required for recirculating flow is approximately 0.6.

## A.5 CONTINUOUS EMISSIONS SAMPLING

Flue gas samples were extracted continuously during furnace operation. A 1/4-in. stainless steel probe with a sintered SS 316 Mott Filter trapped 99.9 percent of particles larger than 2μ. The probe was typically positioned on the furnace centerline in the convective section, downstream of the last cooling tube set. The probe operated properly for temperatures up to 800°F. Compressed air automatically purged the probe at half-hour intervals.

The complete emissions sampling system is depicted in Figure 47. A refrigeration subsystem was located close to the probe to drop out condensate. The sample was pumped into a second conditioner through Teflon lines and then into the electro-optical analyzers. The flowrate through each analyzer was metered to 2.0 scfm and regulated to 12 psig. The instrumentation to determine levels of NO, unburned hydrocarbons, $O_2$, CO, and $CO_2$ is summarized in Table 20. Calibration gases used were 87 ppm NO, 807 ppm $CH_4$, 70 ppm $CH_4$, 4.0 percent CO, 200 ppm CO, 12.0 percent $CO_2$, and 4.96 percent $CO_2$.

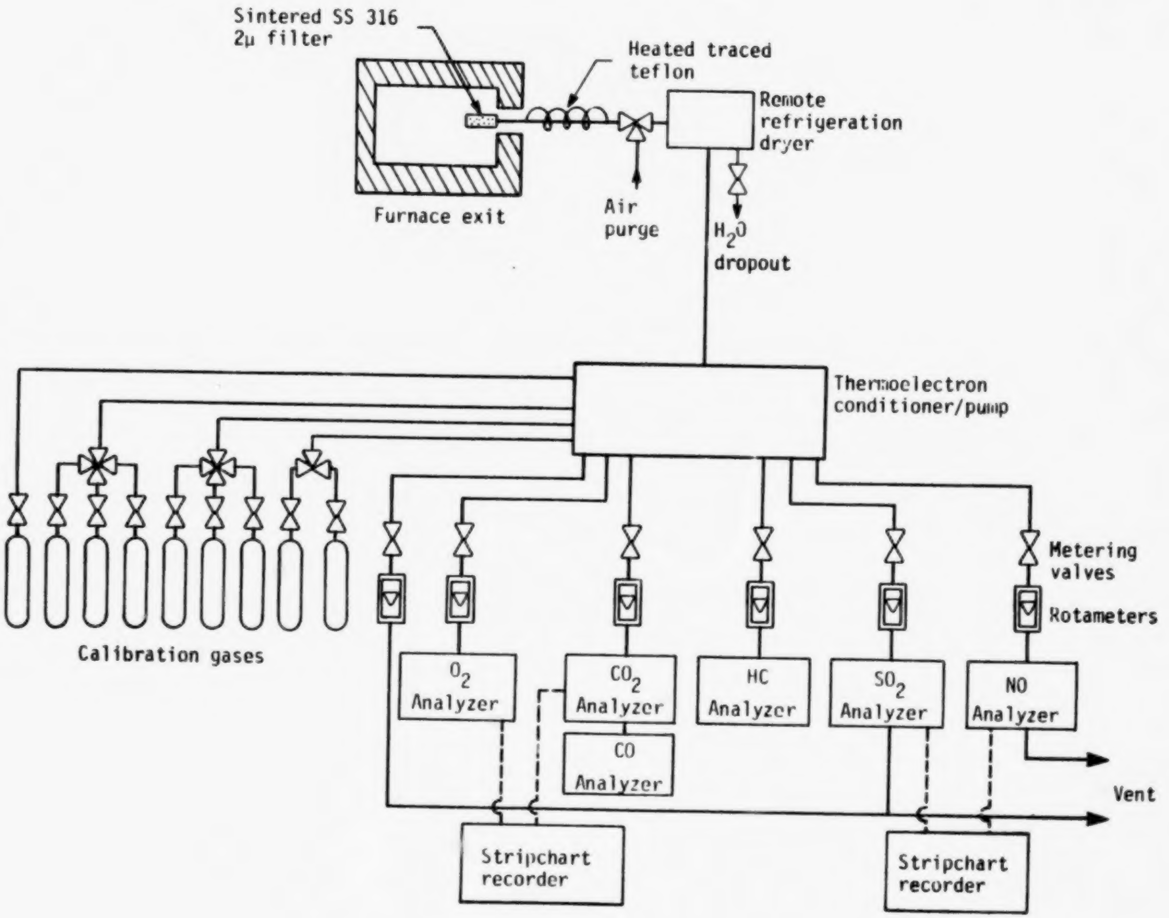
Sintered SS 316
2μ filter
Heated traced teflon
Remote refrigeration dryer
Furnace exit
Air purge
$H_2O$ dropout
Thermoelectron conditioner/pump
Metering valves
Rotameters
Calibration gases
$O_2$ Analyzer
$CO_2$ Analyzer
CO Analyzer
HC Analyzer
$SO_2$ Analyzer
NO Analyzer
Vent
Stripchart recorder
Stripchart recorder

Figure 47. Continuous emissions monitoring system.

TABLE 20. GASEOUS EMISSIONS MONITORING EQUIPMENT

| Instrument | Principal of operation | Manufacturer | Model | Instrument range |
|---|---|---|---|---|
| NO Analyzer | Chemiluminescence | Thermo Electron | 10A | 0 to 2.5 ppm |
| | | | | 0 to 10 |
| | | TECO | -- | 0 to 25 |
| | | | | 0 to 100 |
| | | | | 0 to 250 |
| | | | | 0 to 1,000 |
| | | | | 0 to 2,500 |
| | | | | 0 to 10,000 |
| UHC Analyzer | Flame Ionization Detection | Beckman | 400 | 0 to 100 ppm |
| | | | | 0 to 1,000 |
| | | | | 0 to 10,000 |
| | | | | 0 to 100,000 |
| $O_2$ Analyzer | Micro Fuel Measuring Cell | Teledyne | 326A | 0 to 5 percent |
| | | | | 0 to 10 |
| | | | | 0 to 25 |
| CO Analyzer | Nondispersive Infrared (NDIR) | Beckman | 315B | 0 to 300 ppm |
| | | | | 0 to 900 |
| | | | | 0 to 1,200 |
| CO Analyzer | Nondispersive Infrared (NDIR) | Anarad | AR600R | 0 to 15 percent |
| | | | AR500R | 0 to 1,000 ppm |
| $CO_2$ Analyzer | Nondispersive Infrared (NDIR) | Anarad | AR600R | 0 to 20 percent |
| Sample Gas Conditioner | Refrigerant Dryer-Condenser | Thermo Electron | 600 | 24 scfh |

# APPENDIX B

# DETAILED FURNACE OPERATION

## B.1 FUEL PREPARATION

The fuel oil used for all tests was Shell no. 2 grade distillate oil supplied by Peninsula Oil Company, Mountain View, California. Chemical analyses for atomic composition, heating value, viscosity, and density were provided by Truesdail Laboratories, Los Angeles, California for two batches of distillate oil. Table 21 shows that all properties are uniform to <1% between the lots analysed.

For the baseline studies, the distillate oil was pumped directly from 55-gal drums to the fuel delivery tube. For the single and multiple compound tests, the distillate oil and hazardous waste compounds were pumped in batches into a clean 55-gal drum, which was then installed in the oil delivery system. The distillate oil volume was measured by a Neptune model no. 137 positive displacement totalizing flowmeter to ±5 percent accuracy. The waste compounds were hand-pumped through a Tuthill model no. 800 totalizing flowmeter to ±10% accuracy. The precise waste compound volume fractions in the mixture were subsequently recalculated for each run based on chloride analysis of the fuel provided by Huffman Laboratories, Wheat Ridge, Colorado. The mixture was circulated through the fuel delivery system for 1 hour to ensure adequate mixing.

## B.2 OPERATION SCHEDULE

A vigorous daily testing schedule was required to control the temperature of the furnace gases. The essential dilemma was to produce repeatable temperature profiles uniquely characteristic of a set of furnace operating parameters. One solution was to allow the furnace (walls and gas stream) to reach a steady-state condition. Unfortunately, the time required was on the order of 20 hours. A less time-consuming and more manageable approach was to specify a fixed duration after light-off ($\Delta t'$) after which sampling would begin. This is shown schematically in Figure 48. Note that a different temperature path will be followed according to the initial temperature of the furnace refractory. Therefore, it was necessary to ensure that the wall temperature distribution was the same prior to igniting the oil/waste flame for each test. The black dots in Figure 48 represent a furnace temperature (gas or wall) characteristic of two different firing conditions when the initial wall temperature was $T_3$.

TABLE 21. NO. 2 FUEL OIL ANALYSES

| | Batch No. 1 | Batch No. 2 |
|---|---|---|
| Utimate analysis (wt %) | | |
| Carbon | 85.99 | 86.05 |
| Hydrogen | 12.96 | 13.35 |
| Nitrogen | 0.01 | 0.02 |
| Sulfur | 0.20 | 0.18 |
| Ash | <0.001 | <0.001 |
| Oxygen (by difference) | 0.84 | 0.40 |
| Heat or combustion (Btu/lb) | | |
| Gross | 19,620 | 19,600 |
| Net | 18,440 | 18,440 |
| Kinematic viscosity (cSt) | | |
| at 70°F | 4.3 | 4.5 |
| at 80°F | 3.8 | 3.9 |
| at 90°F | 3.4 | 3.5 |
| Specific gravity at 80°F | 0.840 | 0.837 |

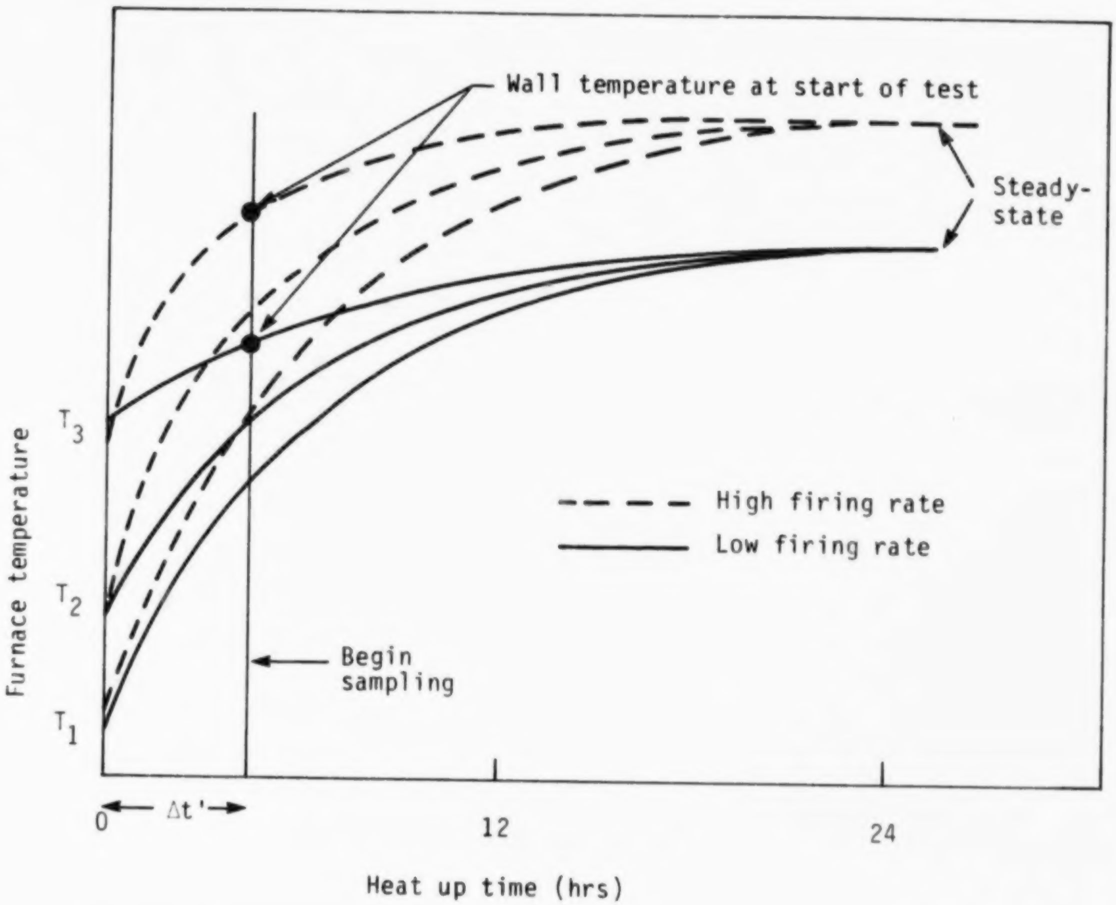

Figure 48. Transient furnace behavior examples.

The repeatability of the time-temperature profiles in the gas phase is dependent not only on keeping Δt' constant for each test, but also the ability to return to the same initial wall temperature. To achieve this the furnace was fired unattended overnight on natural gas between tests. Figure 49 shows the behavior of a representative wall temperature starting from three extreme temperatures and firing on natural gas. When the furnace is fired overnight at a fixed excess air level and firing rate, it approaches a steady state with repeatability of ±25°F, irrespective of the initial temperature on the previous day.

The operation schedule, then, called for switching the furnace from natural gas to oil/waste mixture in the morning. Operating data, emissions, pressures, and temperatures were recorded nominally at 1/2-hour intervals over a 3-hour period. After 3 hours, a series of organic samples would be taken simultaneously with measurement of at least 40 temperatures in the post-flame radiant gases. At the end of the day the furnace was returned to the natural gas firing mode for overnight operation.

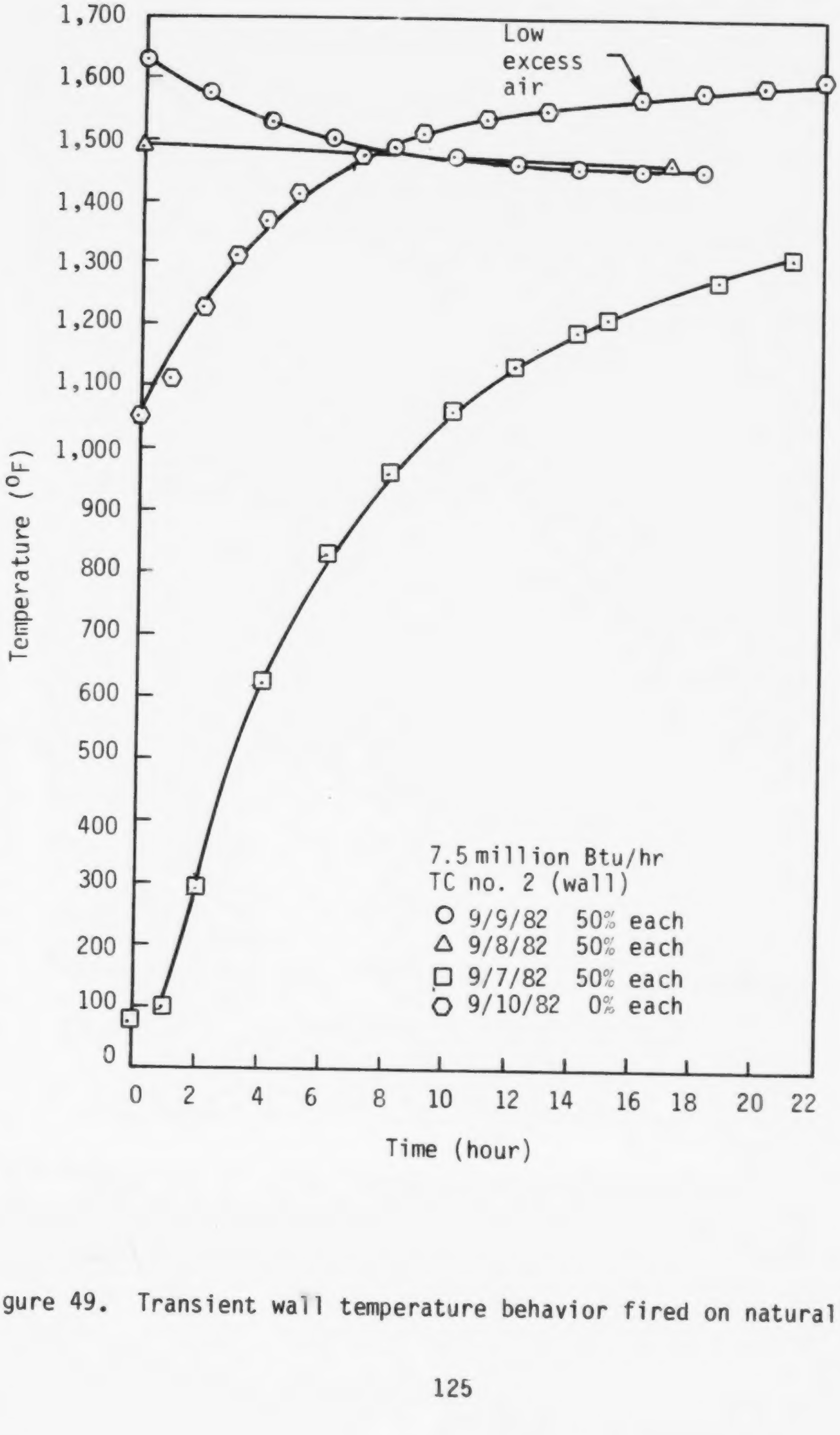

Figure 49. Transient wall temperature behavior fired on natural gas.

# APPENDIX C

## SAMPLING AND ANALYSIS

Sampling and analysis for this project was carried out during the infancy of the VOST protocol. Because of the evolving nature of the VOST during this time, special efforts were taken to ensure the quality of the data. It was decided that the train design used would be qualified by testing with artificial samples in the laboratory. In addition, the analytical procedures were also validated by the use of blind standards and laboratory prepared samples collected from gas streams saturated with HCl and moisture.

Quality assurance was paramount to the study because we were looking for differences among conditions. Therefore the test matrix was directed toward obtaining statistically significant data. The basic points of the program were:

- Validation of the analytical procedures
- Qualification of the sampling train
- Quality control of sample traps
- Use of blanks and duplicates

### C.1 SAMPLING PROCEDURES

The three types of samples drawn during these tests were:

- Tenax for selected organic species
- Bulk gas for moisture content and HCl concentration
- Fuel for total chlorides

Each required a different sampling technique. The procedures have been summarized in Section 3.5 and are described in detail below.

### C.1.1 Tenax (VOST)

Samples for organic analysis were collected from the flue gas duct between the convective heat recovery section and the induced draft exhaust fan (see Appendix A for a detailed description of the facility). Duct gas temperatures were nominally 150°C (approximately 300°F). Three samples were drawn for each run. The sampling train is shown schematically in Figure 3. It consisted of a 1/4-in. SS probe, a heat traced Teflon sampling line (maintained at 150°C (300°F)), an ice water cooled condenser, a Tenax trap, a knock-out impinger, a silica gel filled impinger, a pump, a rotameter, and a dry gas meter. A pressure gauge and shut-off valve were in line between the last impinger and the pump. The Tenax trap was subjected to additional cooling by being wrapped with an ice pack. Early in the program the traps were 25 cm long by 8 mm ID and had standard swagelock fittings with graphite ferrules. Later, the traps were 10 cm long by 12 mm ID.

The system was leak checked by disconnecting the line between the condenser and the sampling line, capping the condenser, pulling a vacuum of approximately 16 in. Hg. on the system, and closing the shutoff valve. The system had to maintain greater than 12 in. Hg. above normal sampling vacuum for 1 minute (see Section C.2). Samples were drawn for 10 to 20 minutes at a rate of 300 or 600 mL/min, the time being adjusted to extract 20 liters of gas or less. The volume drawn was dependent on the expected concentration of the component of interest. The desired level was between 100 and 1,000 ng per trap.

### C.1.2 Bulk Gas

Bulk gas samples were drawn to determine the moisture and hydrogen chloride content of the gas stream. The moisture content was necessary to determine the flue gas flow rates while hydrogen chloride emissions were monitored to perform material balance calculations and for safety considerations. The two data points were obtained with the same sample. The method used was the Texas Air Control Board condenser method. A Greenburg-Smith impinger approximately one-half full of water followed by a straight impinger approximately one-half full of silica gel was used. A measured volume of gas, usually about 10 $ft^3$, was drawn through the impingers at a moderate flow rate while the impingers were partially immersed in an ice bath. The total change in weight of the impingers is the combined weight of the captured moisture and HCl gas. The preliminary moisture content is estimated from the weight gain. This is later corrected when the impinger water chloride analysis is obtained.

### C.1.3 Fuel

Fuel samples were drawn from the fuel feed line during each period that Tenax samples were taken. The procedure for preparing fuel-waste mixtures and sampling them has been given in Appendix B.

## C.2 SAMPLING TRAIN QUALIFICATION

During the period of time that this program was in progress the sampling methodology for organics was in a state of flux. Therefore, the train used for these tests was subjected to a series of qualification tests to insure its ability to collect valid samples. The following performance characteristics were determined:

- Flow rates
- Pressure drops
- Recovery of components (wet and dry streams)
- Breakthrough

The pressure drops across the train at flow rates of 300 and 600 mL/min were determined so that the correct vacuum could be used for leak checks. The early generation traps had pressure drops between 8 and 20 in. Hg., while the later versions had pressure drops on the order of 4 in. Hg. The later generation traps were also much sturdier and easier to handle in the field.

Of highest importance was the determination of recovery efficiencies and potential breakthrough for the PHOC's of interest. A known volume of each PHOC was injected in an air stream as the stream was pulled into the train. The air stream was pretreated by being pulled either through a charcoal trap or a charcoal trap followed by a heated impinger filled with concentrated hydrochloric acid. Recoveries of all components (carbon tetrachloride, chloroform, dichloroethane, and chlorobenzene) ranged between 90 and 130 percent at injection quantities of 50 and 500 ng. Collection efficiency of a single trap ranged betwen 70 and 90 percent.

## C.3 ANALYTICAL PROCEDURE

Analytical procedures began with the preparation of the traps. Each trap was baked at 225°C for 16 hours with nitrogen purging at a rate of approximately 10 mL/min. The trap was then analyzed by GC/Hall to verify that no chlorinated species above 5 ng (as carbon tetrachloride and chlorobenzene) were present. The traps were then sealed and transported to the sampling site. Upon being returned to the laboratory the samples were stored in a refrigerator until analyzed.

Analysis of the traps was begun by desorbing in a reverse direction at 200°C with approximately 100 mL nitrogen onto a 1 percent SP-100 carbopak B 60/80 mesh gas chromatographic column held at 60°C. Following desorbtion of the trap the GC column temperature was ramped up at a rate of 20°C/min to 220°C and held for 20 minutes. The detector was a Hall electrolytic conductivity detector set in the halogen mode. Standards were run by spiking a blank trap with approximately 100 ng of each component of interest. Samples were injected with an internal standard (bromofluroethane) prior to analysis. Retention times and response factors were monitored relative to the internal standard.

## C.4 ANALYTICAL PROCEDURE VALIDATION

Under ideal conditions, the detection limit of the system was found to be about 0.5 ng per trap. Excellent reproducibility (RSD 6.5 percent) was obtained at concentrations of 100 ng each chlorobenzene, carbon tetrachloride, chloroform, and 1,2-dichloroethane spiked directly on the trap. The recoveries averaged 92 percent at 100 ng per trap, 85 percent at 10 ng per trap, and 70 percent at 1.0 ng per trap. Results of samples spiked into various gas streams were discussed above. The detector response was found to be linear in the range 1 to 2,000 ng. Reproducibility of retention time was ±0.1 percent for a series of five traps spiked with chlorobenzene and bromoflouroethane at 1 to 100 ng, and analyzed sequentially.

# APPENDIX D

# DATA HANDLING AND REDUCTION PROCEDURES

This program generated a large volume of diverse types of data. The data handling plan is presented in this section to illustrate the origins and reduction algorithms.

## D.1 GENERAL DATA FLOW

Four broad classes of data were collected: facility design data, furnace operating data, sampling data, and analysis data. The sequence of data reduction steps and how the data is used to determine the desired results is shown in Figure 50. Raw data collected in any disciplinary area (e.g., analysis) is first reduced to a set of numbers that will be used in the first phase of integration and reduction. Combining results from the first phase of interdisciplinary integration gives the first level or primary results. Primary results are the hard numbers of a study, which are then further manipulated and integrated to achieve secondary or comparative results. Thus the following sequence of data reduction will occur.

Analysis data is reduced to give specie concentration per sample, while sampling data is reduced to give quantity of material sampled. These are combined to generate specie concentration in a particular stream. This data is combined with mass flowrate data to give specie DRE's, a hard or primary result. The next step combines and integrates the data from different runs and conditions and identifies directional DRE trends from specified changes in certain operation parameters, the furnace conditions.

The following sections will present, on a technical discipline basis, the various raw data collected. The last section will show how primary results were computed. (Section 5.6 discusses the modeling output.) Facility design data is given in Appendices A and B. Kinetic data were available outside the program (2 to 4, 30, 32 to 34) and will not be discussed in depth.

## D.2 FURNACE OPERATION DATA

This section describes in detail the raw data collected by the furnace operating engineer. Data were collected which were relevant both to experimental results and operating safety. Furnace operating data were collected on five different field data forms. Examples of portions of data sheets for run C-3 are shown in Figures 51 and 52. Data from this run (C-3)

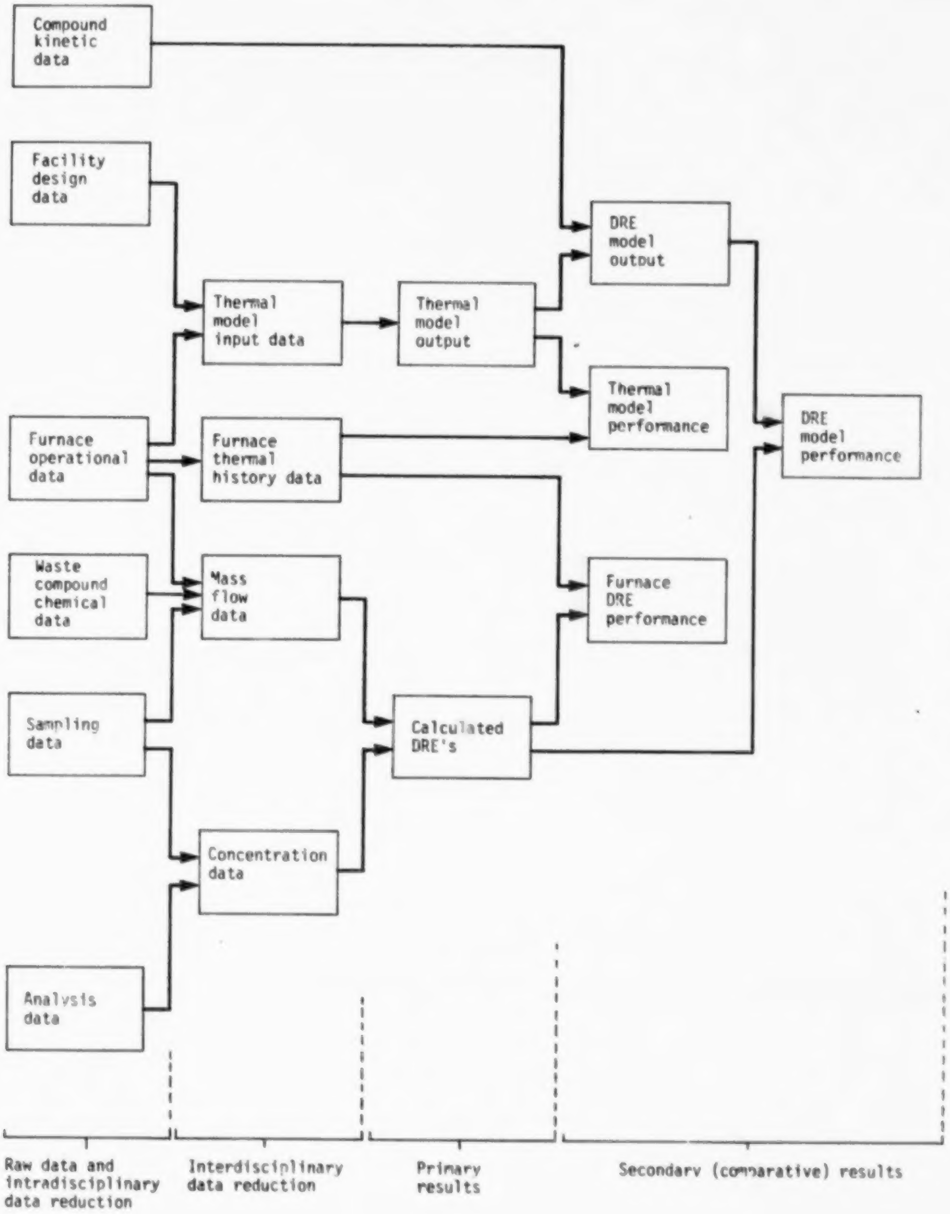
Compound kinetic data
Facility design data
Thermal model input data
Thermal model output
DRE model output
Thermal model performance
Furnace operational data
Furnace thermal history data
DRE model performance
Waste compound chemical data
Mass flow data
Furnace DRE performance
Sampling data
Calculated DRE's
Concentration data
Analysis data
Raw data and intradisciplinary data reduction
Interdisciplinary data reduction
Primary results
Secondary (comparative) results

Figure 50. Major steps for the general data reduction sequence.

Furnace Data Sheet 1
Run Number: C-3
Date: 4/7/83
Operator: Garman

Primary Operating Data
Fuel: Distillate/CB-CT
Nozzle: 10 gph -- 70°A

| 1<br>Time | 2<br>Gas rota-meter | 3<br>Gas firing rate* | 4<br>Oil barrel number | 5<br>Oil rota-meter | 6<br>Oil temper-ature | 7<br>Oil volume flow† | 8<br>Oil firing rate‡ | 9<br>Oil pressure | 10<br>Air Temper-ature | 11<br>Anemo-meter |
|---|---|---|---|---|---|---|---|---|---|---|
| 24 hr | x/100 | Million Btu/hr | 1<br>2<br>3 | | °F | gal/hr | Million Btu/hr | psig | °F | volts |
| 1215 | | | | | | | | | | |
| 1255 | | | 2G | 17.0 | 87 | 5.8 | 0.80 | 40 | 74 | 4.0 |
| 1341 | | | 2G | 17.0 | 91 | 5.8 | 0.80 | 40 | | 4.0 |
| 1408 | | | 2G | 17.0 | 91 | 5.8 | 0.80 | 40 | | 4.0 |
| 1453 | | | 2G | 16.9 | 89 | 5.8 | 0.80 | 40 | 70 | 4.0 |
| 1612 | | | 2G | 16.8 | 87 | 5.8 | 0.80 | 39 | 60 | 3.95 |
| 1629 | | | | | | | | | | |
| 1648 | 52 | | | | | | | | | 3.6 |

| 12<br>Air volume flow | 13<br>Furnace pressure | 14<br>Air preheat temper-ature | 15<br>Fuel tube position | 16<br>Swirl | 17<br>Total excess air | 18<br>Total excess air | Comments |
|---|---|---|---|---|---|---|---|
| cfm | in. $H_2O$ | °F | in. | 0-8 | ($O_2$) % | ($CO_2$) % | |
| 150 | -0.4 | 356 | 7 15/16 | 7.5 | 24 | 26 | Relit on oil 2G good flame |
| 150 | -0.3 | 358 | 7 15/16 | 7.5 | 23 | 25 | |
| 150 | -0.5 | 356 | 7 15/16 | 7.5 | 23 | 26 | |
| 150 | -0.7 | 356 | 7 15/16 | 7.5 | 22 | 25 | |
| 148 | -0.6 | | 7 15/16 | 7.5 | 23 | 26 | Soot buildup |
| | -2.0 | | | 7.5 | | | Oil flame off<br>Gas on |

* Calculated at 5 psig, 77°F, and 1,050 Btu/scf.
† From chart 1 oil rotameter calibration chart.
‡ Calculated from fuel heating value.

Figure 51. Sample raw data sheets 1 and 2 for run C-3.

Furnace Data Sheet 2
Run Number: C-3
Date: 4/7/83
Operator: Garman

Primary Temperature Data
Fuel: Distillate/CB-CT
Nozzle: 10 gph -- 70°A

| 1 | 2 | 3 | 4 | 5 | 6 | 7 | 8 | 9 |
|---|---|---|---|---|---|---|---|---|
| Time | Wall B-1 K1 | Wall C-1 K2 | Wall C-5 K3 | Wall D-5 K4 | Wall E-5 K5 | BDRY gas F-3 K6 | Furnace exit K7 | Conv sec wall K8 |
| 24 hr | °F | °F | °F | °F | °F | °F | °F | °F |
| 1230 | 1,070 | 1,190 | 629 | 934 | 1,011 | 921 | 420 | 330 |
| 1258 | 1,163 | 1,230 | 632 | 1,080 | 998 | 958 | 428 | 324 |
| 1344 | 1,246 | 1,275 | 632 | 1,156 | 999 | 989 | 437 | 313 |
| 1412 | 1,263 | 1,291 | 632 | 1,177 | 1,004 | 1,003 | 438 | 309 |
| 1445 | 1,270 | 1,299 | 631 | 1,180 | 1,010 | 1,004 | 435 | 305 |
| 1620 | 1,293 | 1,322 | 630 | 1,203 | 1,017 | 1,007 | 431 | 296 |

| 10 | 11 | 12 | 13 | 14 | 15 | 16 | 17 |
|---|---|---|---|---|---|---|---|
| ID fan stack K10 | Bag-house K1' | Therminol K8' | Conv sec gas (CO) K9' | Conv sec gas (HI) K10' | Sample gas K11' | Comb gas* R2 | Range |
| °F | °F | °F | °F | °F | °F | °F | ±°F |
| 268 | 85 | 169 | 1,118 | 725 | 339 | 1,325 | 20 |
| 273 | 86 | 177 | 1,146 | 744 | 342 | 1,385 | 15 |
| 284 | 86 | 180 | 1,191 | 757 | 351 | 1,420 | 20 |
| 275 | 86 | 182 | 1,189 | 767 | 347 | 1,410 | 10 |
| 277 | 85 | 181 | 1,188 | 762 | 350 | 1,420 | 10 |
| 272 | 83 | 178 | 1,176 | 760 | 345 |  |  |

* At position D-2 centerline.

Figure 51. Sample raw data sheets 1 and 2 for run C-3 (Concluded).

Furnace Data Sheet 3
Run Number: C-3
Date: 4/7/83
Operator: Garman

Furnace Gas Temperatures

| 1 | 2 | 3 | 4 | 5 | 6 | 7 | 8 | 9 | 10 |
|---|---|---|---|---|---|---|---|---|---|
| Axial location | Wall | Time start | Time end | 0" min | 0" max | 1" min | 1" max | 2" min | 2" max |
| Sec-port | L R T | 24 hr | 24 hr | Temperature, °F | | | | | |
| D-2 | L | 1534 | 1536 | 1,455 | 1,480 | 1,516 | 1,534 | 1,532 | 1,550 |
| C-3 | L | 1537 | 1539 | 1,597 | 1,618 | 1,666 | 1,678 | 1,695 | 1,716 |
| E-2 | L | 1542 | 1544 | 1,317 | 1,328 | 1,374 | 1,387 | 1,390 | 1,397 |
| B-4 | L | 1545 | 1547 | 1,580 | 1,596 | 1,667 | 1,669 | 1,686 | 1,704 |
| F-2 | L | 1606 | 1610 | 1,138 | 1,179 | 1,280 | 1,288 | 1,312 | 1,321 |

| 11 | 12 | 13 | 14 | 15 | 16 | 17 | 18 | 19 | 20 |
|---|---|---|---|---|---|---|---|---|---|
| 3" min | 3" max | 4" min | 4" max | 8" min | 8" max | 12" min | 12" max | 16" min | 16" max |
| Temperature, °F | | | | | | | | | |
| 1,539 | 1,552 | 1,553 | 1,571 | 1,551 | 1,558 | 1,531 | 1,537 | 1,500 | 1,518 |
| 1,719 | 1,725 | 1,728 | 1,744 | 1,739 | 1,750 | 1,642 | 1,656 | 1,604 | 1,620 |
| 1,409 | 1,417 | 1,432 | 1,447 | 1,418 | 1,428 | 1,376 | 1,390 | 1,374 | 1,379 |
| 1,710 | 1,721 | 1,708 | 1,737 | 1,728 | 1,739 | 1,764 | 1,772 | 1,827 | 1,841 |
| 1,345 | 1,362 | 1,326 | 1,344 | 1,318 | 1,324 | 1,321 | 1,338 | 1,287 | 1,292 |

Figure 52. Examples of raw data sheets 3, 4, and 5 (data from run C-3).

Furnace Data Sheet 4
Run Number: C-3
Date: 4/7/83
Operator: Garman

Heat Extraction Data

| 1<br>Time<br>24 hr | 2<br>Left waterwall flow<br>gpm | 3<br>Right waterwall flow<br>gpm | 4<br>Left inlet temp<br>°F | 5<br>Right outlet temp<br>°F | 6<br>Left outlet P-1<br>°F | 7<br>Left outlet P-2<br>°F | 8<br>Left outlet P-3<br>°F |
|---|---|---|---|---|---|---|---|
| 1301<br>1548<br>1555 | 14.0 | 13.5 | 97 | 97 | 134 | 137 | 130 |

| 9<br>Right Outlet P-1<br>°F | 10<br>Right outlet P-2<br>°F | 11<br>Right outlet P-3<br>°F | 12<br>Quarl vol flow<br>gpm | 13<br>Quarl inlet<br>°F | 14<br>Quarl outlet<br>°F |
|---|---|---|---|---|---|
| 123 | 135 | 138 | 5.5 | 94 | 112 |
| | | | 5.5 | 97 | 116 |

Waterwall panel code
Top view

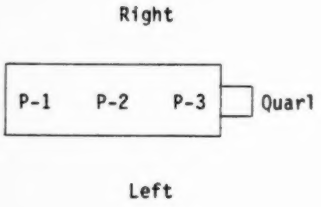

Figure 52. Examples of raw data sheets 3, 4, and 5 (data from run C-3) (Continued).

Furnace Data Sheet 5
Run Number: C-3
Date: 4/7/83
Operator: Garman

Continuous Monitor Readouts

| 1 | 2 | 3 | 4 | 5 | 6 |
|---|---|---|---|---|---|
| Time | $O_2$ | $CO_2$ | CO | NO | UHC |
| 24 hr | mole % | mole % | ppm | ppm | ppm |
| 1257 | 4.3 | 12.2 | 30 | 77 | 7.5 |
| 1343 | 4.1 | 12.3 | 20 | 87 | 1.0 |
| 1411 | 4.2 | 12.2 | 30 | 92 | ND |
| 1449 | 4.0 | 12.3 | 20 | 96 | 4.0 |
| 1617 | 4.1 | 12.2 | 30 | 95 | ND |

Note: All data is on a dry v/v basis.
UHC is as propane.

Figure 52. Examples of raw data sheets 3, 4, and 5 (data from run C-3) (Concluded).

will be used throughout the section. Following is a description of the most significant items for DRE calculation and modeling considerations. The presentation is broken into sections parallelling the data sheets. In the text, each data point is identified with a number corresponding to the data sheet on which it is found, followed by a number corresponding to its column on the example sheet. For example, the gas firing rate is found on the first data sheet, third column, and is identified as 1-3.

### D.2.1 Furnace Data Sheet 1 -- Primary Operating Data

1-1 Time: The absolute time at which data is collected, generally at 30- to 45-min intervals

1-2 Gas rotameter: The natural gas fuel rotameter flowrate measurement. This value is used to set the overnight idle rate for the furnace.

1-3 Gas firing rate: The natural gas firing rate calculated from the rotameter reading. Pressure is assumed to be 0.34 atmospheres (5 psig), temperature 25°C, and the heat content 39 million joules/cubic meter (1,050 Btu/scf). The gas firing rate is maintained at a consistent setting for overnight operation to insure uniform starting conditions at the beginning of each run, typically 0.23 megawatts (0.8 million Btu/h)r.

1-4 Oil barrel number: Normally, three barrels of fuel-waste mixture are made up for each run. This number identifies which mixture is being fired for analytical purposes.

1-5 Oil rotameter: The distillate oil/waste mixture flowrate reading. The rotameter calibration is based on the density and viscosity of the distillate oil.

1-6 Oil temperature: The distillate oil/waste temperature at the rotameter. The rotameter is particularly sensitive to liquid viscosity which is, in turn, temperature dependent. The fuel temprature varies between 20° and 50°C depending on the ambient conditions.

1-7 Oil volume flow: The calculated volume flowrate is based on rotameter reading and temperature, and ranges between 19 and 34 L/hr (5 and 9 gal/hr). The value is read from a predetermined chart as depicted in Figure 53.

1-8 Oil firing rate: This is a calculated value based on distillate oil heating value and volume flow. For this program it was targeted to be either 0.23 or 0.35 megawatts (0.8 or 1.2 million Btu/hr). The value is read from a precalculated chart shown in Figure 54.

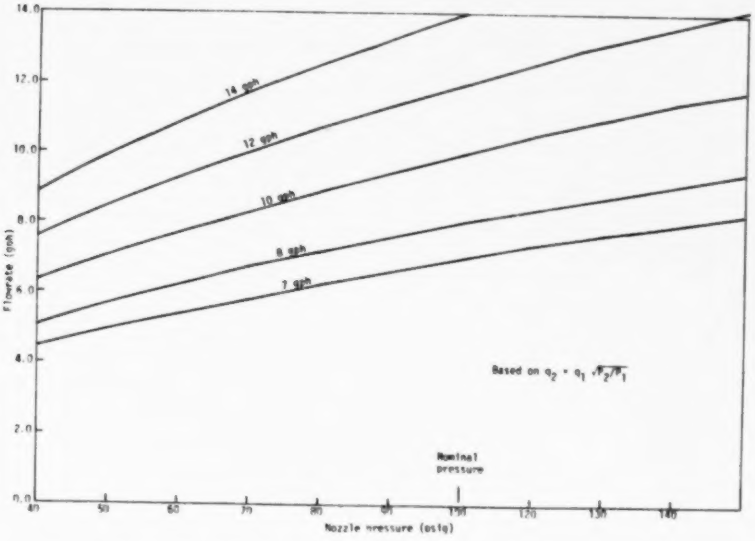

a. Determining distillate fuel flow rate from nozzle pressure

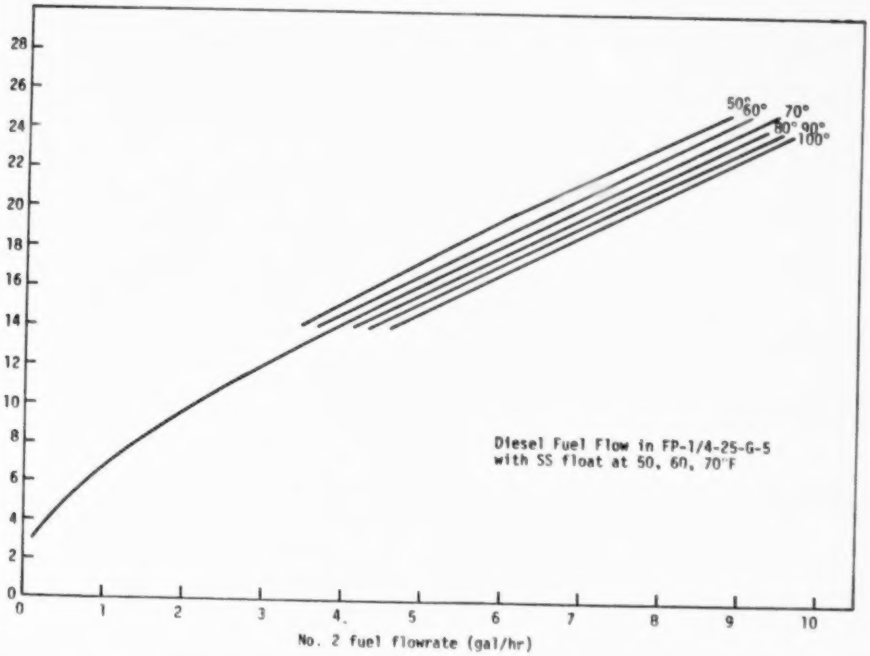

b. Determining distillate fuel flow rate from fuel rotameter setting

Figure 53. Examples of control charts for furnace operation.

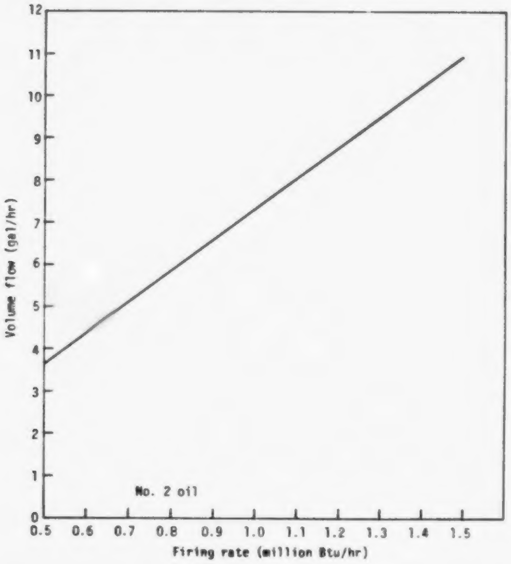

a. Determining firing rate from fuel flow rate (pure distillate)

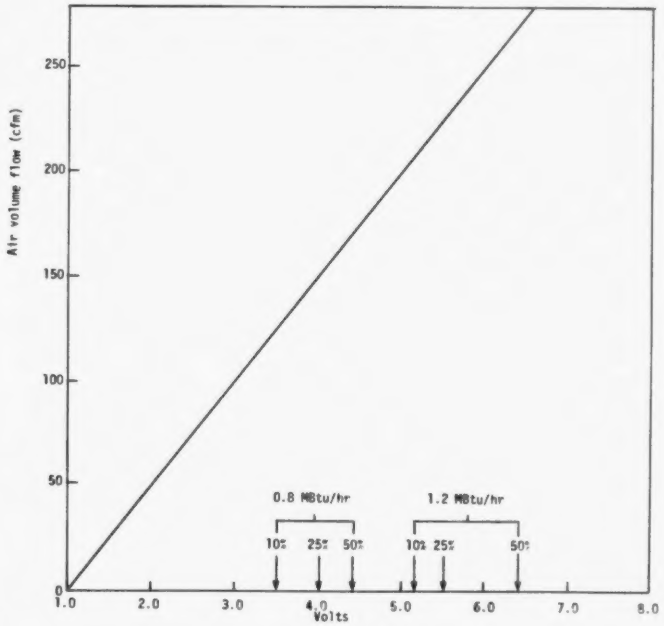

b. Determining air flow rate from anemometer reading

Figure 54. Examples of control charts for furnace operation.

1-9 Oil pressure: The distillate oil/waste mixture pressure immediately upstream of the fuel delivery nozzle. The pressure is significant for several reasons. It is an indicator of the extent of atomization which may have a large effect on destruction efficiency, and it provides an independent verification of flowrate. The nozzles used are calibrated such that 100 psig (690 kPa) corresponds roughly to the nozzle flow rating. Typically 10.0 gph (0.6 L/min) rated nozzles were used over the pressure range of 40 to 80 psig (275 to 552 kPa).

1-10 Air temperature: The ambient air temperature

1-11 Anemometer voltage: The voltage measured across the hot wire anemometer

1-12 Total air flow: The total actual combustion air flowrate (acfm) based on the hot wire anemometer voltage output. The value is read from a calibration chart as shown in Figure 54. The air preheat temperature measurement (1-10) allows conversion to scfm.

1-13 Furnace pressure: The pressure measured at the center of the firebox. It is a measure of the degree of air leakage into the furnace; the more negative the pressure, the greater the addition of ambient air into the postflame gas stream. The induced draft fan is adjusted to minimize the in-leakage, but maintain slightly subatmospheric pressure.

1-14 Air preheat temperature: The temperature measured at the burner entrance, nominally 177°C (350°F)

1-15 Fuel tube position: A distance measurement related to the axial position of the fuel delivery tube within the burner. A low value indicates downstream penetration of the point of injection, and a short bulk residence time. This parameter was not significantly varied during the program.

1-16 Swirl: Burner swirl setting on a scale of 0 to 8. See Section 3.2 for a discussion of the impact of swirl.

1-17 Total excess air ($O_2$): Combustion stoichiometry calculated based on oxygen in the exhaust assuming distillate oil firing. Excess air levels were targeted to be 10, 25, and 50 percent by iterative adjustment of furnace pressure and combustion air delivery. Values are read from the chart example in Figure 55.

1-18 Total excess air ($CO_2$): Combustion stoichiometry calculated based on carbon dioxide in the exhaust

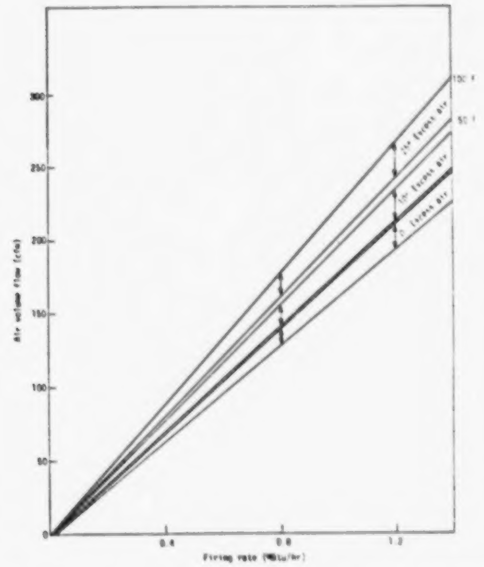

a. Determining air flow rate necessary for a given firing rate and desired excess air rate

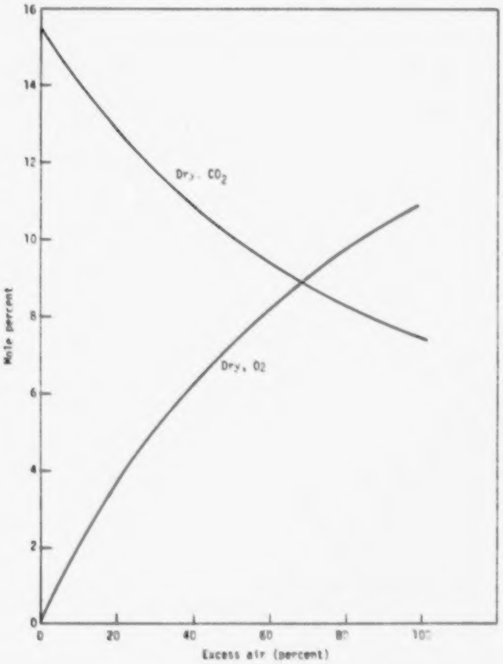

b. Determining actual excess air rate from $CO_2$ or $O_2$ concentration

Figure 55. Control charts for furnace operation.

### D.2.2 Furnace Data Sheet 2 -- Primary Temperature Data

2-1 Time: The absolute time when a set of readings was taken

2-2 to 2-6 Wall temperatures: Temperatures at various locations in the refractory walls of the firebox

2-7 to 2-16 Gas temperatures: Temperatures of the gas stream at various locations throughout the pilot unit.

2-17 Range: The range over which the temperature at the centerline of the firebox at cross section D-2 was observed to fluctuate in a 30-sec period

### D.2.3 Furnace Data Sheet 3 -- Furnace Gas Temperatures

3-1 Axial location: The cross section identifier for a set of sampling ports. The cross sections at which samples were taken are designated B-4, C-3, D-2, E-2, and F-2, with B-4 the closest to the burner face. See Figure 3-2 for the positions of each cross section.

3-2 Wall: The wall designation for the port from which the location of the thermocouple reading is measured. The walls are designated L for left, R for right, and T for top as one faces downstream with the gas flow.

3-3 Time start: The time at which the measurements for a particular cross section began

3-4 Time stop: The time at which the measurements for a particular cross section was completed

3-5 to 3-20 Temperatures: The high and low temperature measured over an approximately 10-sec time span at each designated distance from the wall at the particular cross section

### D.2.4 Furnace Data Sheet 4 -- Heat Extraction Data

4-1 Time: The time at which the measurements were read

4-2 and 4-3 Waterwall flow: The volume flowrate of water in the waterwalls within the firebox

4-4 to 4-11 Inlet and outlet temperatures: The measured inlet and outlet temperatures of the water flowing in the waterwalls

4-12 Quarl flowrate: The flowrate of water in the burner quarl. This is measured because the quarl extracts a significant amount of heat from the burner

4-13 and 4-14 Quarl inlet and outlet temperatures: The temperatures of the quarl cooling water

### D.2.5 Furnace Data Sheet V -- Continuous Monitor Readouts

5-1 Time: The time at which the monitor charts were read

5-2 to 5-6 Gas specie concentration: The measured concentration of the particular specie (oxygen, carbon dioxide, carbon monoxide, nitric oxide, and unburnt hydrocarbon) sampled in the furnace convective section and measured by continuous emissions analysis. The values are on a dry volume/volume basis.

## D.3 SAMPLING DATA

Three different gas phase samples were collected in addition to the continuous monitoring samples for oxygen, carbon dioxide, carbon monoxide, and nitrogen oxides taken as part of the furnace operation. These samples were for the moisture determination, the chloride concentration, and the volatile organics concentration. No sampling was done for semivolatile organics because the selected POHC's were all within the volatile designations. Sampling data was recorded on two sheets, the Preliminary Moisture Determination Data Sheet (Figure 56) and the Volatile Organic Sampling Train Data Sheet (Figure 57). The gas sample drawn for determination of moisture content was also used for the chloride emission rate sample. Table 22 indicates the type of data obtained from the reduction of the sampling data. These are the values that are carried forward in the data reduction scheme to be integrated with the sampling data to calculate emission rates. The gas volumes have been corrected from "actual" (as sampled) to standard. Standard gas volumes are defined at 68°F and 1 atmosphere of pressure. The following subsections define the various pieces of data on each sheet and explain how they are used.

### D.3.1 Sampling Data Sheet 1 -- Preliminary Moisture Determination

1-1 Barometric pressure: Used with dry gas meter temperature to correct gas volume to a standard volume. Expressed in inches of mercury and measured usually once during the sampling day.

1-2 Clock time: The time, on a 24-hr basis, at which the sampling was started and stopped.

1-3 Dry gas meter reading: The actual reading of the dry gas meter before and after sampling.

1-4 Flow meter reading: The instantaneous rate of flow of the sampled gas stream as read on a rotameter.

1-5 Dry gas meter temperature: The temperature of the gas stream passing into the dry gas meter. Used to calculate the standard volume sampled.

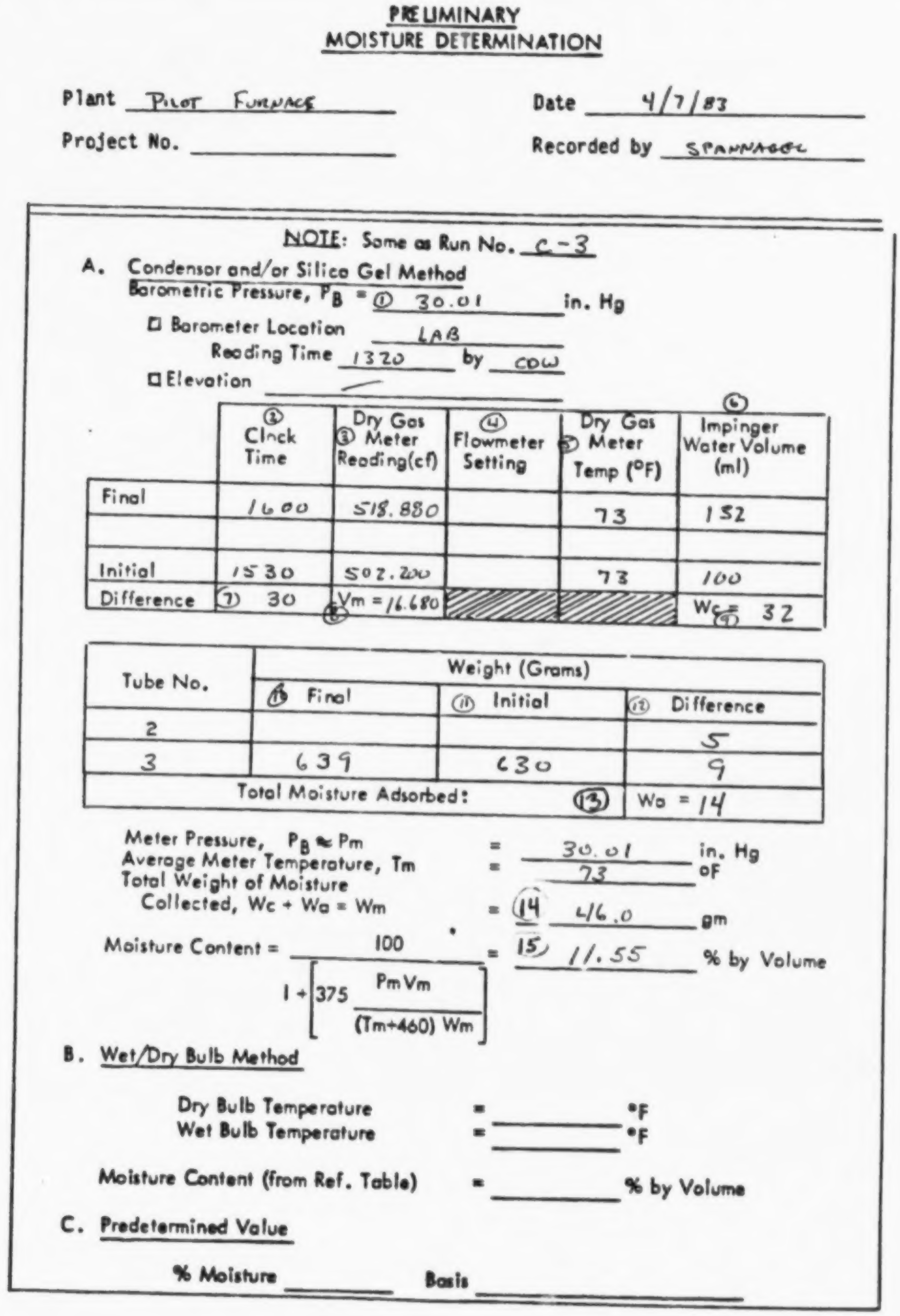

PRELIMINARY
MOISTURE DETERMINATION

Plant Pilot Furnace

Date 4/7/83

Project No. ____

Recorded by Spannagel

NOTE: Same as Run No. C-3

A. Condensor and/or Silica Gel Method

Barometric Pressure, $P_B$ = ① 30.01 in. Hg

☐ Barometer Location LAB

Reading Time 1320 by COW

☐ Elevation —

| | ② Clock Time | Dry Gas ③ Meter Reading(cf) | ④ Flowmeter Setting | Dry Gas ⑤ Meter Temp (°F) | ⑥ Impinger Water Volume (ml) |
|---|---|---|---|---|---|
| Final | 1600 | 518.880 | | 73 | 152 |
| | | | | | |
| Initial | 1530 | 502.200 | | 73 | 100 |
| Difference | ⑦ 30 | ⑧ Vm = 16.680 | ▨ | ▨ | ⑨ Wc = 32 |

| Tube No. | Weight (Grams) | | |
|---|---|---|---|
| | ⑩ Final | ⑪ Initial | ⑫ Difference |
| 2 | | | 5 |
| 3 | 639 | 630 | 9 |
| Total Moisture Adsorbed: | | ⑬ | Wa = 14 |

Meter Pressure, $P_B \approx P_m$ = 30.01 in. Hg

Average Meter Temperature, Tm = 73 °F

Total Weight of Moisture Collected, Wc + Wa = Wm = ⑭ 46.0 gm

$$\text{Moisture Content} = \frac{100}{1+\left[375\,\frac{P_m V_m}{(T_m+460)\,W_m}\right]} = ⑮\ 11.55\ \%\text{ by Volume}$$

B. Wet/Dry Bulb Method

Dry Bulb Temperature = ____ °F

Wet Bulb Temperature = ____ °F

Moisture Content (from Ref. Table) = ____ % by Volume

C. Predetermined Value

% Moisture ____ Basis ____

Figure 56. Example of raw data for moisture train and gas phase chloride sampling.

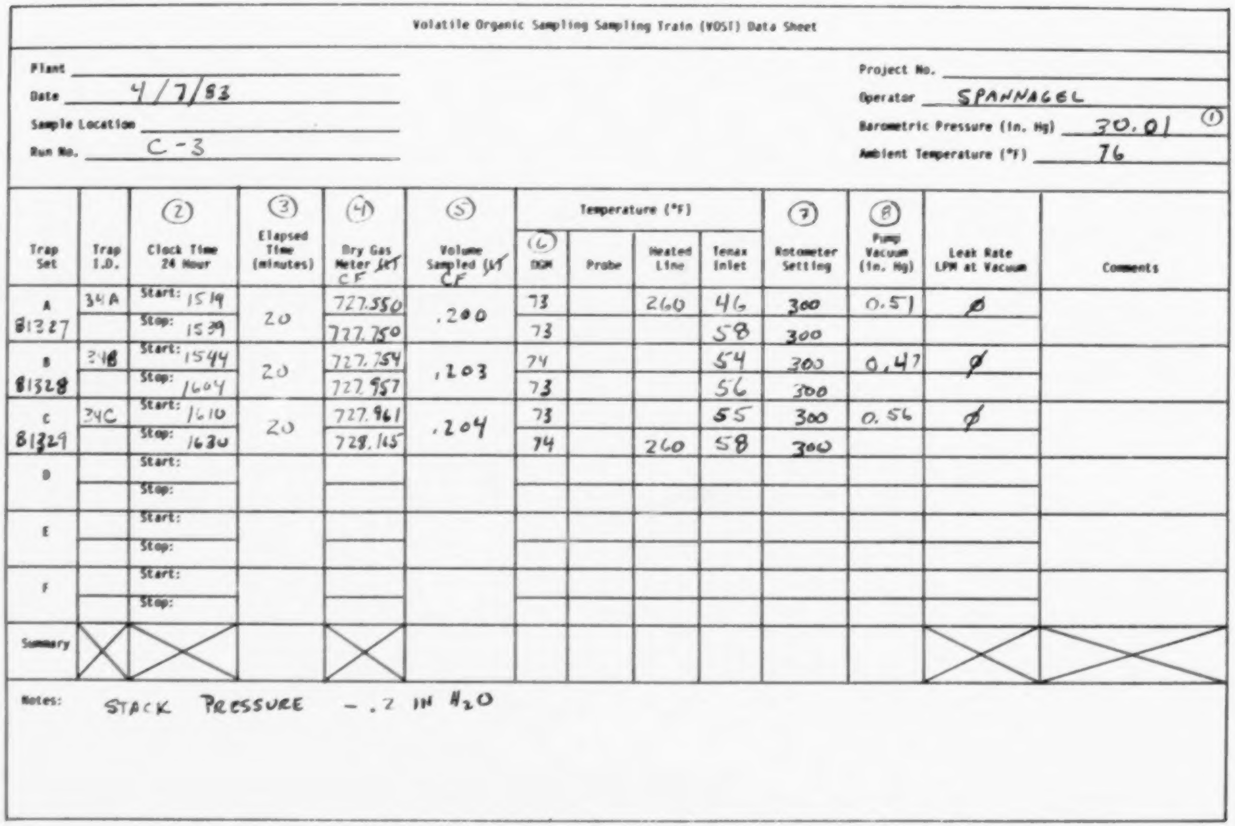

Volatile Organic Sampling Sampling Train (VOST) Data Sheet

Plant
Date 4/7/83
Sample Location
Run No. C-3

Project No.
Operator SPANNAGEL
Barometric Pressure (in. Hg) 30.01 ①
Ambient Temperature (°F) 76

| Trap Set | Trap I.D. | ② Clock Time 24 Hour | ③ Elapsed Time (minutes) | ④ Dry Gas Meter ~~(L)~~ CF | ⑤ Volume Sampled ~~(L)~~ CF | Temperature (°F) ⑥ DGM | Temperature (°F) Probe | Temperature (°F) Heated Line | Temperature (°F) Tenax Inlet | ⑦ Rotometer Setting | ⑧ Pump Vacuum (in. Hg) | Leak Rate LPM at Vacuum | Comments |
|---|---|---|---|---|---|---|---|---|---|---|---|---|---|
| A<br>81327 | 34A | Start: 1519 | 20 | 727.550 | .200 | 73 |  | 260 | 46 | 300 | 0.51 | 0 |  |
|  |  | Stop: 1539 |  | 727.750 |  | 73 |  |  | 58 | 300 |  |  |  |
| B<br>81328 | 34B | Start: 1544 | 20 | 727.754 | .203 | 74 |  |  | 54 | 300 | 0.47 | 0 |  |
|  |  | Stop: 1604 |  | 727.957 |  | 73 |  |  | 56 | 300 |  |  |  |
| C<br>81329 | 34C | Start: 1610 | 20 | 727.961 | .204 | 73 |  |  | 55 | 300 | 0.56 | 0 |  |
|  |  | Stop: 1630 |  | 728.165 |  | 74 |  | 260 | 58 | 300 |  |  |  |
| D |  | Start: |  |  |  |  |  |  |  |  |  |  |  |
|  |  | Stop: |  |  |  |  |  |  |  |  |  |  |  |
| E |  | Start: |  |  |  |  |  |  |  |  |  |  |  |
|  |  | Stop: |  |  |  |  |  |  |  |  |  |  |  |
| F |  | Start: |  |  |  |  |  |  |  |  |  |  |  |
|  |  | Stop: |  |  |  |  |  |  |  |  |  |  |  |
| Summary | ☒ | ☒ |  | ☒ |  |  |  |  |  |  |  | ☒ | ☒ |

Notes: STACK PRESSURE -.2 IN $H_2O$

Figure 57. Example of a typical VOST raw data sheet.

### TABLE 22. EXAMPLE OF REDUCED SAMPLING DATA READY FOR INTEGRATION WITH ANALYTICAL DATA AND FURNACE OPERATING DATA

Sampling Data Summary

Run C-3

Date 4/7/83

Moisture content 11.55%

| | | Dry Gas Volume | |
|---|---|---|---|
| | Sample | SCF | L |
| HCl and moisture | | 16.745 | 470.8 |
| VOST | 81327 | 0.200 | 5.62 |
| | 81328 | 0.203 | 5.71 |
| | 81329 | 0.204 | 5.72 |

1-6 Impinger water volume: The amount of water in the first impinger of the sampling train. Note that this value is usually a weight rather than a volume.

1-7 Clock time difference: The actual elapsed sampling time. The product of 1-7 and 1-4 should give a cross check to the value 1-8.

1-8 Dry gas meter reading difference ($V_m$): The net actual cubic feet of dry gas sampled.

1-9 Impinger water volume difference ($W_c$): The net change in water volume (mass) in the first impinger of the train. When this is on a weight basis the calculated moisture content must later be corrected for absorption of gases such as HCl and $SO_2$.

1-10 and 1-11 The initial and final weights of any other impingers in the train. This usually includes an empty impinger and one partially filled with silica gel. This ensures that the gas volume measured at the dry gas meter is relatively dry.

1-12 to 1-14 The weight gains of the individual impingers and the net weight gain. This is interpreted to be water.

1-15 Moisture content: The calculated percent moisture content on a volume basis. Note the correction requirement in 1-9.

### D.3.2 Sampling Data Sheet 2 -- VOST Data Sheet

2-1 Barometric pressure: The recorded barometric pressure during sampling.

2-2 Clock time: Same as Item 1-2, previous page.

2-3 Elapsed time: The actual duration of the sampling period for a given sample.

2-4 Dry gas meter: The actual readings of the dry gas meter at the start and stop of sampling.

2-5 Volume sampled: The actual dry gas volume sampled in cubic feet.

2-6 Temperature (DGM): The temperature of the gases in the dry gas meter.

2-7 Rotameter setting: The volume flowrate of gas as measured by the VOST rotameter. Value in milliliters per minute. Note that the rotameter setting and the elapsed time allow a cross check on the volume sampled.

2-8 Pump vacuum: The vacuum drawn on the system by the sampling pump. This value acts as a warning of leaks.

## D.4 ANALYTICAL DATA

There were three different raw data sets of analytical data taken; for chloride analysis, for organic chloride analysis, and for the Tenax volatile organic analysis by gas chromatography. Of these, only the last requires an in-depth discussion. The actual reduced data arriving from the laboratory appears as Table 23. This section details the data reduction steps used to achieve the compound levels reported for the VOST Tenax chromotographic analysis.

Raw chromatographic data is obtained as a chromatogram and/or a printout of peak relative retention times and areas. Typical plots are shown for a standard and a real sample in Figure 58. (See Appendix C for a detailed description of the analytical procedure.) To determine the quantity of one compound in one sample eleven different pieces of raw data must be used, and ten different logic or mathematical operations conducted. The sequence is illustrated in Figure 59. In the more automated systems, such as GC/MS, this is done by computer, but the system still must be programmed and calibrated. Whether the system is automated or manual, this data reduction sequence contains subjective aspects and requires careful attention. When performed manually, this data reduction is done in two steps and has been carried out in an example case in the data sheets illustrated in Figures 60 and 61. The following subsections detail the items found on these sheets.

### D.4.1 Analytical Data Sheet 1 -- Standard Injection GC Run

1-1 Samples: The identity numbers of the samples for which this standard injection is valid. Usually those samples run during the same shift or half-shift depending on the stability and reproducibility of the instrument.

1-2 Peak number: The number of the peak as it occurs on the chromatogram in sequence from the point of injection.

1-3 Identity: The compound identity of the peak. This is usually established by injecting individual compounds on the analytical system and comparing relative retention times when the standard is prepared.

1-4 Retention time: The time from the point of injection to the occurence of the peak. This is the primary value by which a peak is identified by gas chromatography on all detection systems except mass spectroscopy. Mass spectroscopy uses this value as a preliminary screening identifier. This value is printed out by automated plotter integrators, but is manually determined by measuring the distance on the chromatogram from the point of injection to the peak and correlating with the chromatogram chart drive speed.

TABLE 23. EXAMPLE OF AN ANALYTICAL DATA SUMMARY FORM (RUN C-3)

Analytical Data Summary

Run: C-3

Date: 4/7/83

Fuel/Waste Analysis

Chloride 3.44 wt % (3.47 wt % duplicate)

Moisture train analysis:

Total chloride 710 mg

VOST Tenax analysis:

| | ng/sample | | | | |
|---|---|---|---|---|---|
| Sample Ident | $CHCl_3$ | $CCl_4$ | (TCE) | (PCE) | PhCl |
| 818327 | 590 | 700 | 40 | 620 | <5 |
| 818328 | 780 | 970 | 40 | 870 | <5 |
| 818329 | 510 | 480 | 80 | 420 | <5 |

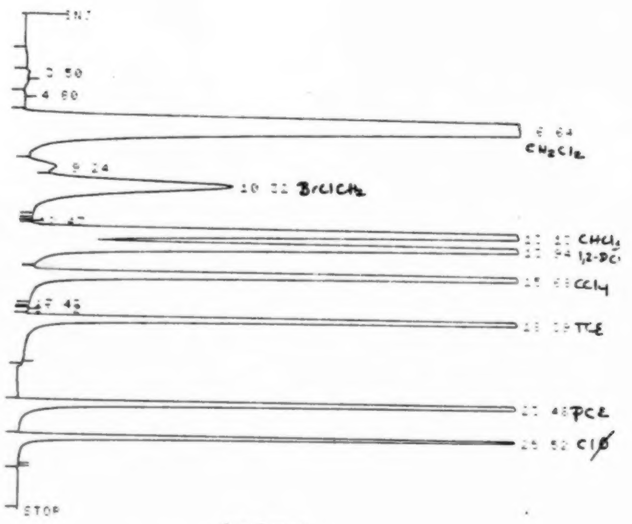

```
                Area Percent
   RT   Type    Area

   3.50              8721     .022 29
   4.80              3237     .008 272
   6.64           9932579   25.38
   9.24   T        316036     .807 6
  10.32   TM      2638512    6.743
  13.13           5440454   13.9
  13.94   M       4886447   12.49
  15.68           4954714   12.66
  17.43   T          1083     .002 768
  18.39           4943969   12.63
  23.48           3995594   10.21
  25.52   T       2010462    5.138
```

a. Standard

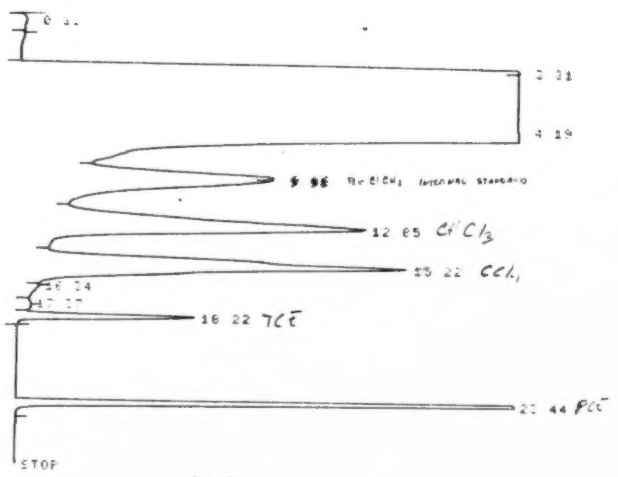

```
                Area Percent
   RT   Type    Area

    .33             37075     .030 59
   3.31           3491035    2.88
   4.19   *M     99999999   82.51
   9.86   M       2117886    1.747
   9.98   M       2606396    2.15
  12.85   M       4939373    4.075
  15.22   M       4245692    3.503
  18.22            738742     .609 5
  23.44           3027368    2.498
```

b. Sample

Figure 58. Typical standard and sample chromatographic traces.

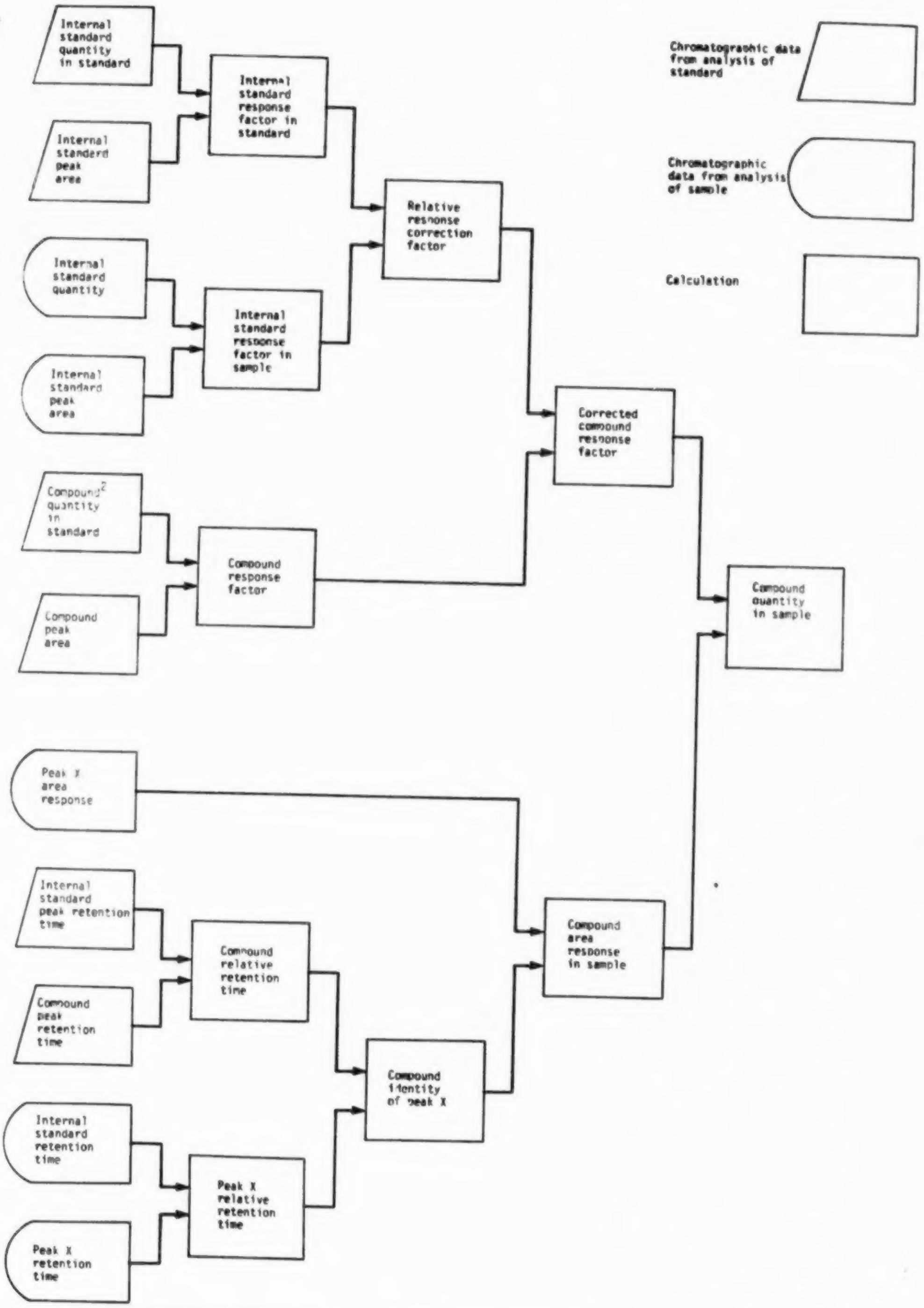
Internal standard quantity in standard
Internal standard peak area
Internal standard response factor in standard
Internal standard quantity
Internal standard peak area
Internal standard response factor in sample
Relative response correction factor
Compound$^2$ quantity in standard
Compound peak area
Compound response factor
Corrected compound response factor
Compound quantity in sample
Chromatographic data from analysis of standard
Chromatographic data from analysis of sample
Calculation
Peak X area response
Internal standard peak retention time
Compound peak retention time
Compound relative retention time
Internal standard retention time
Peak X retention time
Peak X relative retention time
Compound identity of peak X
Compound area response in sample

Figure 59. Preliminary data reduction steps for gas chromatographic data from a Tenax trap.

Analytical Data Sheet 1
Date: 4/7/83
Samples: [1] 818327-329, 332-334

Standard GC Run
Operator ____________________

| [2] Peak no. | [3] Identity | [4] Retention time (min) | [5] Relative retention time | [6] Quant inject (ng) | [7] Peak area $cts \times 10^{-3}$ | [8] Resp factor $ng \times 10^4/ct$ |
|---|---|---|---|---|---|---|
| 1 | $CH_2Cl_2$ | 6.65 | 0.64 | 1,000 | 9,933 | 1.01 |
| 2 | $BClCH_2$ | 10.32 | 1.00 | 1,000 | 2,639 | 3.79 |
| 3 | $CHCl_3$ | 13.13 | 1.27 | 1,000 | 5,440 | 1.84 |
| 4 | 1,2-DCA | 13.94 | 1.35 | 1,000 | 4,886 | 2.05 |
| 5 | $CCl_4$ | 15.68 | 1.52 | 1,000 | 4,955 | 2.02 |
| 6 | TCE | 18.39 | 1.78 | 1,000 | 4,944 | 2.02 |
| 7 | PCE | 23.48 | 2.28 | 1,000 | 3,996 | 2.50 |
| 8 | $C_6H_5Cl$ | 25.52 | 2.47 | 1,000 | 2,010 | 4.98 |

Figure 60. Example of analytical raw data for a standard showing the first step of data reduction. The data is from the third VOST train of run C-3.

Analytical Data Sheet 2
Sample GC Run

Date: 4/7/83
Operator ____________________

Sample: [1] 818329 Internal std: [2] $\mathrm{BRClCH_2}$ Peak no. [3] 3+4
Retention time [4] 10.32 Quantity 1,000 ng [5] Response factor [6] 3.79*
Retention time [7] 9.86 Quantity 1,000 ng [8] Response factor [9] 2.12†
Response correction factor [10] 0.56

| [11] Peak no. | [12] Ret time (min) | [13] Rel ret time | [14] Identity | [15] Std resp factor (ng x$10^4$/ct) | [16] Corr resp factor (ng x$10^4$/ct) | [17] Area (ct x$10^{-3}$) | [18] Quantity (ng) |
|---|---|---|---|---|---|---|---|
| 1 | 3.31 | 0.34 | ? | (1) | 0.56 | 3,491 | (195) |
| 2 | 4.19 | 0.42 | ? | (1) | 0.56 | >$10^5$ | (>5,600) |
| 3 | 9.86 | 1.00 | $\mathrm{BrClCH_2}$ | 3.79 | 2.12 | 4,724 | 1,000 |
| 4 | 9.98 | | | | | | |
| 5 | 12.85 | 1.30 | $\mathrm{CHCl_3}$ | 1.84 | 1.03 | 4,939 | 509 |
| 6 | 15.22 | 1.54 | $\mathrm{CCl_4}$ | 2.02 | 1.13 | 4,246 | 480 |
| 7 | 18.22 | 1.85 | TCE | 2.02 | 1.13 | 739 | 84 |
| 8 | 23.44 | 2.38 | PCE | 2.50 | 1.40 | 3,027 | 423 |

* From standard injection.
† From sample injection.

Figure 61. Example of analytical raw data for sample showing final steps in the preliminary (intradisciplinary) data reduction.

1-5 Relative retention time: The time of appearance of a peak relative to a known internal standard. Calculated by dividing the retention time of the internal standard into the retention time of the peak in question.

1-6 Quantity injected: The absolute mass of the standard compound that was injected. This value is calculated from the concentration of the material in the standard solution and the quantity (volume) of standard solution injected.

1-7 Peak area: The area under the peak of the compound in question. The value represents an integrated electronic signal from the detector of the instrument, and is usually referred to as area counts.

1-8 Response factor: The mass of compound represented by an area count. This is a measure of the sensitivity of the detector to the compound, and is the number used to quantitate peaks. A larger number indicates less detector sensitivity to the particular compound. In the example shown in Figure 60 it can be seen that the Hall detector is 2.5 times less sensitive to chlorobenzene than to most of the other compounds measured.

### D.4.2 Analytical Data Sheet 2 -- Sample Injection GC Run

2-1 Sample: The identity number of the sample being analyzed.

2-2 Internal standard: The compound co-injected with the sample and to be used as the internal standard for determining relative retention times and relative response factors.

2-3 Peak number: The number(s) of the peak(s) in the sample chromatogram identified as the internal standard.

2-4 Retention time: The retention time of the internal standard compound from the standard injection chromatogram (data sheet 1).

2-5 Quantity: The quantity of the internal standard compound in the standard chromatogram.

2-6 Response factor: The response factor of the internal standard compound in the standard chromatogram.

2-7 Retention time: The retention time of the internal standard compound in the sample chromatogram.

2-8 Quantity: The quantity of the internal standard compound injected with the sample.

2-9 Response factor: The response factor of the internal standard compound in the sample.

2-10 Response correction factor: The correction factor for responses of compounds in the sample. This will be applied to the response factor of the respective compounds in the standard to determine the corrected response factor to be used for the sample.

2-11 Peak number: Same as item 1-2 in Section D.4.1.

2-12 Retention time: Same as item 1-4 in Section D.4.1.

2-13 Relative retention time: As for 1-5 in Section D.4.1.

2-14 Identity: The compound identification assigned to the given peak. Peaks are usually identified as being a given compound if their relative retention time is within 0.1 of the corresponding peak relative retention time in the standard. For example, from Figure 61, peak 5 has a retention time relative to bromochloromethane of 1.30. The closest peak in the standard is chloroform with a retention time relative to bromochloromethane of 1.27. Some subjective judgment enters here because 1,2-dichloroethane has a relative retention time of 1.35. This is resolved by reviewing the overall pattern and noting how more readily identifiable peaks are shifted.

2-15 Standard response factor: The response factor of the identified compound in the standard (data sheet 1, item 8).

2-16 Corrected response factor: The response factor of the compound after being corrected for the change in the response factor of the internal standard. Calculated by multiplication of 2-10 and 2-15.

2-17 Area: Same as item 1-7 in Section D.4.1.

2-18 Quantity: The calculated quantity of the compound in the sample. Determined by multiplying 2-16 and 2-17.

## D.5 DATA INTEGRATION

Once all the data from each of the project disciplinary areas (furnace operation, sampling, and analysis) for a given test have completed the first (intradisciplinary) data reduction step, they must be integrated and further reduced. Refering back to Figure 50, one may see the integration and reduction steps. The reduction depicted in the bottom half of the figure and leading up to the box labeled "Furnace DRE Performance" is discussed in this section. The reduction is carried out on four standardized data sheets to insure consistency. Example data sheets are shown in Figures 62 to 65. The input and calculations necessary to generate each datum is identified with a bracketed number. The data are defined and described below. Although many of the items appear to be self-explanatory, they have been included to ensure completeness.

Run: ____________________

Date: ____________________

| | Compound | [1] MW | [2] $\rho$ (g/mL) | [3] Volume (mL) | [5] Volume fraction ($mL/mL_{tot}$) | [6] Wt/vol ($g/mL_{tot}$) | [8] Weight fraction ($g/g_{tot}$) |
|---|---|---|---|---|---|---|---|
| A | | | | | | | |
| B | | | | | | | |
| C | | | | | | | |
| D | | | | | | | |

[4] $mL_{tot}$ = ________ [7] $\rho_{tot}$ = ________

| | [9] Chloride fraction ($g_{cl}/g$) | [10] Carbon fraction ($g_c/g$) | [11] Chloride fraction ($g_{cl,i}/g_{tot}$) | [13] Carbon fraction ($g_{c,i}/g_{tot}$) |
|---|---|---|---|---|
| A | | | | |
| B | | | | |
| C | | | | |
| D | | | | |

[12] $g_{cl}/g_{tot}$ = __________ [14] $g_c/g_{tot}$ = __________

[4] = $\Sigma$ [3]

[5] = [3]/[4]

[6] = [2] x [5]

[7] = $\Sigma$ [6]

[8] = [6]/[7]

[9] = 35.5 x $N_{cl}$/[1]

[10] = 12 x $N_C$/[1]

[11] = [8] x [9]

[12] = $\Sigma$ [11]

[13] = [8] x [1]

[14] = $\Sigma$ [13]

Data Reduction Form 1 -- Waste Calculations

Figure 62. Example of data reduction sheet for calculating DRE values (part 1).

Run: ____________________

Date: ____________________

[15] Weight fraction chloride in feed ($g_{cl}/g_f$) __________

[16] Weight fraction waste in feed ($g_w/g_f$) __________ [16] = [15]/[12]

[17] Weight fraction fuel in feed ($g_2/g_f$) __________ [17] = 1.00 - [16]

[18] Feed density ($\rho_f$) __________ [18] = .843 x [17] + [7] x [16]

[19] Volume fraction waste ($mL_w/mL_f$) __________ [19] = [16] x [18]/[7]

[20] Measured feed rate ($lb_f/hr$) __________

[21] Corrected feed rate ($lb_f/hr$) __________ [21] = [20] (.58 + 0.5 x [18])

[22] Corrected feed rate ($g_f/min$) __________ [22] = 7.56 x [21]

[23] Feed rate waste ($g_w/min$) __________ [23] = [16] x [22]

| | Compound | [24] Feedrate (g/min) | [25] Feedrate (lb/hr) |
|---|---|---|---|
| A | | | |
| B | | | |
| C | | | |
| D | | | |

[24] = [8] x [23]　　[25] = [24]/7.56

[26] Carbon content in fuel ($g_c/g_{\#2}$) __________

[27] Carbon content in feed ($g_c/g_f$) ________ [27] = [26] x [17] + [14] x [16]

[28] Carbon feedrate ($g_c/min$) __________ [29] ($lb_c/hr$) __________

[28] = [22] x [27]　　[29] = 7.56 x [28]

Data Reduction Form 2 -- Feed Rate Calculations

Figure 63. Example of data reduction sheet for calculating DRE values (part 2).

Run: ______________________

Date: ____________________

### A. Moisture Fraction

[30] Moisture weight gain (g) __________

[31] Chloride weight gain (g) __________

[32] Net weight gain (g) __________ [32] = [30] - [31]

[33] DSCF sampled __________

[34] SCF water __________ [34] = .04832 x [32]

[35] Moisture fraction $Bw_o$ __________ [34]/([33] + [34])

[36] Dry gas fraction __________ 1.00 - [35]

### B. Flue Gas Composition

| Specie | [37] Dry mole fraction | [38] Wet mole fraction | [39] MW | [40] Wt Cont |
|---|---|---|---|---|
| A Oxygen | __________ | __________ | [32] | __________ |
| B Carbon dioxide | __________ | __________ | [44] | __________ |
| C Nitrogen | __________ | __________ | [28] | __________ |
| D Water | | [35] __________ | [18] | __________ |

[41] Flue gas MW __________

[38] = [36] x [37]   [40] = [38] x [39]   [41] = $\Sigma$ [40]

[42] Flue gas flow rate (lb/hr) __________

[42] = ([21] x [27] x [41])/(12 x [38B])

[43] Flue gas flow rate (wscf/min) __________

[43] = 6.423 x [42]/[41]

Data Reduction Form 3 -- Flue Gas Composition and Flowrates

Figure 64. Example of data reduction sheet for calculating DRE values (part 3).

Run: ____________________

Date: ____________________

Set:

[44] Dry gas volume sampled (dscf) __________
[45] Wet gas volume sampled (wscf) __________
$[45] = [44]/[36]$

Emission Rates

| Compound | [46] Quantity (ng/sample) | [47] Concentration (μg/wscf) | [48] Rate (g/min) | [49] Rate (lb/hr) |
|---|---|---|---|---|
| A | | | | |
| B | | | | |
| C | | | | |
| D | | | | |

$[47] = [46]/([45] \times 10^3)$

$[48] = [43] \times [47] \times 10^{-6}$

$[49] = [48]/7.56$

DRE's

| | [50] C/Co | [51] DRE |
|---|---|---|
| A | | |
| B | | |
| C | | |
| D | | |

$[50] = [48]/[24]$

$[51] = (1.00 - [50]) \times 100$

Data Reduction Form 4 (A-C) -- Emission Rate and DRE Calculations

Figure 65. Example of data reduction sheet for calculating DRE values (Part 4)

### D.5.1 Data Reduction Form 1 -- Waste Composition Calculations

1-1 Molecular weight: The molecular weight of the individual waste compound

1-2 Density: The density of the individual waste compound at 200°C and 101 kPa (one atmosphere pressure)

1-3 Volume: The measured volume of the individual waste compound added to the waste blend when the waste blend was prepared. The sum of all 1-3 values.

1-4 Milliliters total: The total volume of the particular waste blend

1-5 Volume fraction: The volume fraction of the particular waste compound in the waste blend. Calculated by dividing 1-3 by 1-4.

1-6 Weight per unit volume: The weight of the individual waste compound per unit volume of the waste blend. Determined from the density times the volume fraction (1-2 times 1-5).

1-7 Total density: The density of the waste blend, calculated by summing 1-6. This is an approximation that does not account for molal-mixing effect. The error is expected to be less than 1 percent for the compounds and blends prepared in this program.

1-8 Weight fraction: The fraction of the blend by weight that is associated with the individual waste compound (1-6 divided by 1-7).

1-9 Chloride fraction: The fraction of the weight of the individual compound that is chlorine (molecular weight of chlorine times the number of chlorine atoms in the waste compound divided by the molecular weight of the compound).

1-10 Carbon fraction: The fraction of the weight of the individual compound that is carbon (the molecular weight of carbon times the number of carbon atoms divided by the molecular weight of the compound).

1-11 Chloride fraction in waste: The contribution of the individual compound to the total chloride in the waste (1-8 times 1-9).

1-12 Chloride fraction total: The weight fraction of chloride in the waste blend.

1-13 Carbon fraction in waste: The contribution of the individual compound to the total carbon in the waste (1-8 times 1-10).

1-14 Carbon fraction total: The weight fraction of carbon in the waste blend.

### D.5.2 Data Reduction Form 2 -- Feed Rate Calculations

2-15 Weight fraction chloride in feed: The amount of chloride in the fuel plus waste mixture as fed to the furnace. This is a laboratory analysis number.

2-16 Weight fraction waste in feed: The weight fraction of the fuel plus waste mixture that is contributed by the waste. Calculated by dividing 2-15 by 1-12.

2-17 Weight fraction fuel in feed: The portion of the feed (by weight) that is No. 2 distillate oil (one minus 2-16).

2-18 Feed density: the density of the waste soup plus fuel mixture. Calculated by adding the fractions of the density contributed by the fuel and the soup respectively.

2-19 Volume fraction waste: The fraction of the feed (fuel plus waste) by volume that is waste or soup.

2-20 Measured feed rate: The fuel plus waste feed rate as measured by the fuel feed system.

2-21 Corrected feed rate: The feed rate of fuel plus waste corrected for the change in density caused by addition of the waste to the No. 2 distillate oil. The original measuring device (rotometer) is calibrated to a fluid density or No. 2 distillate. The algorithm used here is empirically derived from the particular rotometer calibration curve, and the equations for rotameter flows.

2-22 Corrected feed rate: Same as above but in metric units. The number 7.56 is the multiplier to change pounds per hour to grams per minute.

2-23 Feed rate waste: The feed rate of the waste alone.

2-24 and 2-25 Feed rate: The feed rates of the individual components of the waste soup in both English and metric units.

2-26 Carbon content in fuel: The analyzed carbon content of the No. 2 distillate oil.

2-27 Carbon content in feed: The calculated carbon content of the feed (fuel plus waste soup).

2-28 and 2-29 Carbon feed rate: The feed rate of carbon to the furnace in both English and metric units.

### D.5.3 Data Reduction Form 3 -- Flue Gas Composition and Flowrates

3-30 Moisture weight gain: The weight gain of the moisture train impingers (from Section D.3.1, item 1-14).

3-31 Chloride weight gain: The amount of chloride ion collected in the moisture train.

3-32 Net weight gain: The amount of weight gain attributed to moisture only. The weight gain of the moisture train less the weight gain attributed to chloride.

3-33 DSCF sampled: The number of dry standard cubic feet of gas sampled with the moisture train (from Section 4.3.1, item 1-8).

3-34 SCF water: The number of standard cubic feet that the water collected in the moisture train represent.

3-35 Moisture fraction: The corrected moisture fraction of the flue gas.

3-36 Dry gas fraction: The fraction of the flue gas that is dry gas.

3-37 Dry mole fraction: The mole fraction of the dry flue gas represented by the given compound (A-D). These values are instrument measured values. Note that carbon monoxide is not listed. Carbon monoxide was never measured at a high enough level to contribute significantly to the flue gas flowrate, the ultimate goal of this series of calculations.

3-38 Wet mole fraction: The mole fraction of the wet flue gas represented by the individual compound (A-D).

3-39 Molecular weight: The molecular weight of the individual compound (A-D).

3-40 Molecular weight contribution: The contribution to the molecular weight of the flue gas by the particular specie (A-D).

3-41 Flue gas molecular weight: The calculated molecular weight of the flue gas.

3-42 and 3-43 Flue gas flowrate: The flowrate of flue gas in units of mass and volume.

### D.5.4 Data Reduction Form 4 -- Emission Rates and DRE's

4-44 Dry gas volume sampled: The measured amount of dry gas sampled in the organic sampling train for the particular set of traps under study and corrected to standard conditions.

4-45 Wet gas volume sampled: The value from above (4-44) corrected for the moisture content of the flue gas.

4-46 Quantity: The amount of the particular specie measured in the particular set of traps. This datum is a laboratory reported number.

4-47 Concentration: The calculated concentration of the given specie in the flue gas stream.

4-48 and 4-49 Rate: The calculated mass flowrate of the specie out of the combustor in English and metric units.

4-50 C/Co: The penetration fraction of the particular specie. The fraction of the amount of the material injected that passed through the combustor.

4-51 DRE: The destruction and removal efficiency of the system with respect to the particular specie.